DOE/NV/10872--T208

University of Nevada, Las Vegas

Mechanical Properties of Tuffaceous Rocks Under Triaxial Conditions

by

Moses Karakouzian and Nick Hudyma

Geomechanics Research Group

Department of Civil and Environmental Engineering
4505 Maryland Parkway
Box 454015
Las Vegas, Nevada 89154-4015
(702) 895-0959/3701
FAX (702) 895-3936

December, 1994

DISCLAIMER

ABSTRACT

Yucca Mountain has been designated as a potential site for a high level nuclear waste repository. Part of the site characterization program is an investigation of the mechanical properties of the tuffs which comprise Yucca Mountain. This study tested specimens of TCw tuff in triaxial compression to observe the effects of confining pressure, saturation, strain rate, and anisotropy on the compressive strengths and Young's Moduli of the specimens. Test results have shown that increasing the confining pressure increased the compressive strength and generally increased the Young's Modulus. Saturation appears to lower both the compressive strength and Young's Modulus of the specimens. Increasing strain rates increases the compressive strengths, but lowers the Young's Modulus values. There appears to be a stiffness anisotropy where the specimens are stiffer perpendicular to the orientation of the lithophysal cavity orientation. Correlations with porosity have shown an increase in porosity generally lowers both the compressive strength and the Young's Modulus of the specimens. From the triaxial tests, the Mohr - Coulomb strength parameters have also been determined. A comparison between the strengths and modulus values from this study, values from previous studies and the suggested values reveal that the

values computed for this study are generally lower than the previously published data. This discrepancy may be due to sample and specimen differences between the studies.

TABLE OF CONTENTS

LIST OF FIGURES

LIST OF TABLES

ACKNOWLEDGMENTS

First and foremost, I would like to thank Dr. Moses Karakouzian for his help towards the completion of this thesis and for the opportunity to work with him on the Rock Properties of Yucca Mountain Project. His vast knowledge of laboratory testing techniques and mechanical properties of geomaterials stimulated numerous beneficial conversations, many of which have helped me both academically and in my research. I would also like to extend my thanks to Dr. G. Frederick, Dr. S. Ladkany, and Dr. S. Moujaes, who all served on my graduate committee. Also, thanks go to Lynn for her understanding of the time requirements needed to finish this thesis.

INTRODUCTION

In order to design, license, construct, operate, and decommission a repository at Yucca Mountain, the behavior and properties of the tuffs which make up the mountain must be studied (DOE, 1988). The intact rock properties of the tuffs at Yucca Mountain are being used for three purposes:

- for direct use in analysis and design of mined openings, shafts and boreholes,
- to determine the spatial distribution of intact rock properties in the Yucca Mountain tuffs, and
- to help predict rock-mass and in-situ rock properties.

Some of the intact rock properties which must be studied include Young's Modulus and compressive strength. Young's Modulus is used to characterize the elastic deformation of the tuffs under an applied load. This elastic constant is required for the design, modeling, and analysis of openings in the tuffs and for how the tuffs will deform elastically after excavation and emplacement of waste. The compressive strengths are used for analysis and modeling in-situ rock strength and the stability of subsurface openings (Tillerson and Nimick, 1984). Rock strength depends on the rate of loading or strain. It is possible that the

compressive strength of the tuffs at Yucca Mountain is rate dependent (DOE, 1988).

The objective of this study is to investigate the effect of confining pressure, saturation, strain rate and specimen anisotropy on the compressive strength and Young's Modulus of Tiva Canyon Tuff specimens which are from the thermo - mechanical unit TCw. The study is comprised of five parts. A background section provides some brief information on the geology of Yucca Mountain, factors affecting mechanical properties of rock specimens and lists the available data on the mechanical properties of Tiva Canyon Tuff and the thermo - mechanical unit TCw. Next, a section detailing the experimental approach used for this study is given. This section deals with core sampling, experimental design, and test procedures. Following the experimental approach section is a results section. This section addresses how the test results were computed and lists the test results. Next, the discussion of results section provides insight into the effects of the test conditions, anisotropy, and porosity on the compressive strength and Young's Modulus of the tuff specimens. This section also calculates the Mohr - Coulomb strength parameters and compares previous mechanical property data with the compressive strength and Young's Modulus data from this study. Finally, all of the observations from this study are presented in the conclusions section. The Appendix

contains specimen data and the stress - strain curves from each test triaxial compression test.

BACKGROUND

Geology

Yucca Mountain, located in the state of Nevada, is currently being studied as a potential site for a mined geologic disposal system for high level nuclear waste. Yucca Mountain is situated on land controlled by three Federal agencies: the Bureau of Land Management (BLM), the Department of Energy (DOE) and the U.S. Air Force. By road, Yucca Mountain is located approximately 160 km (100 miles) northwest of Las Vegas (Site Characterization Plan, Volume I, Part A). The location of the Nevada Test Site (NTS) and Yucca Mountain within the state of Nevada is shown in Figure 1.

Yucca Mountain is located in the southwestern portion of the Great Basin, a subprovince of the Basin and Range physiographic province (DOE, 1988). The mountain consists of a cluster of elongated, north-trending ridges and lateral spurs which rise from the Amargosa desert (elevation 800 m) to a flat, faulted summit area (elevation 1800 m), 25 km to the north as shown in Figure 2 (Fox et. al., 1990).

Geophysical surveys and surficial drilling have determined that Yucca Mountain is made up of a sequence of tuffaceous rocks between 1.5 and

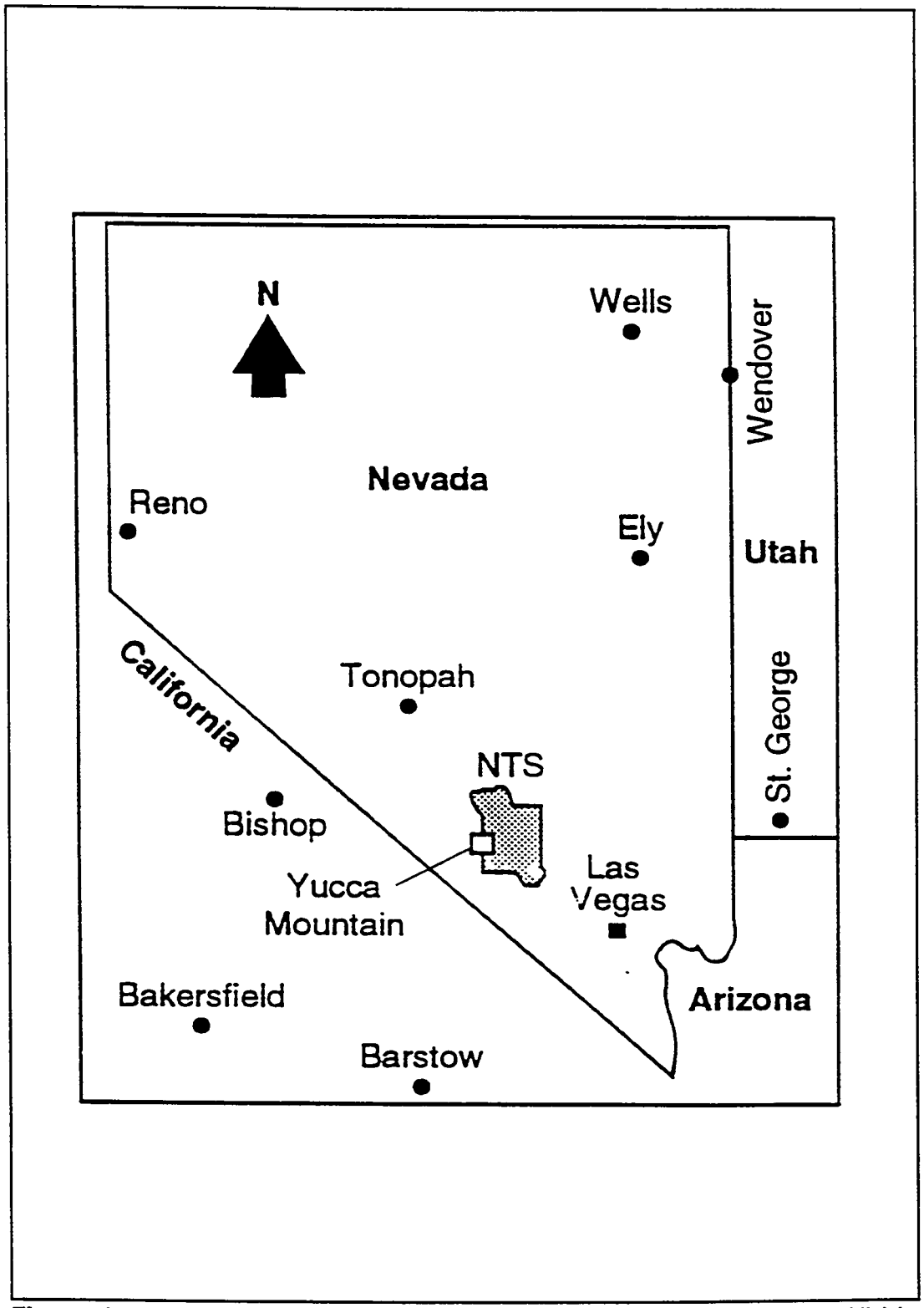

Figure 1. Location of the Nevada Test Site and Yucca Mountain Within the State of Nevada (Wilder, 1993).

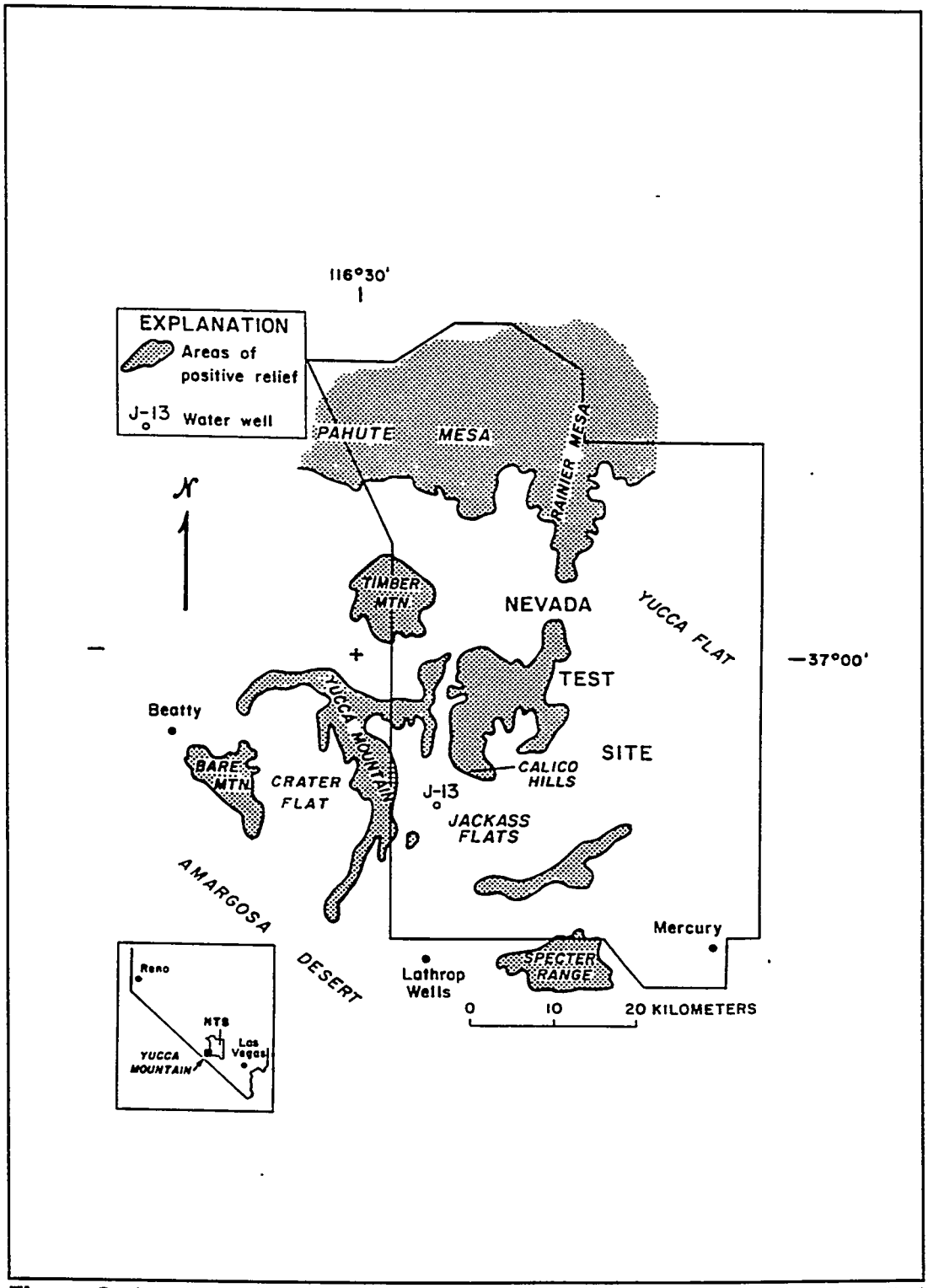

Figure 2. Location of Yucca Mountain and Other Areas of Positive Relief Within the Nevada Test Site (Scott et. al., 1983).

4 km thick overlying a preCenozoic basement complex (Scott et. al., 1983). The tuffaceous rocks of Yucca Mountain which have been penetrated by surficial drilling follow this nomenclature: major ash flows of a particular eruptive cycle are referred to as a formation and individual cooling units of a particular eruptive cycle are referred to as members (Fox et. al., 1990).

The tuffs, which make up Yucca Mountain, listed in descending order are:

- Paintbrush Tuff Formation, which is comprised of:
  - Tiva Canyon Member,
  - Yucca Mountain Member,
  - Pah Canyon Member,
  - Topopah Spring Member,
- Tuffaceous Beds of Calico Hills Formation,
- Crater Flat Tuff Formation, which is comprised of:
  - Prow Pass Member,
  - Bullfrog Member,
  - Tram Member, and
- Lithic Ridge Tuff Formation (Scott et. al., 1983, and DOE, 1988).

The above formations and members are shown in Figure 3, which was derived from correlations between select drill holes from Yucca Mountain (DOE, 1988).

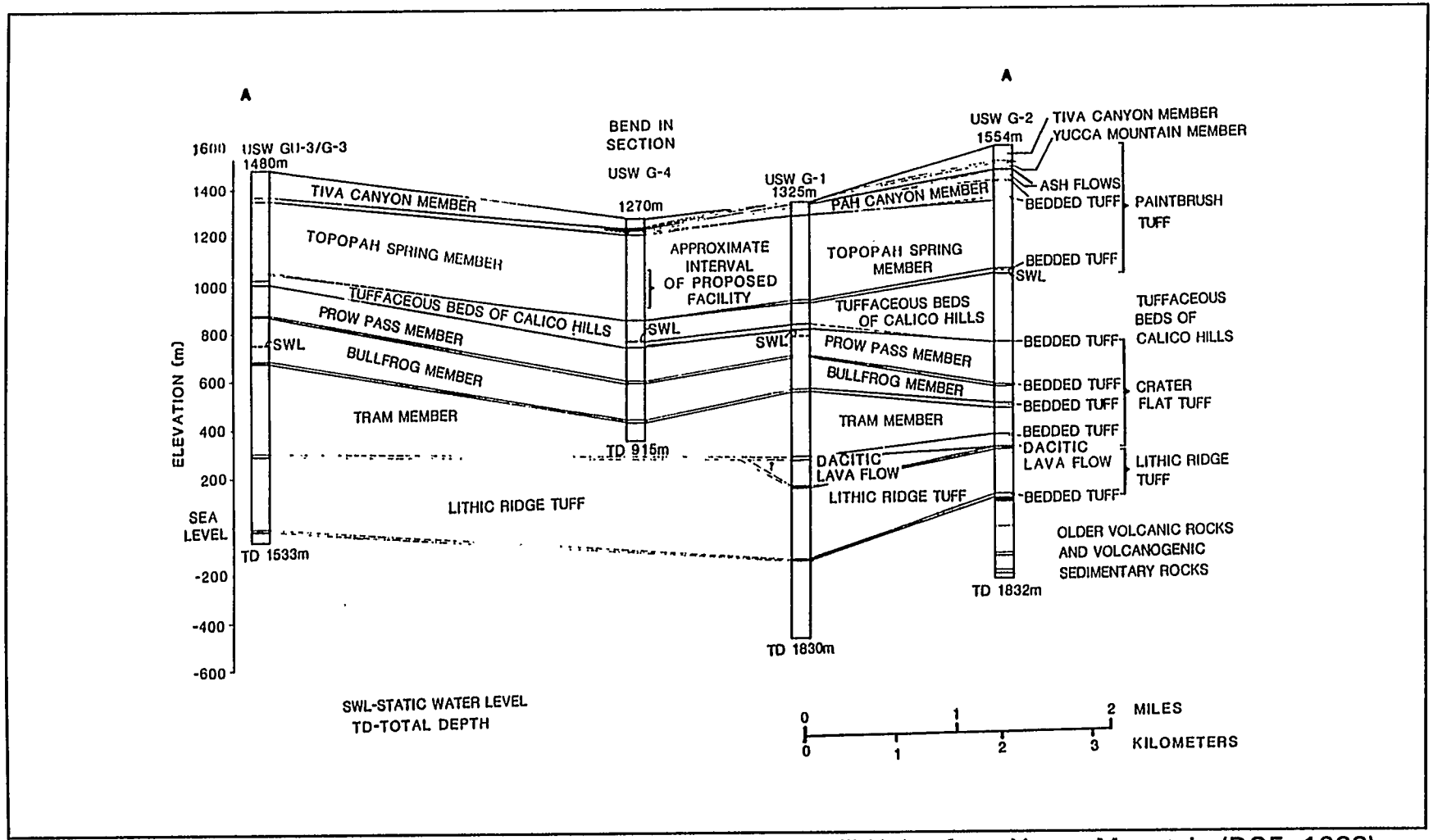

Figure 3. North - South Stratigraphic Correlation Between Select Drill Holes from Yucca Mountain (DOE, 1988).

The tuffaceous rocks of Yucca Mountain were formed during a 10 million year period, from 16 Ma to 6 Ma, during which 6 major eruptive cycles occurred and silicic ash flows were deposited over an area of 13000 km^2. Each major eruptive cycle was comprised of several eruptions of chemically similar, silicic pryroclastic ejecta and perhaps, several nuee ardentes. Generally, individual ash flows are chemically zoned from more silicic at the base to less silicic near the top. However, successive ash-flows of a particular eruptive cycle show a general trend towards a high average silica content. The viscosity of these ash flows was very low and they formed sheets which ponded in low areas with tongues extending outwards along favorably oriented valleys. These paleotopographic variations caused the ash flows to intertongue and wedge out to form a modern day complex three dimensional distribution of tuff (Fox et. al., 1990).

The Tiva Canyon Member of the Paintbrush Tuff formation erupted from the Claim Canyon Cauldron (Scott et. al., 1983) about 12.5 Ma (DOE, 1988). It consists of moderately to densely welded tuff, compositionally zoned from high silica rhyolites at the base and central portions to quartz latites which form the densely welded caprocks near the top of the member (Scott et. al., 1983).

The Tiva Canyon Member has been further subdivided into eight zones. From top to bottom, these zones are:

- Caprock zone
- Upper Cliff zone
- Upper Lithophysal zone
- Clinkstone zone
- Lower Lithophysal zone
- Hackly zone
- Columnar zone
- Basal zone

Some of the zones within the Tiva Canyon Member have been further subdivided (Scott et. al., 1983, and Scott and Bonk, 1984).

The geological stratigraphy of the tuff units of Yucca Mountain do not readily lend themselves to describing the material properties of their associated formations because the formations may contain more than one type of rock. Most formations at Yucca Mountain contain at least two types of tuff: welded ashflows and bedded tuffs (Ortiz et. al., 1984). Ortiz et. al. (1984) have divided the geological stratigraphic tuff units of Yucca Mountain into thermo - mechanical units, which is shown in Figure 4. This study has only tested specimens from the thermo - mechanical unit TCw.

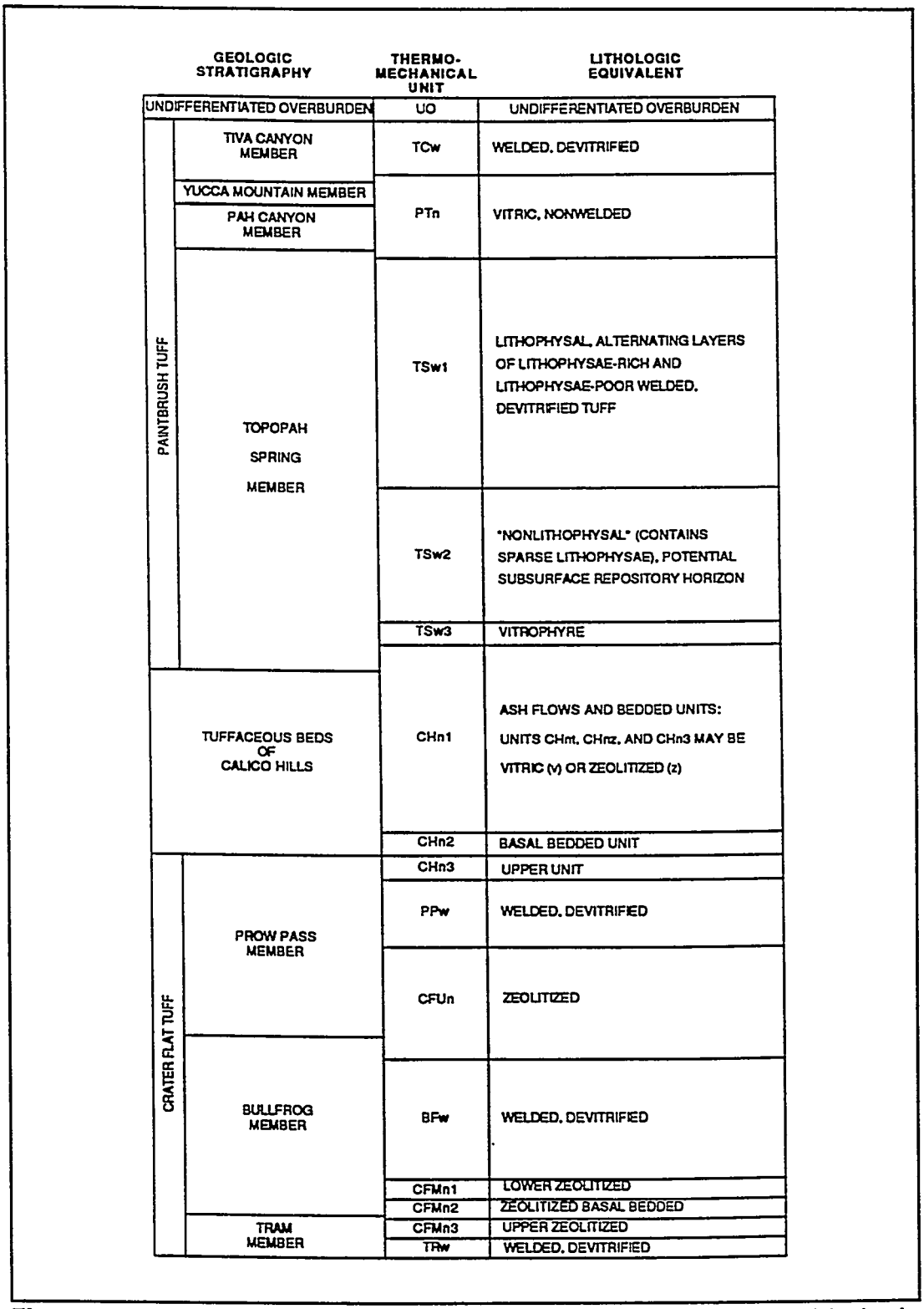

Figure 4. Stratigraphy, Thermo - Mechanical Units and Lithologic Equivalent of the Tuffs at Yucca Mountain (Lin et. al., 1992).

Factors Affecting Mechanical Properties

There are many factors which influence the compressive strengths and Young's Moduli of rock specimens in laboratory testing. These factors can be divided into two main groups: inherent factors and test conditions. This section discusses the inherent factors and test conditions which were examined for this study and their effects on the compressive strengths and Young's Moduli of rock specimens.

Inherent Factors

Inherent factors are those factors which are found in the rock itself, such as porosity, mineralogy, anisotropy, and density. This discussion is limited to porosity and anisotropy, which were the only inherent factors determined for this study.

For mechanical purposes, pores are the most important constituent in a rock because they are the weakest portion of a rock. The pores may influence the strength and deformation properties of a rock specimen (Franklin and Dusseault, 1989). Much work has been done to establish relationships between porosity and parameters such as electrical resistivity, compressional wave velocity, permeability, compressive strength, Young's Modulus, Poisson's Ratio, and axial strain at failure of tuffs from the Nevada Test Site (Nelson and Anderson, 1992, and Price,

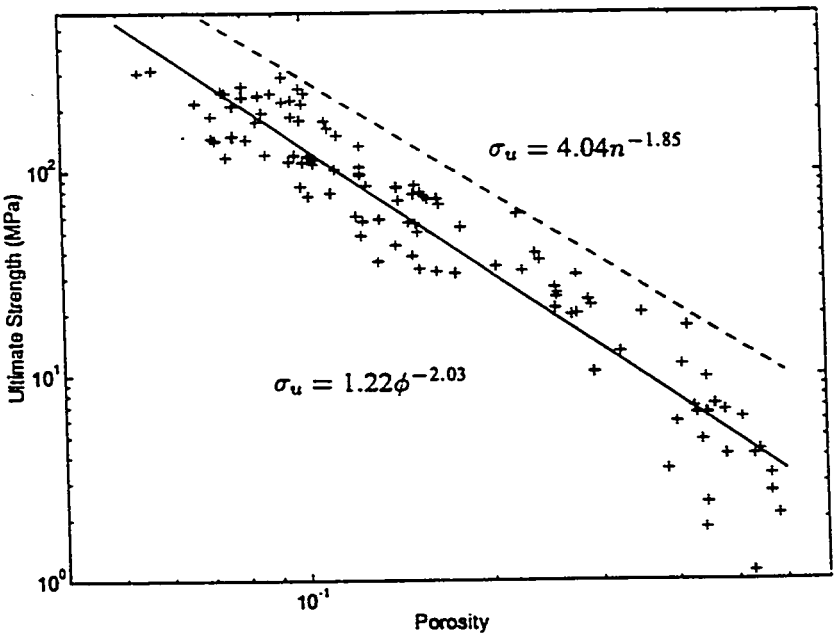

Figure 5. (a) Effect of Porosity on Compressive Strength and (b) Effect of Porosity on Young's Modulus (Price et. al, 1993).

1983). Figure 5 shows two plots which demonstrate the effect of porosity on the ultimate strength (Figure 5a) and on Young's Modulus (Figure 5b). These tests were performed on specimens of Yucca Mountain tuff under unconfined conditions, at room temperature, saturated, and at a constant axial strain of 10^{-5} s^{-1}. If Figure 5, n represents the functional porosity (volume fraction of porosity + volume fraction of clay (Montmorillonite)) and ϕ represents volume fraction of porosity. It is apparent that an increase in porosity decreases both the ultimate strength and the Young's Modulus of Yucca Mountain tuff (Price et. al., 1993).

Olsson and Jones (1980) measured the porosity of the Tiva Canyon Tuffs which they tested. The measured porosities ranged from 8.8% to 54%. The measured values were 8.8%, 8.8%, 8.8%, 26.7%, and 54.0%.

Another inherent factor which may affect the mechanical properties of rock specimens tested in the laboratory is the anisotropy of the specimen. Anisotropy of rock properties occurs as a result of endogenous and exogenous factors. Endogenous factors are associated with the process of rock formation, such as the structure and texture of sedimentary rocks, or the lithophysal cavities in tuffaceous rocks. Exogenous factors are associated with the influence of the surrounding environment. Examples of exogenous factors include the effect of

pressure and temperature (Kwasniewski, 1993). Anisotropy in tuffs from Yucca Mountain may be due to the alignment of microcracks, lithophysal cavities, or mineral grains. Microcracks may develop along grain boundaries of extrusive igneous rocks, such as tuff, as the rock mass cools (Martin et. al., 1992).

When the ash flow sheets which make up Tiva Canyon Tuff were initially deposited, trapped gases may have formed gas pockets called lithophysal cavities. These cavities, which are preserved in the tuff, are spherical to highly oblate voids ranging in size from less than 1 cm to 30 cm in diameter. Surrounding the cavities is a thin ($\sim$1 mm) inner rim of vapor phase crystals. Outside this rim is another rim of pale colored altered rock matrix. This outer rim is usually about 1 cm thick.

There are two major lithophysal zones within the Tiva Canyon Member, the Upper Lithophysal zone and the Lower Lithophysal zone. Field relations suggest that these zones are continuous sheets and are a result of two separate, gas-rich eruptive pulses. These cavities will influence effective hydraulic conductivities, decrease the rock thermal conductivities and bulk densities and will alter the mechanical properties of the Tiva Canyon Member (Scott et. al., 1983). Tillerson and Nimick (1984) state the lithophysal cavities are expected to decrease the strength of the tuffs.

The anisotropy of strength and deformation properties can be

observed by testing specimens of different orientations from within the same rock block. In an attempt to measure the degree of anisotropy of the elastic moduli of tuffs from the Nevada Test Site, Olsson and Jones (1980) measured independently the axial and transverse strains during hydrostatic loading. A typical plot of the two strains during hydrostatic loading is shown in Figure 6.

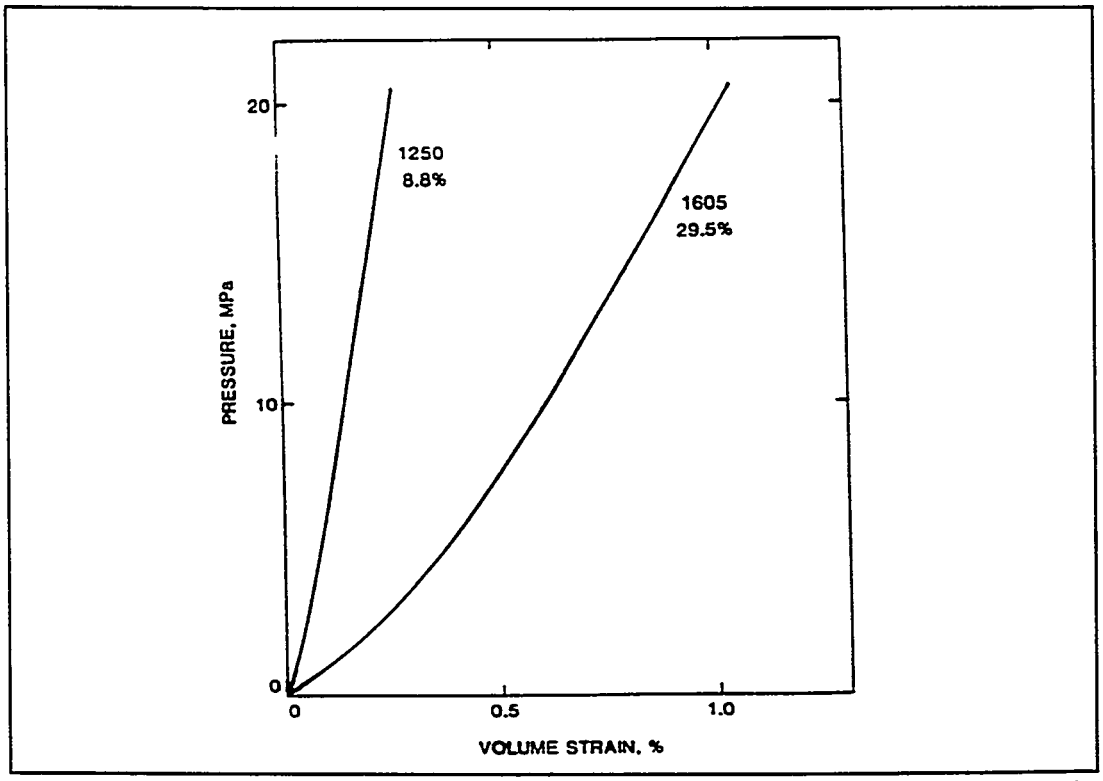

Figure 6. Axial and transverse strains of a tuff sample during hydrostatic loading. The tuff sample was from the Nevada Test Site (Olsson and Jones, 1980).

The ratio of the slopes from the linear portions of the two curves (K_{axial} and $K_{transverse}$) was considered to be a measure of anisotropy. The ratios ranged from near 7 for welded tuffs to near 0.1 for non - welded

tuffs. The terms used, K_{axial} and $K_{transverse}$, should not be confused with the bulk modulus, K. These values, K_{axial} and $K_{transverse}$, can be considered to be "Young's" Modulus values measured under proportional loading, but they are not true values of Young's Moduli (Olsson and Jones, 1980). Olsson and Jones (1980) also state that "welded tuff is stiffest perpendicular to bedding", which is approximately vertical.

Martin et. al. (1992) measured the anisotropy of a welded tuff (Topopah Spring Tuff) from Yucca Mountain. Their results state that the tuff can be considered transversely isotropic with the axis of symmetry normal to the bedding plane. The tuff was significantly more compliant normal to the layering than within the bedding plane. Thus, the vertical direction was the slow direction for the P waves and the Young's Modulus was lower perpendicular to the bedding than it was parallel to the bedding (Martin et. al., 1992). Other studies, Price et. al., 1985; 1987, have stated that the axis of symmetry is perpendicular to the preferred orientation of the shard matrix, which is a result of gravity and flow during deposition of the ash flow. The anisotropy is thought to be produced by the preferred orientation of the shard matrix and perhaps, the pore distribution (Martin et. al., 1992).

Test Conditions

Test conditions under which rock specimens are tested affect the

compressive strength and the Young's Modulus of the specimen. The test conditions which were varied in this study were confining pressure, saturation, and strain rate.

Most rocks show an increase in compressive strength with an increase in confining pressure (Goodman, 1989). The confining pressure hampers the growth of the largest cracks within a rock specimen. The largest cracks can no longer cause fracture, thus a further increase in load is possible. This is the cause of the increase in strength with and increase in confining pressure (Dyskin et. al., 1994). Olsson and Jones (1980) state that confining pressure appears to have no significant effect on Young's Modulus for volcanic tuffs from the Nevada Test Site. Nimick et. al. (1985) state that a variation of confining pressure between 0 and 10 MPa produced no definite trend in Young's Moduli for the Topopah Spring Tuff specimens they tested.

Water saturation of silicic rocks, such as tuff, tends to weaken rock specimens in two ways: by chemical effects and by mechanical effects. The chemical weakening effect of water is caused by a reduction of surface energy at grain boundaries and at the tips of internal flaws (Franklin and Dusseault, 1989). The surface energy is a measure of the work required to produce a unit area of surface by a reversible and isothermal process. Both surface energy and mechanical strength of a solid depend on the strength of its bonds (Swolfs, 1972). Water tends

to hydrolyze strong silicon-oxygen bonds (-Si-O-Si-) into weaker hydroxyl groups (-Si-OH), and thereby weaken the bonds at crack tips within the specimen (Franklin and Dusseault, 1989). The weakened crystals deform plastically by dislocation-propagated slip (Griggs, 1967).

Mechanically, water can affect the strength of rock specimens through the coupling of diffusion and deformation which can cause non-equilibrium pore pressure. That is, if the rock specimen is compacting, the pore pressure will increase and if the rock specimen is dilating, the pore pressure will decrease. These altered pore pressures can influence the strength of rock specimens in accordance with the principle of effective stress. To determine whether chemical or mechanical effects of water saturation are dominant, one can perform tests on saturated and unsaturated specimens at various strain rates. Then, the strength can be plotted as a function of strain rate and, if the trend of the lines passing through the points of saturated and dry specimens are parallel, the primary effect of water saturation is said to be chemical (Olsson and Jones, 1980).

Saturated and dry compression tests have been run on specimens of Grouse Canyon Tuff and Calico Hills Tuff to determine the effects of water saturation on the compressive strength of the two tuffs. Saturated Grouse Canyon Tuff showed an average of 30% compressive strength decrease over air dried specimens (Price, 1983). The saturated

Calico Hills Tuff specimens showed a 23% decrease in compressive strength over air dried specimens (Tillerson and Nimick, 1984).

An increase in the strain rate will generally increase the compressive strength of a rock specimen. The strength variation with strain rate variation is most likely due to stress concentrations at the tips of internal flaws in the rock specimen. Slow strain rates allow local time dependent crack growth whereas fast strain rates precludes time dependent crack growth and gives higher compressive strengths (Franklin and Dusseault, 1989).

Tillerson and Nimick (1984) cite several studies on the effect of strain rate on the compressive strengths of tuffs from the Nevada Test Site. Data from these studies indicate that there is an average strength decrease of three to six percent for every factor of 10 decrease in strain rate. However, Price et. al. (1987) have stated that there is a general increase in strength with a decrease in strain rate with both saturated (4% ultimate strength increase per decade decrease in strain rate) and dry specimens (11% strength increase per decade decrease in strain rate) of Topopah Spring Tuff. Martin et. al. (1993) tested Topopah Spring Tuff at strain rates of 10^{-9} s^{-1} and compared their results to tests conducted by Price et. al. (1987), who tested the same tuff at strain rates of 10^{-7} to 10^{-3} s^{-1}, to determine the effect of strain rate on the moduli and effective strengths of saturated specimens. They found that

at strain rates between 10^{-9} s^{-1} and 10^{-5} s^{-1}, the strengths decreased with decreasing strain rate. At a strain rate of 10^{-3} s^{-1}, the strengths decreased from those tested at 10^{-5} s^{-1}. Martin et. al. (1993) attribute this strength anomaly to a build up of pore pressure which causes hydrofracturing and reduced strengths.

Studies have shown that an increase in strain rate (loading rate) increases the Young's Modulus of rock specimens (Judd, 1963 and Price et. al., 1987). However, specimens of tuff tested by Price et. al. (1987) have shown the opposite trend, a decrease in Young's Modulus with an increase in strain rate. Young's Modulus decreased 6% with a decrease in strain rate from 10^{-5} to 10^{-7} s^{-1}. Also, Nimick et. al. (1984) state that there is no definite trend in Young's Modulus for specimens of Topopah Spring Tuff tested at strain rates of 10^{-7} s^{-1}, 10^{-5} s^{-1}, and 10^{-7} s^{-1}.

Available Data of Mechanical Properties

Table 1 summarizes the total testing effort of Tiva Canyon Tuff, prior to this study. The lack of test data for the thermo - mechanical unit TCw has prompted the Reference Information Base (RIB), Version 4.4 (DOE, 1991) to recommend using the uniaxial compressive test results from thermo - mechanical unit TSw1 (Topopah Spring Member, alternating lithophysae - rich and lithophysae - poor, poorly welded, devitrified tuff) as representative for the TCw thermo - mechanical unit (Lin et. al, 1993).

Lin et. al. (1992) state that the mechanical properties of TCw should resemble the lithophysae - poor TSw2 more than the lithophysae - rich TSw1 because the description of the TCw in thermo - mechanical units figure (Figure 4) did not report any lithophysae in the Tiva Canyon

Table 1. Previous Test Data of Tiva Canyon Tuff (after Lin et. al., 1993; Price, 1983; and Olsson and Jones, 1980)

Confining Pressure	Strain Rate	Test Temperature	Number of Specimens	Compressive Strength
Unconfined	10^{-4} s^{-1}	Room Temperature	2	7.03 & 364 MPa (1020 & 53000 psi)
10 MPa (1450.3 psi)	10^{-4} s^{-1}	Room Temperature	1	406 MPa (59000 psi)
20 MPa (2900.6 psi)	10^{-4} s^{-1}	Room Temperature	1	895 MPa (130000 psi)
20.7 MPa (3002.1 psi)	10^{-4} s^{-1}	200° C	1	125.7 MPa (18300 psi)
TOTAL NUMBER OF TIVA CANYON TUFF SPECIMENS TESTED			5	

Member (Lin et. al., 1993). Therefore, Lin et. al. (1993) chose the uniaxial compressive strength of TSw2 as being representative of TCw. Table 2 gives the intact rock uniaxial compressive strength, elastic modulus and Poisson's ratio of the thermo - mechanical unit TCw and TSw1 and TSw2 for comparison. The values of Young's Modulus and Poisson's Ratio for the various thermo - mechanical units in Table 2 were derived from the RIB, Version 4.4 (Lin et. al., 1993).

Table 2. Intact Rock Uniaxial Compressive Strength and Elastic Modulus of TCw, TSw1, and TSw2 (after Lin et. al, 1993)

Thermo-mechanical Unit	Uniaxial Compressive Strength (MPa)	Elastic Modulus (GPa)
TCw	161 ± 63	19.9 ± 3.0
TSw1 (lithophysae-rich)	16 ± 5	15.5 ± 3.2
TSw2 (lithophysae-poor)	161 ± 63	21.7 ± 4.6

The Mohr-Coulomb strength properties of Tiva Canyon Tuff were investigated by Olsson and Jones (1980) and the Mohr - Coulomb strength properties for TCw were compiled by Lin et. al. (1993). The strength properties for TCw, TSw1, TSw2 thermo-mechanical units and the Tiva Canyon geologic unit are given in Table 3.

Table 3. Intact Rock Mohr-Coulomb Strength Properties (after Olsson and Jones*, 1980 and Lin et. al., 1993)

Thermo-mechanical or Geologic Unit	Cohesion (MPa)	Angle of Internal Friction
Tiva Canyon*	28.1	68
TCw	36	41
TSw1 (lithophysae-rich)	6	13
TSw2 (lithophysae-poor)	36	41

* For the densely welded upper part of this member, after Olsson and Jones (1980)

It should be noted that the information provided by Olsson and Jones (1980) refers to the densely welded caprock portion of the Tiva Canyon Member. Their testing was performed before the division of the geological stratigraphy into thermo - mechanical units.

Lin et. al. (1993) state that there is insufficient data for the TCw thermo-mechanical unit and that the triaxial testing results from the TSw2 thermo-mechanical unit were used as the Mohr-Coulomb strength properties for the thermo-mechanical unit TCw.

EXPERIMENTAL APPROACH

The experimental approach section deals with three topics: core sampling, experimental design, and test procedures. Test procedures is divided into three sub - sections: triaxial testing apparatus, P - Wave velocities, and saturation apparatus.

Core Sampling

The samples used in this study were obtained from a muckpile in front of the starter tunnel at Yucca Mountain. The muckpile contained rocks which were from the alcove excavation inside the starter tunnel, which is in the TCw thermo - mechanical unit. The samples were removed from the alcove by drill and blast methods and then excavated by mechanical excavators.

Specimens were cored from the muckpile samples of TCw using a thin-walled bit. The specimens were cored in two distinct orientations, parallel and perpendicular to the lithophysal cavities. The specimens were cored in this manner to investigate the anisotropy of the compressive strength and the Young's Modulus of the specimens. The orientation of the specimens with respect to the lithophysal cavity orientation is shown in Figure 7. Each specimen is represented by a

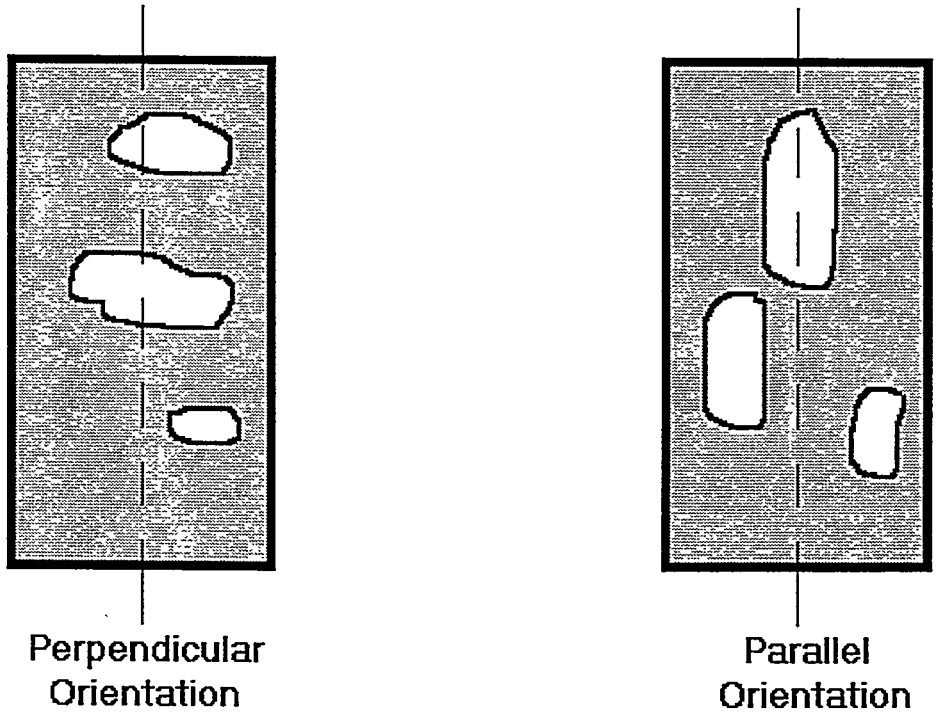

Figure 7. Orientation of Rock Specimens with Respect to the Orientation of the Lithophysal Cavities found in the Samples of TCw Tuff.

number, a letter, and an orientation notation. For example, 726B-PER indicates that the specimen was cored from sample 726, the core was the second one taken from the sample (indicated by the letter B), and the specimen was cored perpendicular to the lithophysal cavity orientation.

Once cored, the specimen ends were cut and ground to the specifications of ASTM D-4543. The specimens were then weighed and measured. Any large, visible lithophysal cavities on the surface of the specimens were filled with epoxy, and the specimens were re - weighed to determine the mass of epoxy used.

Experimental Design

The objective of this study is to investigate the effect of confining pressure, saturation, strain rate and anisotropy on the compressive strengths and Young's Moduli of tuff specimens from the thermo - mechanical unit TCw. Cylindrical specimens have been divided into three sets and tested in triaxial compression. Specimens in SET 1 were tested in an air dried condition under a constant nominal strain rate of 10^{-5} s^{-1} and at confining pressures of 0.1 MPa, 5 MPa, and 10 MPa. Specimens in SET 2 were tested in a saturated condition under a constant nominal strain rate of 10^{-5} s^{-1} and at confining pressures of 0.1 MPa, 5 MPa, and 10 MPa. Specimens in SET 3 were tested in an air dried condition under a constant nominal strain rate of 10^{-4} s^{-1} and at a confining pressure of

10 MPa. Table 4 contains the test conditions and the sample orientations of each set of specimens.

Table 4. Test Conditions of Each Set of Specimens

Test Conditions	SET 1	SET 2	SET 3
Confining Pressure (MPa)	0.1, 5, and 10	0.1, 5, and 10	10
Strain Rate	10^{-5} s^{-1}	10^{-5} s^{-1}	10^{-4} s^{-1}
Saturation Condition	air dried	saturated	air dried
Specimen Orientation	parallel and perpendicular	parallel and perpendicular	parallel and perpendicular

Tables 5 through 7 contain the number of specimens tested at each orientation and each confining pressure for SET 1, SET 2, and SET 3.

Table 5. SET 1 Confining Pressures, Specimen Orientation, and Number of Specimens Tested.

Confining Pressure	Specimen Orientation	Number of Specimens Tested
0.1 MPa (15 psi)	Perpendicular	5
	Parallel	5
5 MPa (725 psi)	Perpendicular	4
	Parallel	4
10 MPa (1450 psi)	Perpendicular	5
	Parallel	3

Table 6. SET 2 Confining Pressures, Specimen Orientation and Number of Specimens Tested.

Confining Pressure	Specimen Orientation	Number of Specimens Tested
0.1 MPa (15 psi)	Perpendicular	2
	Parallel	3
5 MPa (725 psi)	Perpendicular	2
	Parallel	4
10 MPa (1450 psi)	Perpendicular	2
	Parallel	3

Table 7. SET 3 Confining Pressures, Specimen Orientation and Number of Specimens Tested.

Confining Pressure	Specimen Orientation	Number of Specimens Tested
10 MPa (1450 psi)	Perpendicular	1
	Parallel	4

From these three sets of tests, observations of the effect of confining pressure, saturation, strain rate, and specimen orientation on the compressive strength and Young's Modulus for tuff specimens from the thermo - mechanical unit TCw are made. Also, the Mohr - Coulomb Strength Parameters are calculated from the test results from SET 1 and SET 2.

Test Procedures

Triaxial Testing Apparatus

The triaxial testing apparatus used for this study was a servocontrolled triaxial pressure apparatus. The apparatus can simultaneously measure the axial stress, axial and volumetric strains, pore fluid pressure, permeability, compressional wave velocity and the electrical resistivity of a 10- by 20-cm (4- by 8-inch) or a 2.125- by 4.25-inch (NX) sized right cylindrical test specimens during triaxial compression. The apparatus is capable of applying differential axial stresses of up to 585 MPa (85 000 psi) on NX-sized specimens. Confining and pore pressures up to 100 MPa (15 000 psi) can be applied by the apparatus.

The differential axial load is measured by a load cell connected in series with the load piston. Axial displacement is measured with a linear variable displacement transducer which is corrected for measured apparatus distortion. The volumetric strain is measured with a linear variable displacement transducer which is attached to the piston of a multiple-rate syringe pump used for confining pressure control. This value is also corrected for the measured apparatus volume change caused by the application of the axial load.

Voltage outputs from the confining pressure transducer, up- and downstream pore pressure transducers, the load transducer and the

linear variable displacement transducers from the axial displacement and the confining pressure pump are monitored, stored and printed with a microcomputer - based data acquisition system (Donath et. al., 1988). The data acquisition system, ROMTAS (ROck Mechanics Testing and Analysis System), was developed at the University of Nevada, Las Vegas. The outputs are also plotted on an x-y recorder. The microcomputer also provides closed-loop servocontrol of the axial strain rate, confining pressure and pore pressure (Donath et. al., 1988). The triaxial test assembly and loading ram are shown in Figure 8.

P - Wave Velocities

P - Waves, also known as compressional waves, can provide useful correlations to specimen properties such as Young's Modulus and porosity. The P - Wave velocity also provides an indication of deformation - induced microfracturing (Donath et. al, 1988). Housed in the triaxial testing apparatus (top specimen end cap) is a ceramic transducer which converts 0 - to 350 - volt electrical pulses from a puller unit to compressional (P - Waves) waves. These waves are sent through a specimen which is being tested in triaxial compression and then converted back into electrical pulses by another ceramic transducer (housed in the bottom specimen endcap). The electrical pulses are then sent to a receiver which is connected to an oscilloscope. The

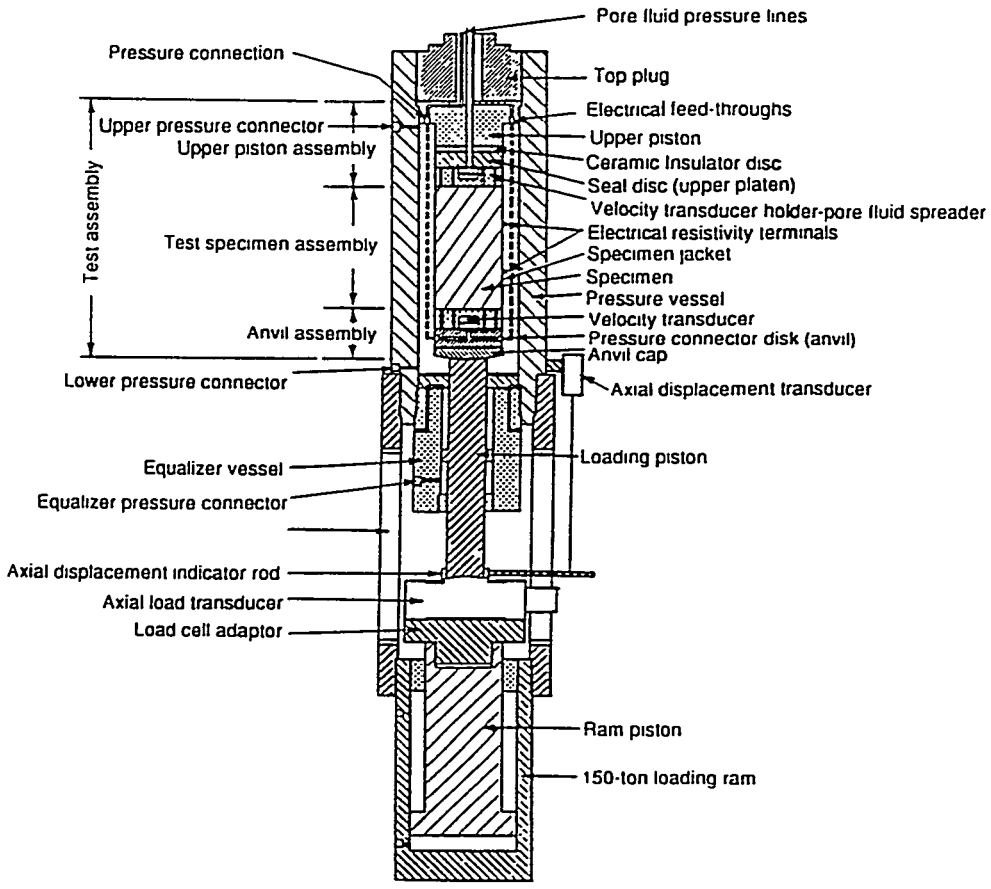

Figure 8. Triaxial Test Assembly and Loading Ram Used in the Triaxial Testing.

oscilloscope is used to read the apparent travel time of the P - Waves through the specimen. The apparent travel time is then corrected for the linear expansion of the triaxial system to obtain the actual velocity of the P - Wave.

Saturation Apparatus

The saturation apparatus consists of a pressure/vacuum chamber, capable of pressures up to 500 psi and a hand pump to produce the confining pressure. According to Boyd et. al. (1994), pressure saturation increases the degree of saturation and achieves saturation faster than vacuum saturation.

The specimens chosen to be saturated were dried for 48 hours at a temperature of 110 ± 5°C. The specimens were then put into the vacuum/pressure chamber and a vacuum was exerted across the specimens and de - ionized water for six hours. The chamber was then flooded with the de - aired de - ionized water and kept under 500 psi pressure for 96 hours (4 days). The specimens were kept submerged in water until testing.

RESULTS

From the triaxial tests, two strains (axial and volumetric) are measured throughout the test and the radial strain is calculated through the following relationship:

$$\frac{\Delta V}{V} = \epsilon_{axial} + 2\epsilon_{radial}$$

The three strains are then plotted against the differential axial stress on the same plot to obtain the specimen's stress - strain curves, as seen in Figure 9, which are typical stress - strain plots for the TCw specimens tested. The differential axial stress does not include the stress from the confining pressure. From the stress - strain curves, several observations can be made regarding the properties of the specimen tested.

- The axial stress - axial strain curve is linear from the start of the test, which indicates that there were few, if any, cracks, fractures, or pores in the rock which were closed by the application of the axial stress. Also, there does not appear to be any yielding at the end of the stress strain curve, which indicates a sudden, brittle failure of the specimen. The shape of this axial stress - axial strain curve is commonly called an elastic stress - strain curve.
- The axial stress - volumetric strain curve is linear throughout the

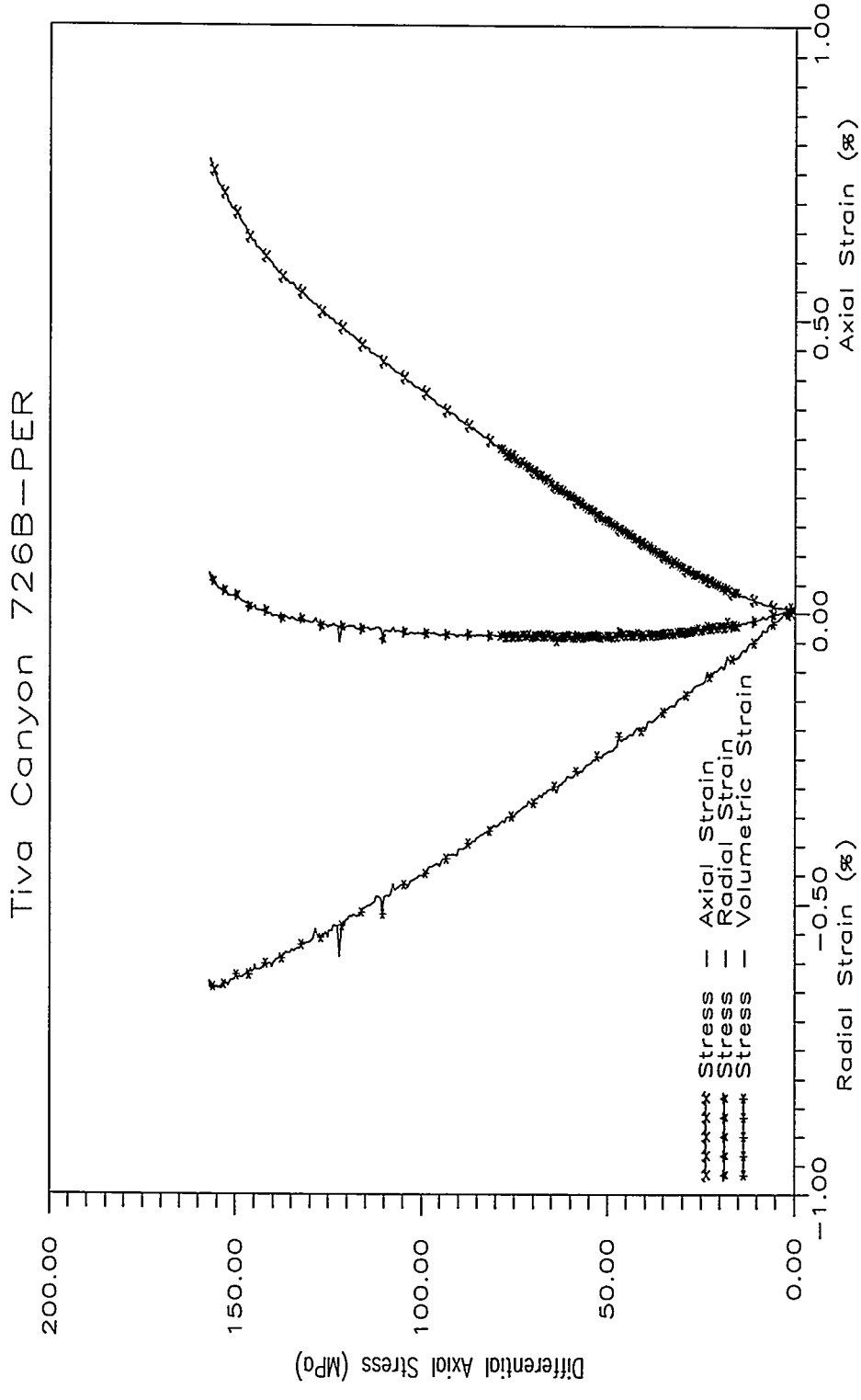

Figure 9. Typical Stress - Strain Curves from Triaxial Testing of TCw Tuff.

test. Figure 9 indicates that the specimen volume is decreasing linearly while the specimen is being loaded. It is interesting to note that near the end of the test, the specimen does not dilate or, increase in volume, because of the formation of microcracks throughout the specimen. This behavior is also indicative of a sudden, brittle failure.

- The axial stress - radial strain curve is linear, until the very late stages of the test. Figure 9 indicates that the specimen radius is increasing linearly throughout most of the test and near the end of the test, close to the onset of failure, the specimen radius begins decrease. Again, the abrupt ending of this curve indicates a sudden, brittle failure.

The term compressive strength, which is used throughout this study, is the ultimate strength because each specimen was loaded to failure. Failure of the specimens was taken as the point of maximum load, after which the specimen lost the ability to hold the maximum load. Young's Modulus was calculated by a least squares fit between ten and fifty percent of the maximum compressive strength. This is the standard method of determining Young's Modulus for tuffaceous rock specimens from Yucca Mountain (Price et. al., 1994). The P-wave velocities used for this study are an average of the velocity readings between ten and fifty percent of the maximum compressive strength. The porosity value is a matrix porosity which has been calculated as follows:

Pore Volume: $$V_v = \frac{M_{sat} - M_{dry}}{\rho_{water}}$$

Sample Volume: $$V_{sample} = Length * \frac{\pi\,(Diameter)^2}{4}$$

Porosity: $$n = \frac{V_v}{V_{sample}}$$

(Brown, 1981)

The test results for this study are presented in tabular form in Tables 8 through 10. Table 8 gives the test results for SET 1, Table 9 gives the test results for SET 2, and Table 10 gives the test results for SET 3. Porosities were not determined for SET 1 and SET 3 because of the possibility of a reduced strength from saturation and re - drying. P - Wave velocities were not determined for the samples in SET 3 because apparatus control took too much operator time to try to read the apparent P - Wave velocities during the test.

Table 8. SET 1 Test Results.

Confining Pressure	Specimen - Orientation	Compressive Strength (MPa)	Young's Modulus (GPa)	Axial Strain at Failure (%)	P-Wave Velocity (km/sec)
10 MPa	726B - PER	157.10	25.05	0.773	4.241
	729D - PER	220.8	25.03	0.958	4.141
	729E - PER	159.04	27.70	0.567	4.222
	736A - PER	126.7	22.00	0.704	4.196
	730D - PER	114.68	22.80	0.555	4.145
	728B - PAR	203.52	25.00	0.865	4.133
	737B - PAR	97.60	28.03	0.406	4.175
	736B - PAR	157.44	21.21	0.804	
5 MPa	726A - PER	129.20	26.10	0.538	4.225
	729C - PER	145.14	21.80	0.738	4.182
	747B - PER	95.30	20.30	0.602	4.038
	746A - PER	134.90	26.20	0.600	
	730C - PAR	159.80	24.47	0.656	4.236
	742C - PAR	83.78	20.95	0.525	
	742A - PAR	87.69	18.38	0.579	
	734D - PAR	140.30	18.72	0.851	
0.1 MPa	734B - PER	77.50	29.00	0.352	
	739A - PER	104.00	31.60	0.397	4.354
	743B - PER	72.30	25.80	0.367	3.863
	749E - PER	95.40	24.70	0.466	4.246
	750E - PER	69.80	21.50	0.370	3.864
	729H - PAR	116.30	28.03	0.475	
	730A - PAR	47.02	16.93	0.435	
	730B - PAR	68.72	22.36	0.376	4.157
	750C - PAR	71.41	15.39	0.600	
	750A - PAR	108.93	18.83	0.652	3.722

Table 9. SET 2 Test Results.

Confining Pressure	Specimen - Orientation	Compressive Strength (MPa)	Young's Modulus (GPa)	Axial Strain at Failure (%)	P - Wave Vel. (km/s)	Porosity (%)
10 MPa	747A-PER	140.54	15.65	0.899	4.325	13.3
	741A-PER	132.12	15.60	0.873	4.433	9.7
	749B-PAR	168.36	15.27	1.042	4.280	14.5
	735C-PAR	125.17	13.73	0.893	4.168	16.2
	729G-PAR	208.30	17.13	1.181	4.395	12.3
5 MPa	726C-PER	135.44	15.00	0.908	4.251	13.0
	750G-PER	42.41	6.88	0.862		18.2
	750D-PAR	129.47	14.61	0.877	4.304	12.9
	727C-PAR	107.63	13.00	0.866	4.336	14.9
	731A-PAR	106.79	13.80	0.775	4.262	15.1
	750B-PAR	90.22	11.02	0.853	4.331	15.1
0.1 MPa	747C-PER	73.25	12.23	0.622	4.364	13.4
	730E-PER	53.63	10.61	0.511	4.252	15.3
	749C-PAR	65.10	8.15	0.778	4.093	15.2
	742B-PAR	57.02	12.00	0.508	4.114	17.7
	750K-PAR	110.96	13.33	0.842	4.303	14.2

Table 10. SET 3 Test Results.

Confining Pressure	Specimen - Orientation	Compressive Strength (MPa)	Young's Modulus (GPa)	Axial Strain at Failure (%)
10 MPa	727A - PER	153.1	13.84	1.095
	726D - PAR	224.8	16.00	1.359
	729F - PAR	183.3	21.61	0.920
	738B - PAR	190.3	21.40	0.972
	746C - PAR	152.7	22.91	0.608

DISCUSSION OF RESULTS

This section presents five major topics. First, the effect of test conditions, namely, confining pressure, saturation, and strain rate, on the compressive strengths and Young's Moduli of the specimens is discussed. Next, the effect of anisotropy and porosity on the compressive strengths and Young's Modulus values is presented. Then, the Mohr - Coulomb strength parameters are calculated for SET 1 and SET 2 specimens. Finally, the results from this study are compared with results from previous studies.

Effects of Test Conditions

Confining Pressure

As stated earlier, an increase in confining pressure tends to increase the compressive strength of rock specimens. This statement is true for the TCw specimens tested for this study. Figure 10 shows a plot of all of the compressive strength data from SET 1 as a function of confining pressure. This plot shows there is large variation of compressive strengths at each confining pressure. At a confining pressure of 0.1 MPa, the compressive strengths range from a low of 47.02 MPa to a high of 116.30 MPa, a difference of 60%. At a confining pressure of 5

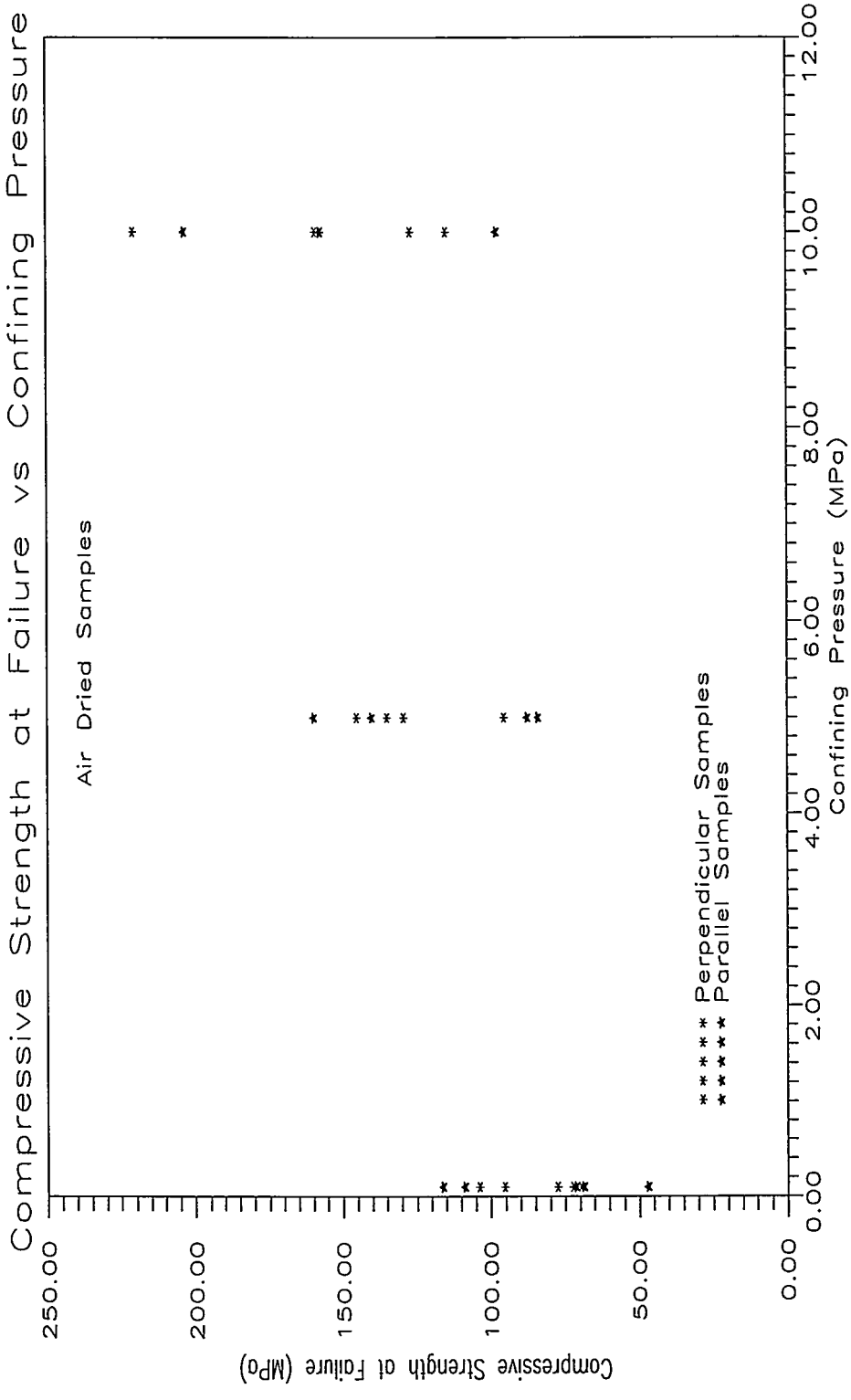

Figure 10. Compressive Strength as a Function of Confining Pressure, SET 1.

MPa, the compressive strengths range from 83.78 MPa to 159.80 MPa, a difference of 48%. At the highest confining pressure, 10 MPa, the compressive strengths range from a high of 220.80 MPa to a low of 97.6 MPa, a difference of 56%. Figure 10 also indicates that there is some overlap in the compressive strength data. That is, a specimen whose compressive strength was determined to be 110 MPa, could have been tested at any one of the three confining pressures. Thus, confining pressure is not a good indicator of compressive strength. There appears to be a general trend of an increase in compressive strength with an increase in confining pressure for SET 1, as seen in Figure 10. With such large variations in data, it may be advantageous to plot the average compressive strengths as a function of confining pressure to help notice any trends. Such a plot is shown in Figure 11.

From Figure 11, it is easy to see the trend of increasing compressive strength with increasing confining pressure. For the perpendicular specimens, increasing the confining pressure 50 times (0.1 MPa to 5 MPa) increased the average compressive strength 1.5 times (82.80 MPa to 126.14 MPa). For the parallel specimens, the same increase in confining pressure produced an average increase in compressive strength of 1.43 times (82.48 MPa to 117.89 MPa). Increasing the confining pressure 100 times (0.1 MPa to 10 MPa) increased the average compressive strength in the perpendicular specimens by 1.86 times

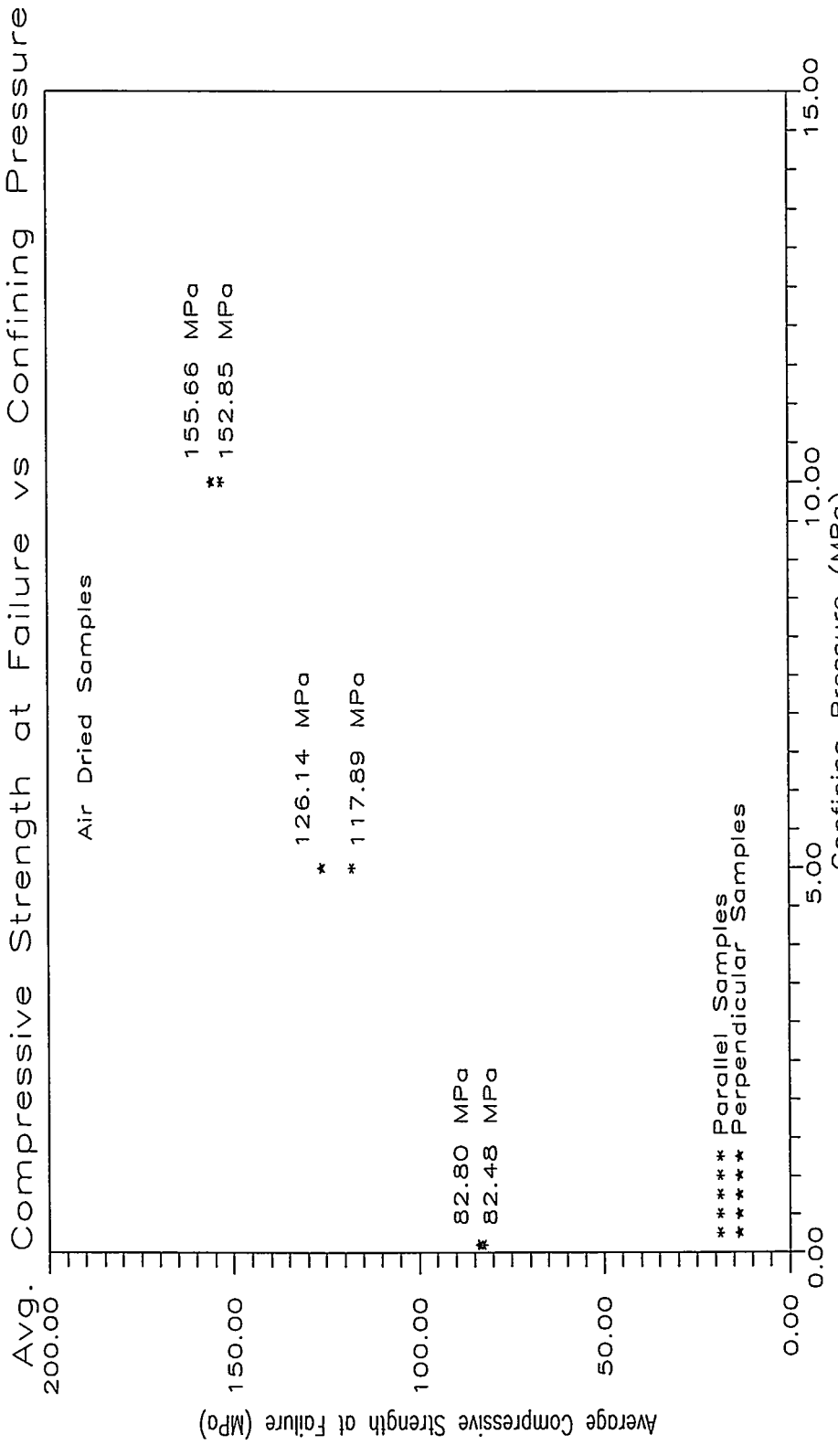

Figure 11. Average Compressive Strength as a Function of Confining Pressure, SET 1.

(126.14 MPa to 155.66 MPa). The corresponding increase for the parallel specimens was 1.85 times (117.89 MPa to 152.85 MPa). It is interesting to note that the average compressive strengths of the perpendicular specimens and the parallel specimens are approximately the same but in each case, the perpendicular specimens have slightly larger average compressive strengths.

Figure 12 shows a plot of the Young's Modulus of SET 1 as a function of confining pressure. As with the compressive strength data, there is a large scatter among the Young's Modulus data at each confining pressure. At 0.1 MPa confining pressure, the modulus values range from 15.39 GPa to 31.6 GPa, a 51% difference. At a confining pressure of 5 MPa, the modulus values range from 18.38 GPa to 26.20 GPa, a 30% difference. At a confining pressure of 10 MPa, the modulus values range from 21.21 GPa to 28.03 GPa, a 24% difference. There is also an overlap in the Young's Modulus data. A specimen with a modulus value of 25 GPa could have been tested at any of the three confining pressures. Thus, confining pressure is not a good indication of modulus values. It also appears that the increase in confining pressure tends to reduce the variability or scatter of the data. With scattered data such as this, it may be advantageous to plot only the average values of Young's Modulus for both specimen orientations as a function of confining pressure. Such a plot is shown in Figure 13.

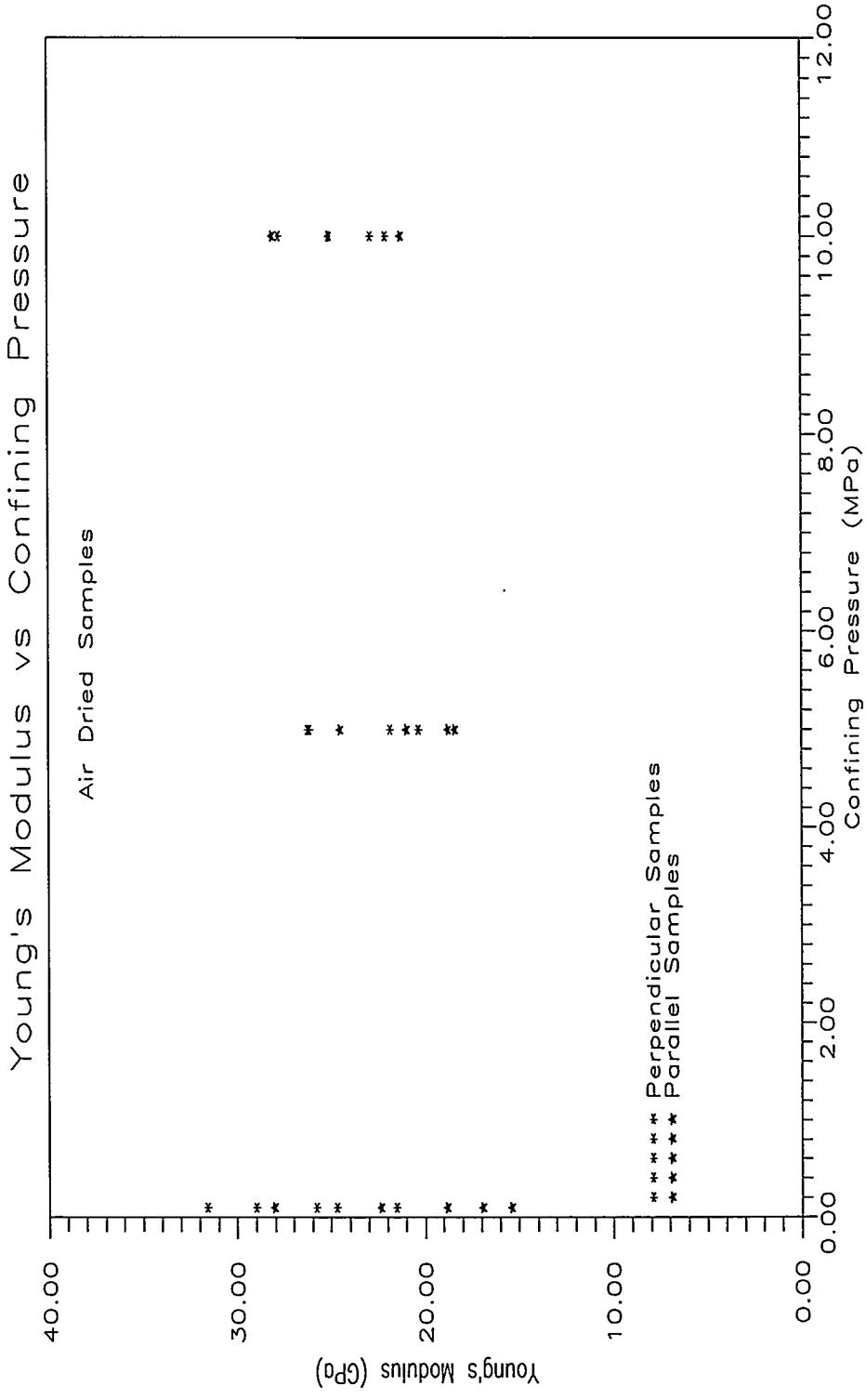

Figure 12. Young's Modulus as a Function of Confining Pressure, SET 1.

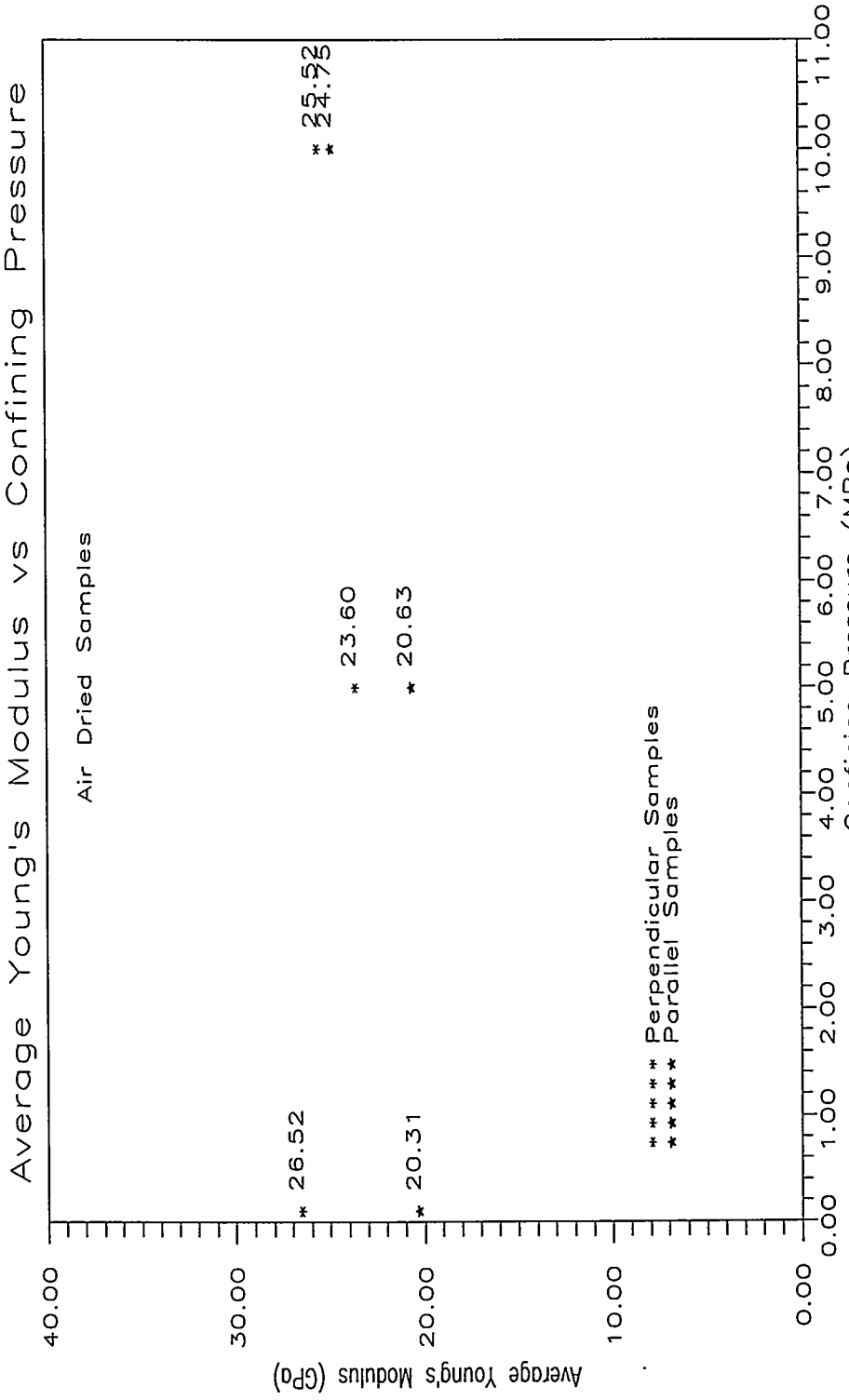

Figure 13. Average Young's Modulus as a Function of Confining Pressure, SET 1.

Figure 13 shows that confining pressure does not seem to influence the average Young's Modulus for the perpendicular specimens. At a confining pressure of 0.1 MPa, the average modulus value for the perpendicular specimens is 26.52 GPa. Increasing the confining pressure to 5 MPa and then to 10 MPa did not affect the average modulus values for the perpendicular specimens. However, the modulus values for the parallel specimens showed an increase with an increase in confining pressure. The modulus values increased from 20.31 GPa to 20.63 GPa to 24.75 GPa with an increase in confining pressure from 0.1 MPa to 5 MPa to 10 MPa. Figure 13 shows that there is a difference between the parallel and perpendicular specimens. The average modulus for the parallel specimens seems to be affected by an increase in confining pressure whereas the confining pressure increase seem to have no effect on the average modulus values of the perpendicular specimens. The effect of confining pressure on the average Young's Modulus may be explained in one of two ways: apparatus/measurement error, or Young's Modulus anisotropy within the TCw thermo - mechanical unit. The explanation is more suited to a discussion on anisotropy, and will be discussed later.

Saturation

In all previous studies performed on dry and saturated tuffs from the

Nevada Test Site, saturation has decreased the compressive strength of the specimens tested (Price, 1983 and Tillerson and Nimick, 1984). No researcher has indicated a change in Young's Modulus with a change in saturation condition.

The average compressive strengths of SET 1 and SET 2 are plotted in Figure 14. The figure shows, that in general, the average strengths of saturated specimens are lower than those of air dried specimens. However, the specimens with the largest average compressive strengths are **saturated** specimens which were cored parallel to the lithophysal cavities and tested at a confining pressure of 10 MPa. At all three confining pressures, there is not a large variation in the strengths. At a confining pressure of 0.1 MPa, the largest average compressive strength is 83.80 MPa (air dried, perpendicular specimens) and the lowest average compressive strength is 63.44 MPa (saturated, perpendicular specimens). This corresponds to a 24.3% strength reduction. At a confining pressure of 5 MPa, the largest average compressive strength is 126.13 MPa (air dried, perpendicular specimens) and the lowest average compressive strength is 88.93 MPa (saturated, perpendicular specimens). This corresponds to a 29.5% decrease in strength. At a confining pressure of 10 MPa, the largest average compressive strength is 167.28 MPa (**saturated**, parallel specimens) and the lowest average compressive strength is 136.33 MPa (saturated, perpendicular specimens). This

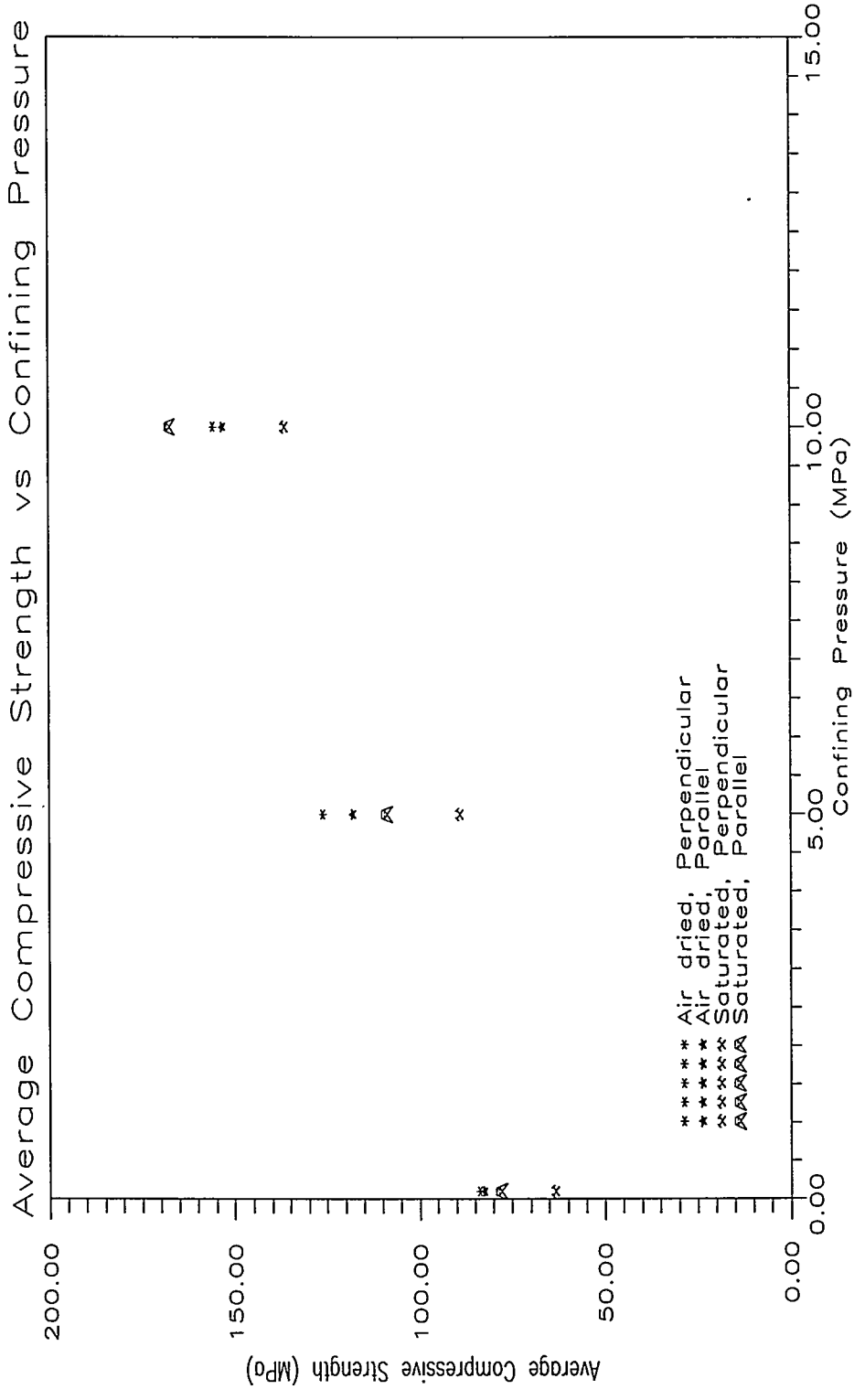

Figure 14. Average Compressive Strength as a Function of Confining Pressure, SET 1 and SET 2.

shows that specimen variability is very high and average values can be very misleading. However, it is interesting to note that the saturated perpendicular specimens consistently had the lowest average compressive strengths. Generally, specimen strength is slightly reduced by saturation, but, due to high specimen variability, the data is inconclusive.

Unlike the compressive strength data, the Young's Modulus values vary between the air dried and saturated specimens. The average Young's Modulus data from SET 1 and SET 2 is averaged and plotted against confining pressure in Figure 15. Figure 15 shows that the saturated specimens have lower average Young's Modulus values. At high confining pressures, the average Young's Moduli decrease from approximately 24.5 GPa (air dried specimens) to approximately 15.4 GPa (saturated specimens), a 37% decrease in average Young's Modulus values. At a confining pressure of 5 MPa, the average Young's Modulus values for the perpendicular specimens decreased approximately 59%. The average Young's Modulus for the parallel specimens at the same confining pressure decreased approximately 37%. At a confining pressure of 0.1 MPa, the average Young's Modulus values for the perpendicular specimens decreased approximately 57%. The average Young's Modulus values for the parallel specimens at the same confining pressure decreased approximately 45%.

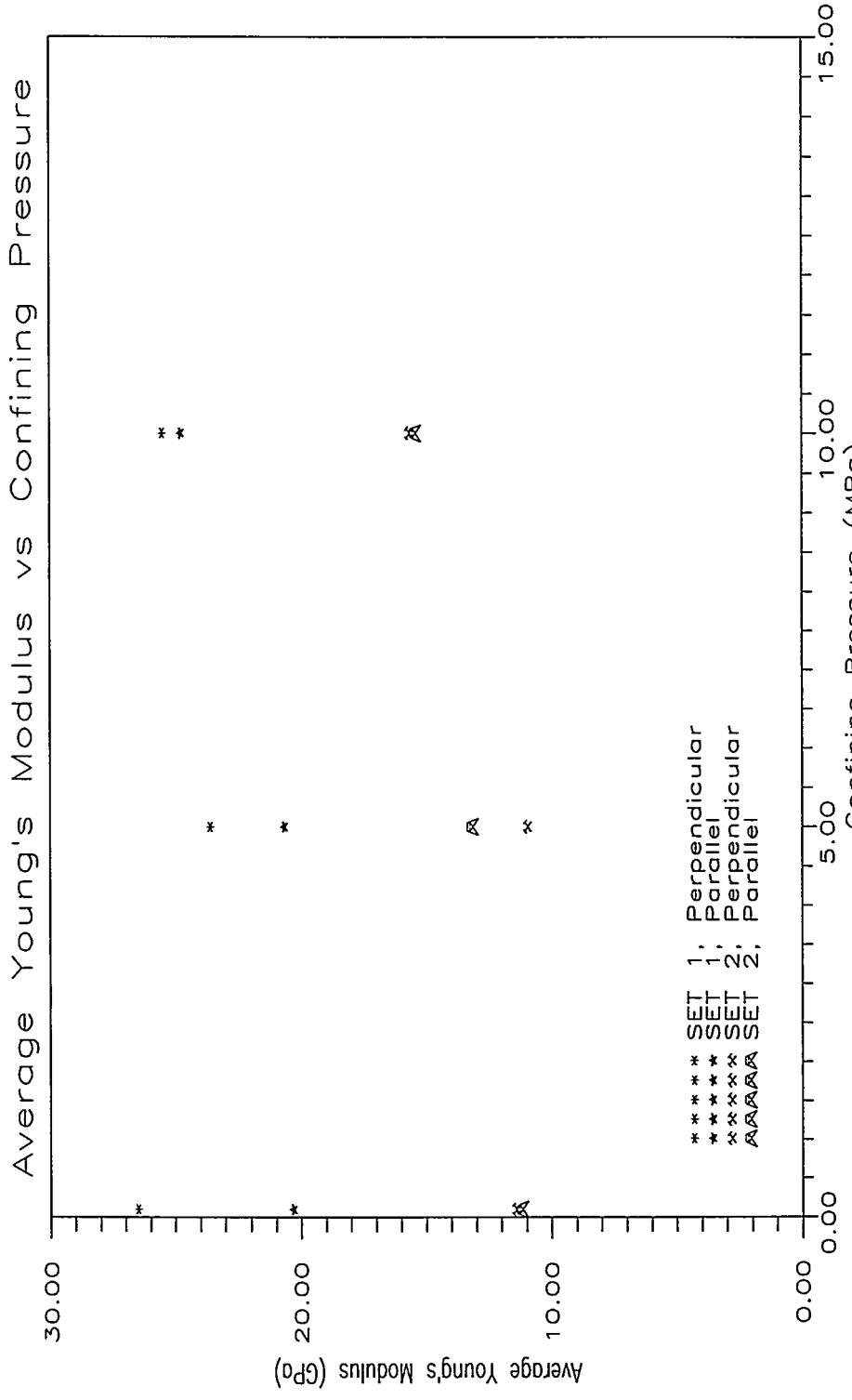

Figure 15. Average Young's Modulus as a Function of Confining Pressure, SET 1 and SET 2.

It appears that the saturated specimens do not exhibit the Young's Modulus anisotropy which is exhibited by the air dried specimens. It is obvious that saturation of specimens from the thermo - mechanical unit TCw causes the specimens to become less "stiff", but the strength is not greatly reduced.

Strain Rate

The strain rate effects on the strength and Young's Modulus of tuffs from the Nevada Test Site have been studied by Price et. al., 1986; Martin et. al., 1993; and Tillerson and Nimick, 1984. Their findings indicated that an increase in strain rate will increase both the compressive strengths and Young's Moduli of the tuffs.

The average compressive strength and average modulus values for SET 1 and SET 3 specimens are shown in Table 11. As expected, an increase in strain rate from 10^{-5} s^{-1} to 10^{-4} s^{-1} increased the strength of air dried TCw specimens. As shown in Table 11, the average compressive strength increased from 154.3 MPa (strain rate of 10^{-5} s^{-1}) to 180.8 MPa (strain rate of 10^{-4} s^{-1}). This is a 14.7% increase in

Table 11. Average Compressive Strength and Moduli Comparison Between SET 1 and SET 3.

SET	STRAIN RATE	AVERAGE COMPRESSIVE STRENGTH (MPa)	AVERAGE YOUNG'S MODULI (GPa)
SET 1	10^{-5} s^{-1}	154.26	24.64
SET 3	10^{-4} s^{-1}	184.84	19.15

average compressive strength.

Table 11 also compares the average Young's Modulus values from SET 1 specimens tested under a confining pressure of 10 MPa with the average Young's Modulus values from SET 3. Surprisingly, the average Young's Moduli for the specimens tested at the higher strain rate showed a 28.63% decrease over the specimens tested at the slower strain rate (19.2 GPa compared to 24.6 GPa). Obviously, there is a great deal of specimen variability since the specimens do not respond as expected to the increase in strain rate. The decrease in Young's Moduli with an increase in strain rate may also be attributed to sample damage from excavation. However, Price (1986) observed the same trend with specimens of Topopah Spring Tuff tested at different strain rates.

Anisotropy

Triaxial testing of air dried specimens from the thermo - mechanical unit TCw, cored in two distinct orientations: perpendicular and parallel

to lithophysal cavities (Figure 7), was performed to observe any anisotropies. The average compressive strengths from SET 1 and their respective confining pressures are plotted in Figure 11. Referring back to this figure, as expected, an increase in strength occurs with an increase in confining pressure. However, this figure indicates that there is no observable compressive strength difference between the parallel and perpendicularly cored specimens. This implies that there is no strength anisotropy for our TCw specimens.

Referring back to Figure 13, the average Young's Modulus from SET 1 plotted as a function of confining pressure shows that there is a distinct difference between the average Young's Modulus for the parallel and perpendicular orientated specimens. This difference may be explained by either a modulus (stiffness) anisotropy or an experimental problem measuring the axial strain of specimens during deformation.

Since there are two possible explanations to the stiffness anisotropy question, an investigation was undertaken to determine if there may be a stiffness anisotropy. A background search discovered that Olsson and Jones (1980) claim that welded tuff is stiffest perpendicular to bedding. Also, Martin et. al. (1992) claim that Topopah Spring Tuff is stiffest parallel to bedding. Obviously, there is some merit in exploring the possibility that there is a stiffness anisotropy.

Martin et. al. (1992) tried to correlate the P - Wave velocities to the

Young's Modulus values. They have also showed that there is an increase in P - Wave velocity with an increase in Young's Modulus for tuffs from the Nevada Test Site. If there is a stiffness anisotropy, the P Wave velocity should be greater in the direction of greater stiffness. Figure 16 shows a plot of the P - Wave velocity as a function of Young's Modulus from SET 1 specimens tested at a confining pressure of 0.1 MPa. It is clear that there is a trend in the data of increasing P wave velocity with an increase in Young's Modulus. On average, the perpendicular specimens have a higher P - Wave velocity than do their parallel counterparts. The perpendicular specimens have an average P Wave velocity of 4.082 km/sec whereas the parallel specimens have an average P - Wave velocity of 3.940 km/sec, a 3.5% difference.

Plotting the P - Wave velocities as a function of confining pressure for the specimens from SET 1 tested under a confining pressure of 10 MPa, the average P - Wave velocities for the two sets of specimens, perpendicular and parallel, should be approximately the same since their Young's Modulus values are approximately the same. The P - Wave velocities from SET 1 tested under a confining pressure of 10 MPa are plotted as a function of Young's Modulus in Figure 17. This figure shows that the data points are clustered around a small area, as expected. The average P - Wave velocity for the perpendicular specimens from SET 1 tested under a confining pressure of 10 MPa is

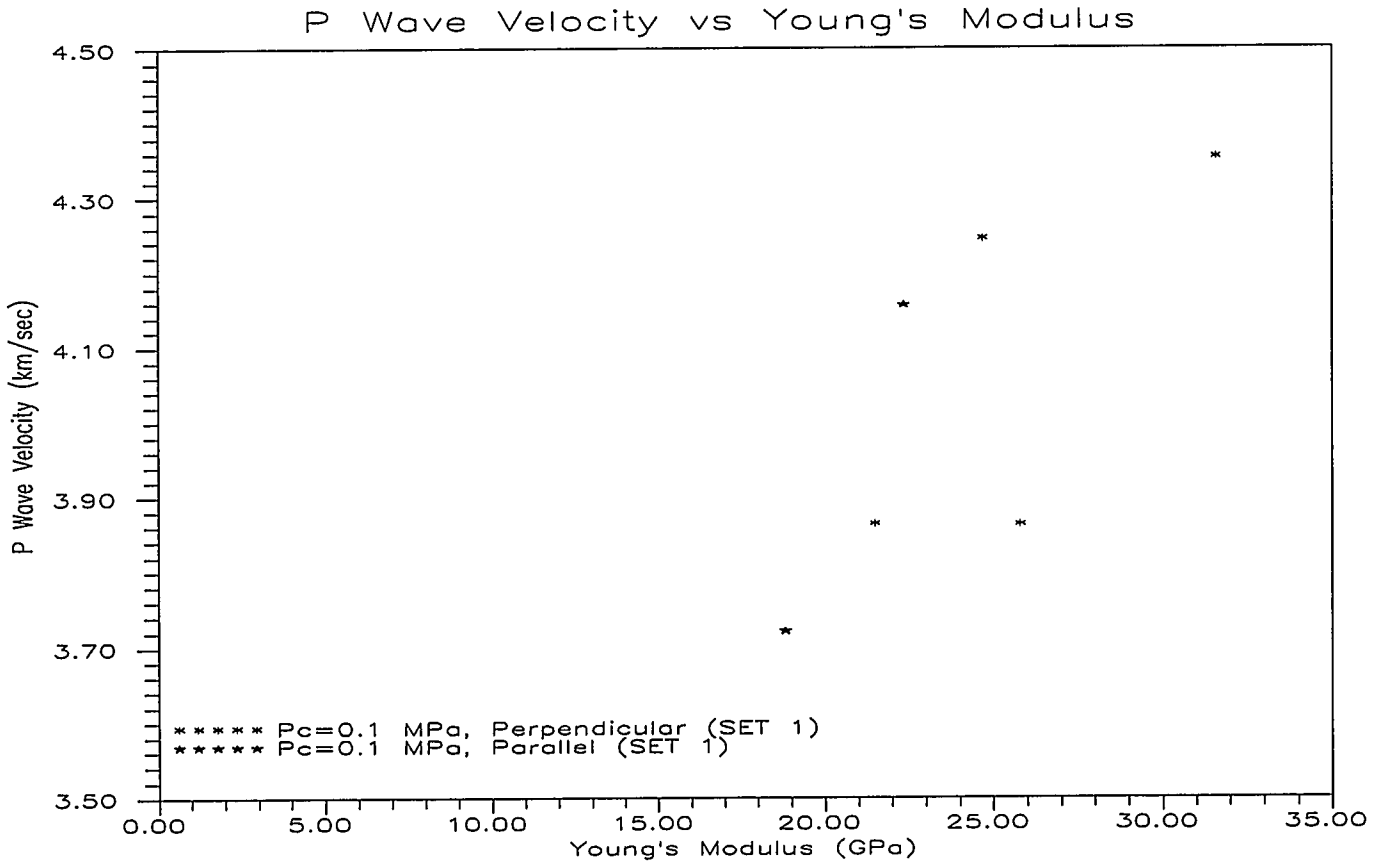

Figure 16. P - Wave Velocity as a Function of Young's Modulus, SET 1 (Specimens Tested at a Confining Pressure of 0.1 MPa).

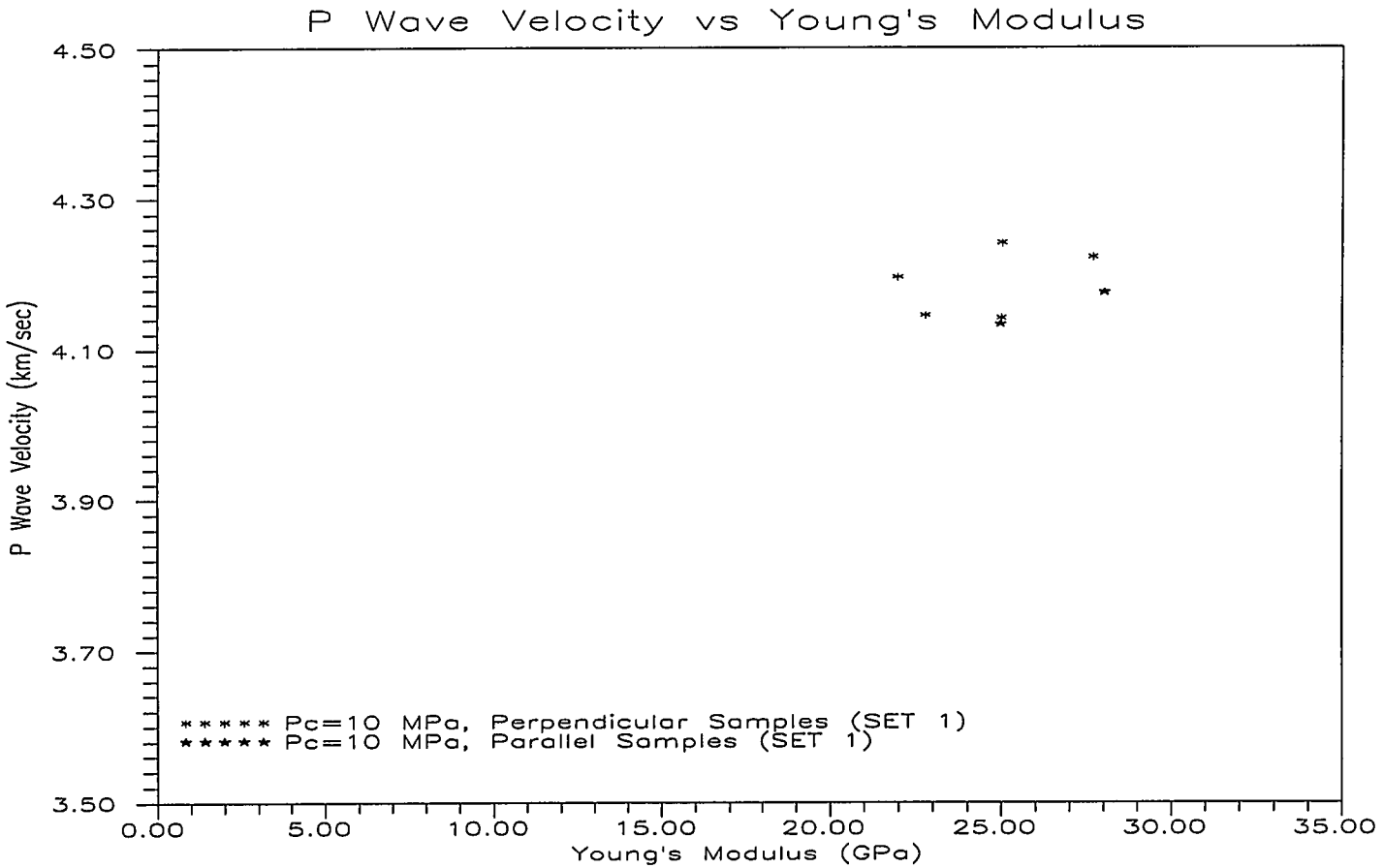

Figure 17. P - Wave Velocity as a Function of Young's Modulus, SET 1 (Specimens Tested at a Confining Pressure of 10 MPa).

4.189 km/sec. The average P - Wave velocity for the parallel specimens from SET 1 tested under the same confining pressure is 4.154 km/sec. The P - Wave velocities of the specimens tested under a confining pressure of 10 MPa are greater than those tested under a confining pressure of 0.1 MPa. This may be due to the increase in Young's Modulus and/or the pressure dependency of the P - Wave velocities. It is a well known fact that the P - Wave velocity is pressure dependent (Carmichael, 1989). Thus, according to the P - Wave velocities, there is a stiffness anisotropy in the TCw specimens which were tested. The specimens are stiffest perpendicular to bedding, or, in the vertical direction.

Another way to investigate a stiffness anisotropy is to look at the stress - strain curves. Since there are many stress strain - curves, and basically, they are all the same: nearly linear until failure where the stress - strain curve drops suddenly, one can look at the end points of the stress - strain curves and see if there is a difference between specimens cut parallel and perpendicular to the lithophysal cavities. Figures 18 and 19 plot an average end point of the stress - strain curves for the three confining pressures from the specimens in SET 1. Around the average end points is a box which defines one standard deviation of the average stress and average strain at each confining pressure. Comparing the two figures, the stress component of each end point is

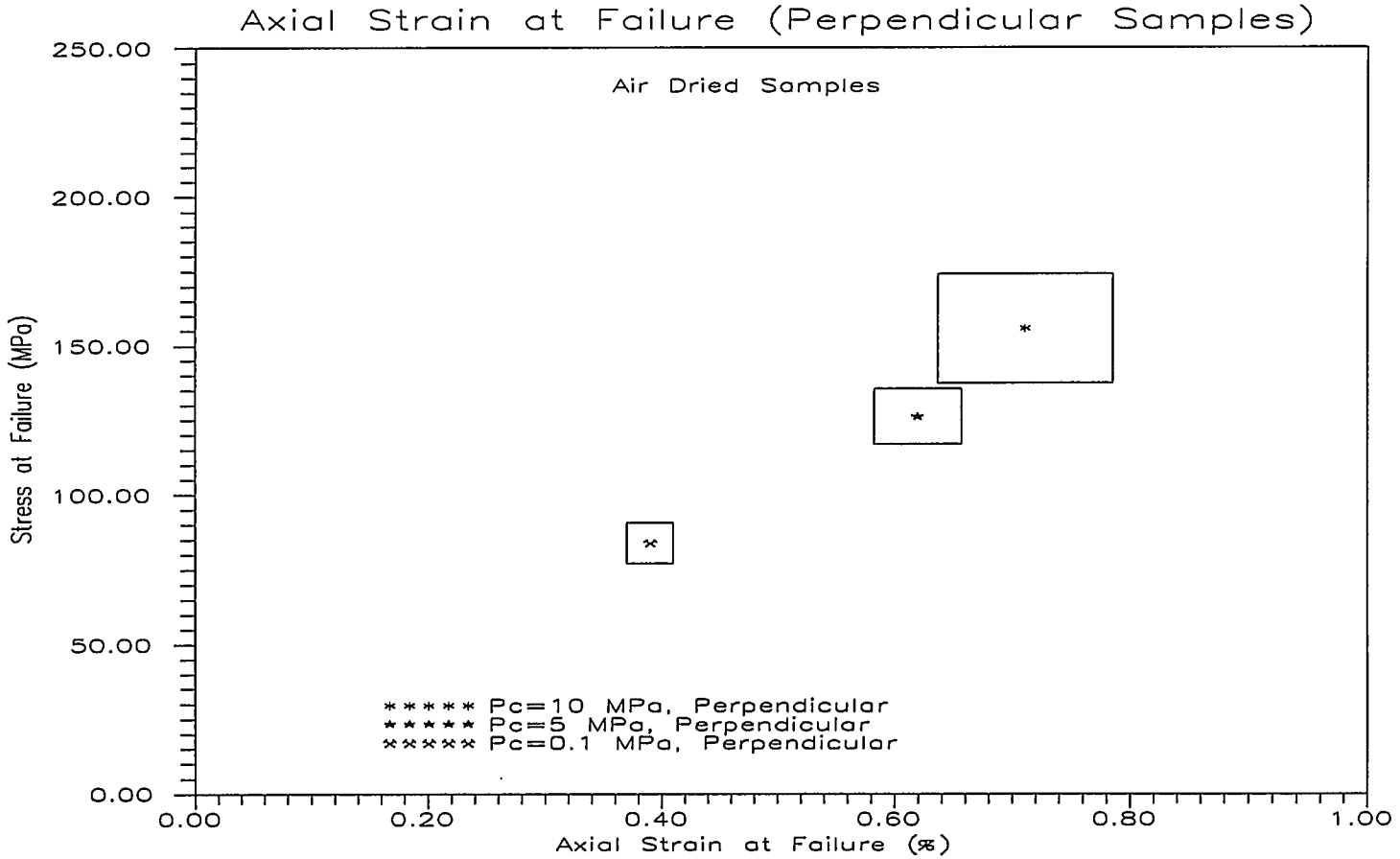

Figure 18. Average Compressive Strength and Axial Strain at Failure and Box Defining One Standard Deviation of Compressive Strength and Axial Strain at Failure, SET 1 (Perpendicular Orientation).

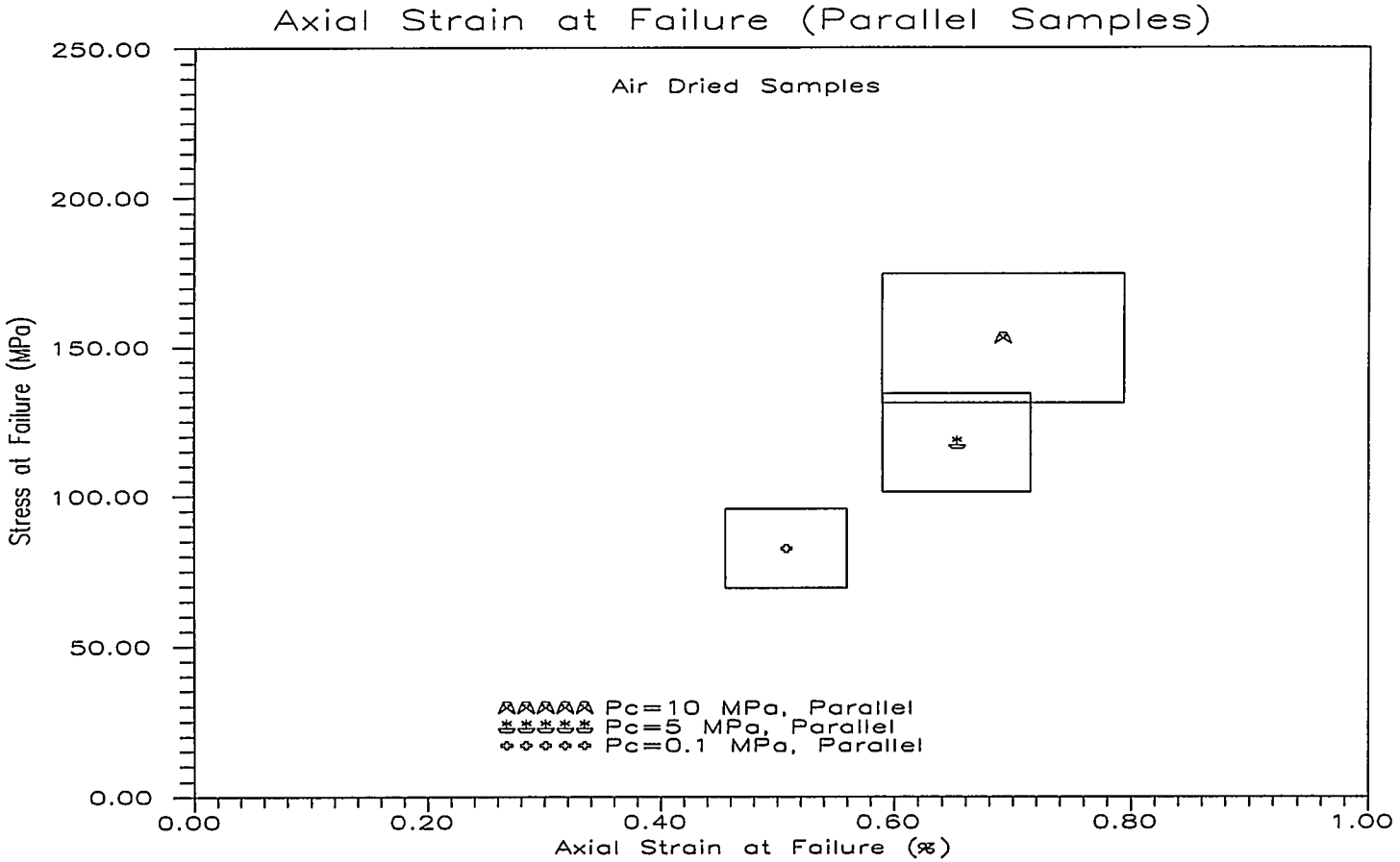

Figure 19. Average Compressive Strength and Axial Strain at Failure and Box Defining One Standard Deviation of Compressive Strength and Axial Strain at Failure, SET 1 (Parallel Orientation).

nearly the same for each confining pressure, which indicates that there is no strength anisotropy. However, the axial strain component of the end points for the parallel specimens is shifted to the right at lower confining pressures. At higher confining pressures, the boxes nearly overlap each other. Obviously, the parallel specimens experience more axial strain at failure but experience the same stress at failure as the perpendicular specimens. Reviewing the Young's Modulus calculation, which is stress divided by strain, for the parallel specimens, which strain more than the perpendicular specimens, the calculated Young's Modulus will be less than the value calculated for the perpendicular specimens. However, at high confining pressures (10 MPa) there does not seem to be an anisotropy because the specimens experience the same amount of stress and axial strain at failure. Thus, according to the stress - strain curves of the specimens tested, there is a stiffness anisotropy in the TCw specimens tested. The specimens are stiffest perpendicular to bedding, or, in the vertical direction.

Porosity

As stated earlier, there have been numerous attempts to correlate rock properties from the tuffs at the Nevada Test Site to their porosities. This section will describe the effect of porosity on the compressive strength and Young's Modulus of saturated TCw specimens. The

porosity values given in this study are volume fraction porosities which were derived from the difference in saturated and dried specimen weights.

Recent studies (Price et. al., 1993 and Martin et. al., 1994) have shown that, in general, an increase in porosity will decrease the compressive strength of tuffaceous specimens from the Nevada Test Site. This is true for the specimens of TCw tested for this study. The porosity and compressive strength data from SET 2 is plotted in Figure 20. As one would expect, there is a general trend indicating a drop in compressive strength with an increase in porosity. The porosity values ranged from approximately 10% to approximately 18%. Within this range of porosities, the maximum compressive strengths ranged from a high of 208.3 MPa to a low of 42.41 MPa. The lowest strength corresponds to the specimen which had the highest porosity.

Figure 20 is also useful in explaining the effect of confining pressure on compressive strength. Two specimens, both with porosities of approximately 15% had compressive strengths of approximately 98 MPa when tested at confining pressures of 5 MPa, whereas two specimens, with porosities of approximately 15%, tested at a confining pressure of 0.1 MPa had maximum compressive strengths of approximately 59 MPa. This is an increase of approximately 40% with an increase in confining pressure of 4900% increase.

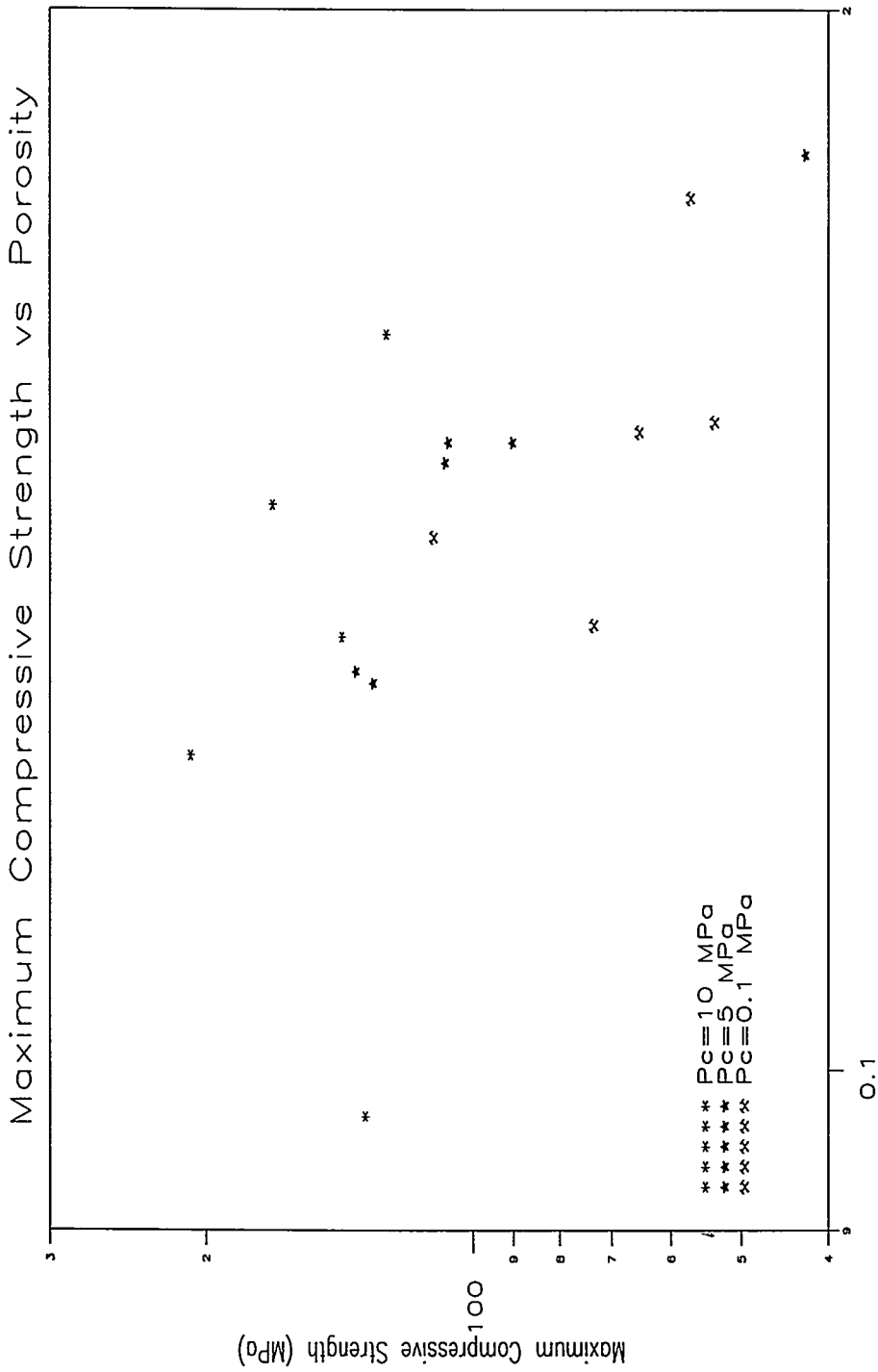

Figure 20. Compressive Strength as a Function of Porosity, SET 2.

An increase in porosity is expected to decrease the Young's Modulus of a rock specimen. This has been shown by Price et. al., 1993 and Martin et. al., 1994 and has been found to be true with the TCw specimens tested for this study. The general trend of the Young's Modulus data from SET 2, when plotted as a function of porosity, such as in Figure 21, is a decrease in Young's Modulus with an increase in porosity. The porosity values ranged from approximately 10% up to approximately 18%. Within this range of porosities, the Young's Modulus values ranged from a high of 17.3 GPa to a low of 6.88 GPa. The lowest modulus value corresponds to the specimen which had the highest porosity.

Mohr - Coulomb Strength Parameters

The classical method of determining the Mohr - Coulomb strength parameters is to draw semi - circles defined by pairs of major and minor principal stresses at failure in τ - σ space. The semi - circles corresponding to failure are joined by a tangent curve or Mohr envelope which defines the upper limit of all possible non - failure states of stress. The straight line version of this envelope is the Mohr - Coulomb strength criterion (Franklin and Dusseault, 1989). The slope of the straight line envelope is ϕ, the angle of internal friction, and the intersection of the envelope with the τ axis is the cohesion of the specimen.

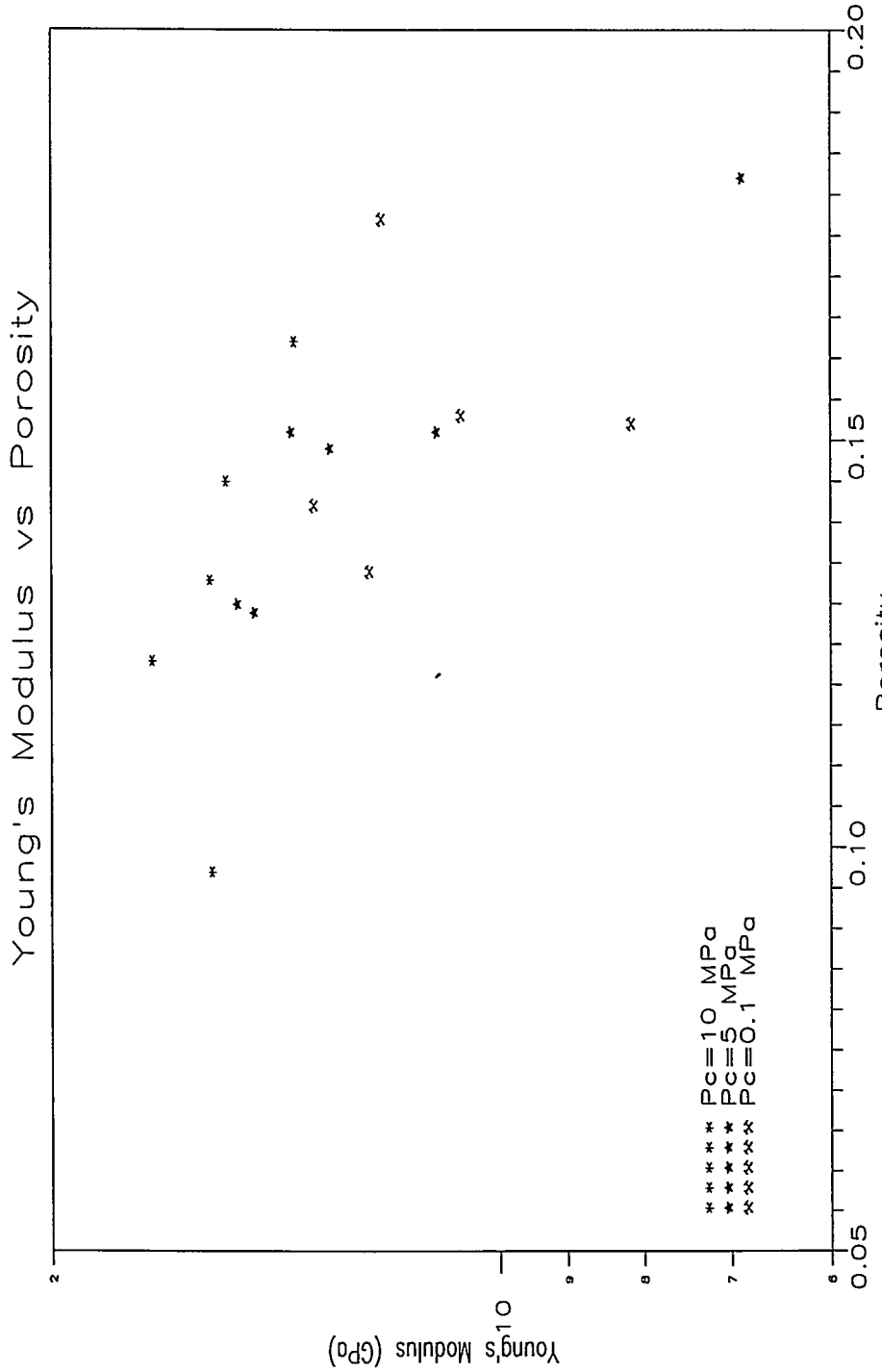

Figure 21. Young's Modulus as a Function of Porosity, SET 2.

Rather than drawing semi - circles in τ - σ space, the Mohr - Coulomb strength parameters can be determined mathematically from values in σ_1 - σ_3 space. The strength parameters can be developed from a least squares curve fit between the axial stress at failure, σ_1, and confining pressure, σ_3. The expression takes the form:

$$\sigma_1 = \sigma_{uc} + N\sigma_3$$

where:

σ_{uc} = unconfined compressive strength

N = confinement factor

σ_{uc} and N are then used to generate a Mohr - Coulomb failure criterion which relates the normal (σ_N) and shear (τ) stresses on the plane of failure to the material constants of cohesion (c) and the angle of internal friction (ϕ). The Mohr - Coulomb criterion takes the form:

$$\tau = c + \sigma_N \tan\phi$$

where:

$$c = \frac{\sigma_{uc}}{2\sqrt{N}}$$

$$\phi = 2(\tan^{-1}\sqrt{N} - 45°)$$

(Lin et. al., 1993)

Figures 22 and 23 show plots of σ_1 vs σ_3 and the least squares curve fit through the data points from SET 1 specimens cored parallel and perpendicular to the lithophysal cavities to calculate the parameters N and σ_{uc} needed to mathematically develop the Mohr - Coulomb strength parameters. From Figures 22 and 23, the following expressions are obtained:

Perpendicular Specimens:

$$\sigma_1 = 85.03 + 7.26\,\sigma_3$$

Parallel Specimens:

$$\sigma_1 = 81.92 + 7.12\,\sigma_3$$

The Mohr - Coulomb strength parameters were calculated using both the classical method and the mathematical method used by Lin et. al. (1993). When using the classical method, three sets of Mohr - Coulomb strength parameters were calculated: a maximum set, an average set and a minimum set. The maximum set was calculated using the maximum values of σ_1 from SET 1, the average set was calculated using an

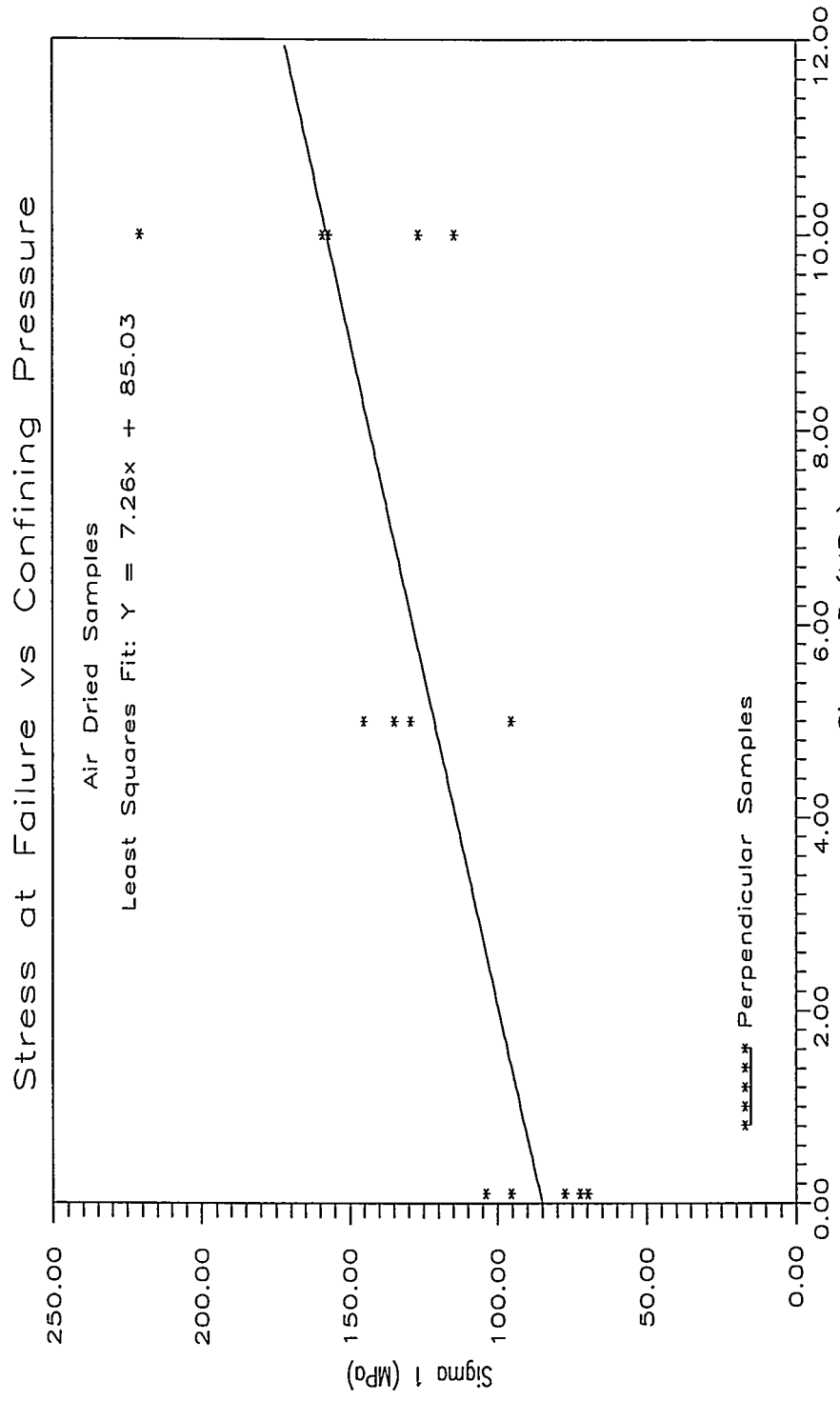

Figure 22. Least Squares Curve Fit - Compressive Strength vs Confining Pressure, SET 1 (Perpendicular Specimens).

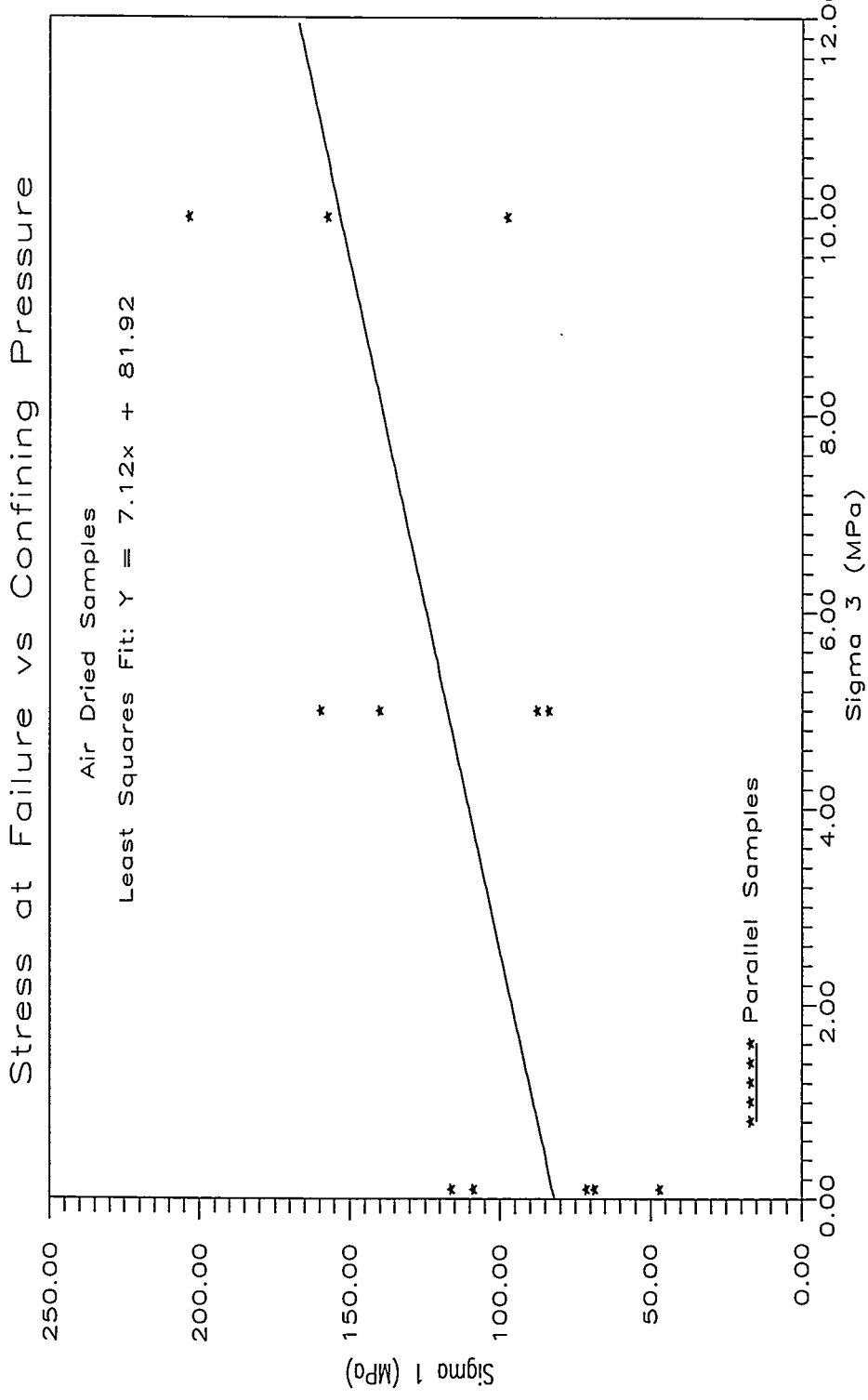

Figure 23. Least Squares Curve Fit - Compressive Strength vs Confining Pressure, SET 1 (Parallel Specimens).

average values of σ_1 from SET 1 and the minimum set was calculated using the minimum values of σ_1 from SET 1. The Mohr - Coulomb strength parameters calculated are given in Table 12 and shown graphically in Figures 24 and 25.

Table 12. Calculated Mohr - Coulomb Strength Parameters of SET 1.

Specimen Orientation	Failure Envelope	ϕ (degrees)	cohesion (MPa)
Perpendicular	Maximum	55.4	16
	Average	50.2	15
	Minimum	41.0	15
	Mathematically Derived	49.3	15.78
Parallel	Maximum	53.5	18
	Average	49.0	15
	Minimum	42.0	11
	Mathematically Derived	48.9	15.35

As shown in Table 12 and Figures 24 and 25, the mathematically derived Mohr - Coulomb strength parameters are almost identical to the average Mohr - Coulomb strength parameters obtained from the classical method. This is because the least squares fit can be considered an average value of σ_1 with a variation of σ_3.

The Mohr - Coulomb strength parameters have also been derived for SET 2 to examine the effect of saturation on the cohesion and the angle

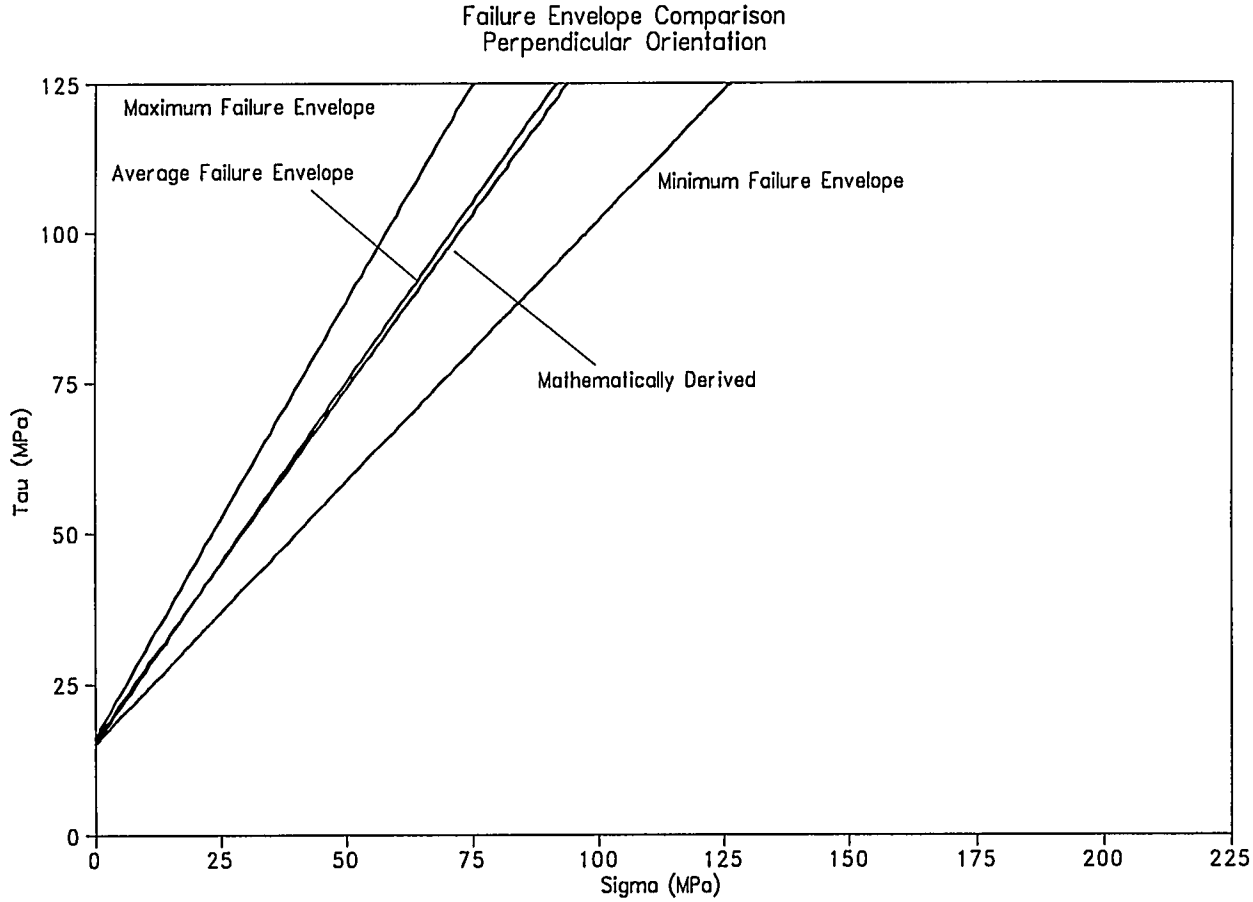

Figure 24. Failure Envelope Comparison, SET 1 (Perpendicular Specimens).

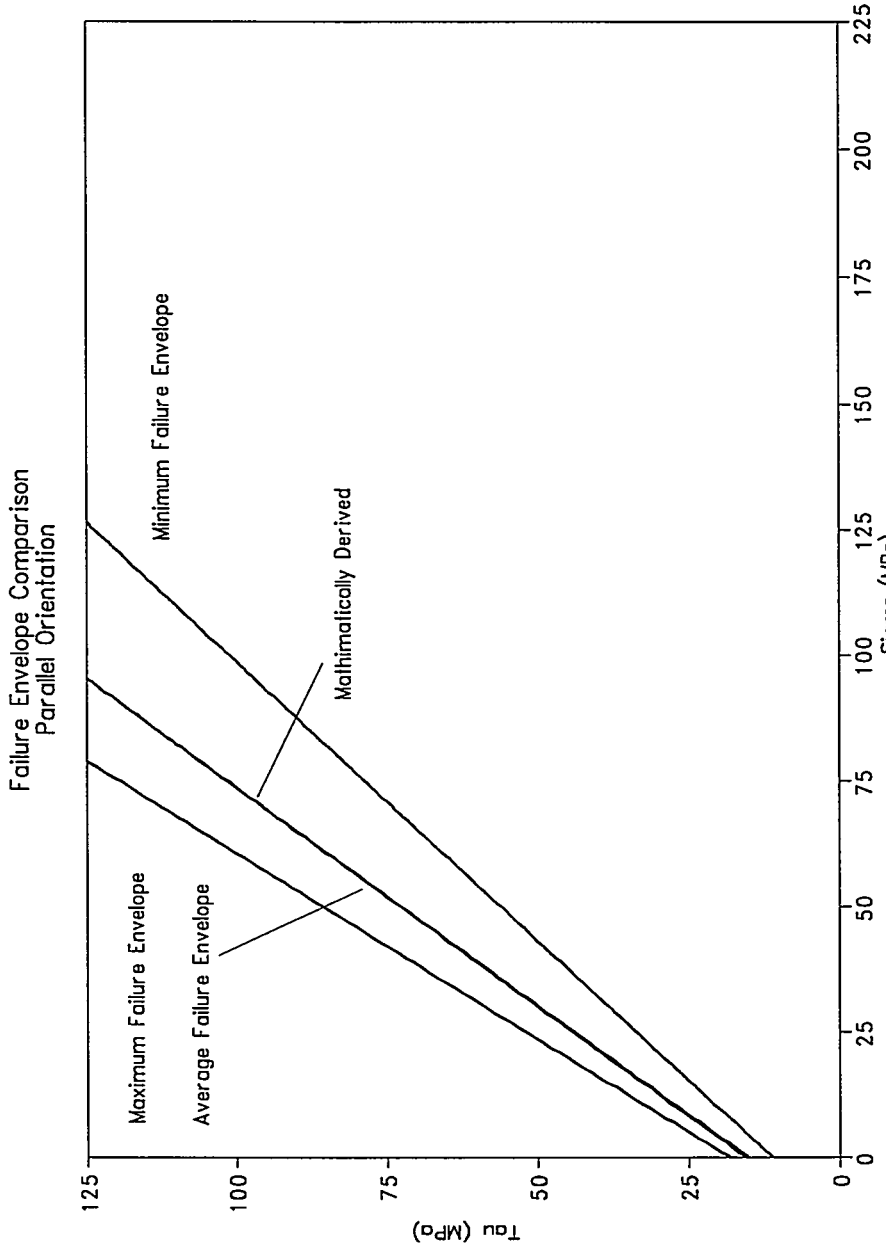

Figure 25. Failure Envelope Comparison, SET 1 (Parallel Specimens).

of internal friction. Since the mathematically derived parameters correlate with the average parameters derived from the classical method of determining the Mohr - Coulomb parameters, only the mathematically derived parameters are calculated for SET 2. Figures 26 and 27 show the plots of σ_1 vs σ_3 and the least squares curve fit through the data to calculate the parameters N and σ_{uc} needed to mathematically develop the Mohr - Coulomb strength parameters. From Figures 26 and 27, the following expression are obtained:

Perpendicular Specimens:

$$\sigma_1 = 59.14 + 7.37\sigma_3$$

Parallel Specimens:

$$\sigma_1 = 71.33 + 9.06\sigma_3$$

Table 13 compares the Mohr - Coulomb strength parameters for the Tiva Canyon Tuff specimens from SET 1 and SET 2.

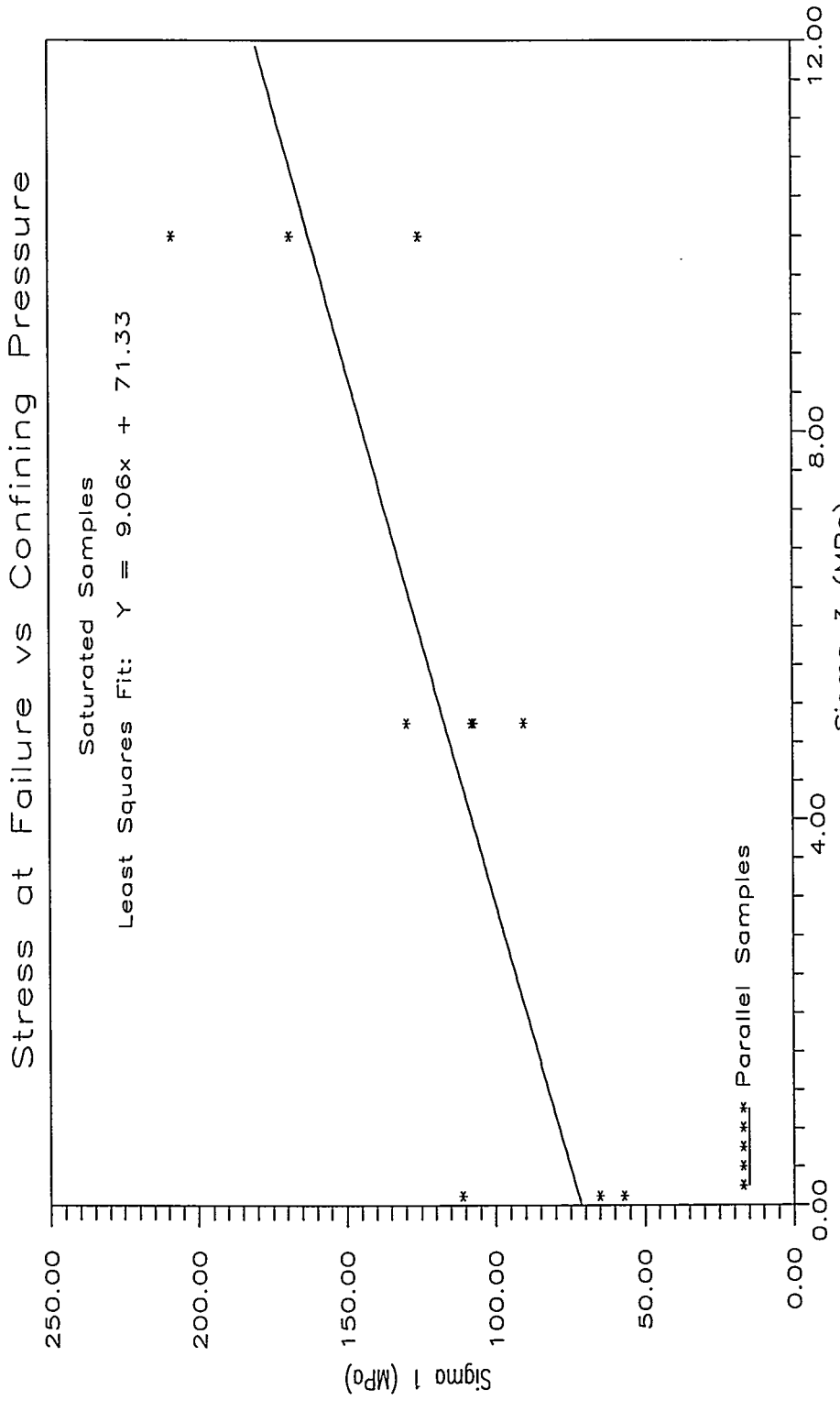

Figure 26. Least Squares Fit - Compressive Strength vs Confining Pressure, SET 2 (Perpendicular Specimens).

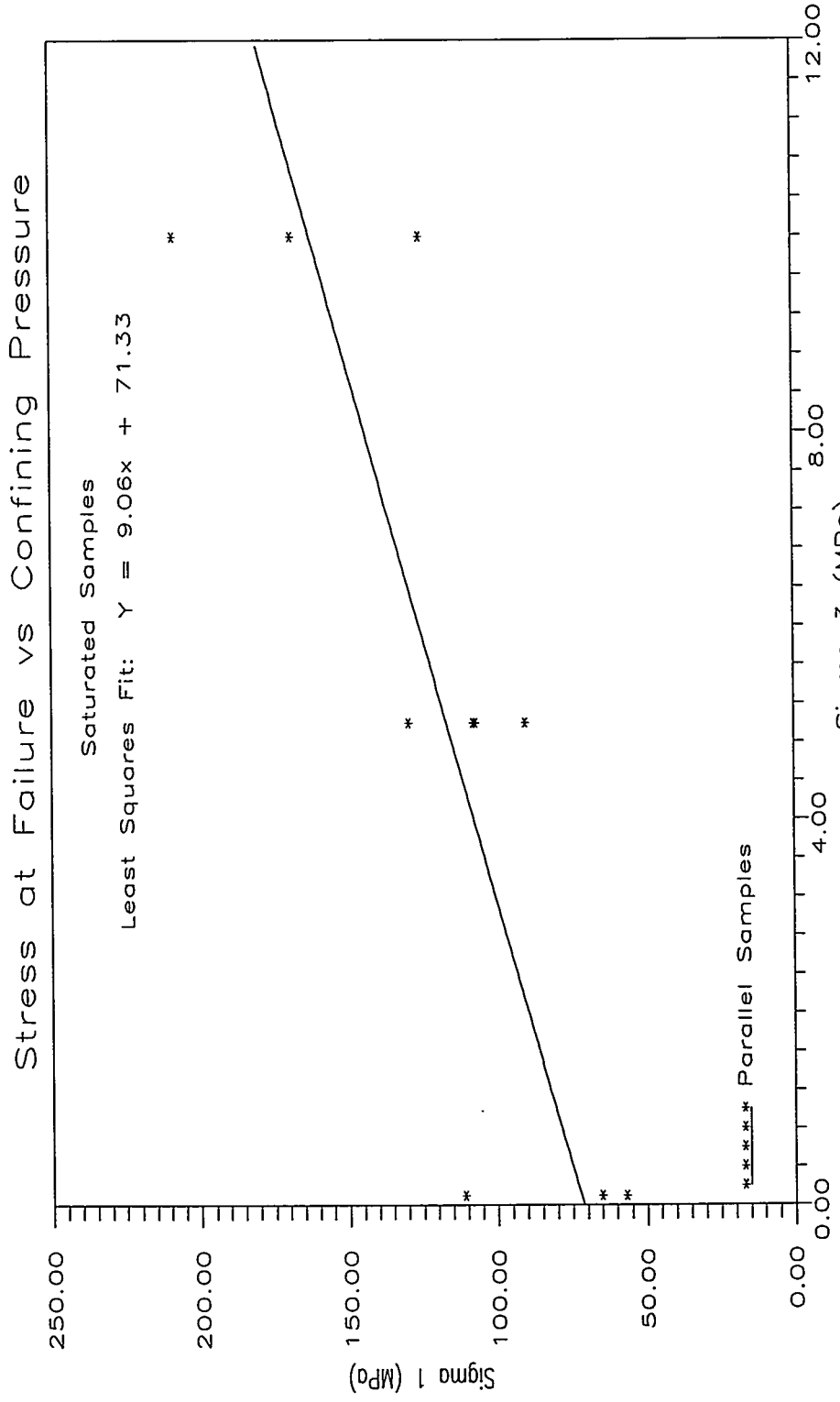

Figure 27. Least Squares Fit - Compressive Strength vs Confining Pressure, SET 2 (Parallel Specimens).

Table 13. Comparison of Mohr - Coulomb Strength Parameters of SET 1 and SET 2.

Set Number	Specimen Orientation	ϕ (degrees)	cohesion (MPa)
SET 1	Perpendicular	49.3	15.78
	Parallel	48.9	15.53
SET 2	Perpendicular	49.6	10.89
	Parallel	53.2	10.85

As shown in Table 13, saturation reduces the cohesion of the specimens, however, the angle of internal friction remains unchanged with saturation.

Comparisons With Previous Data

Compressive Strength Comparison

The easiest way to compare the compressive strength data is in tabular form. Table 14 lists the confining pressures specimens were tested at, average test results from this study, previous test results, and suggested values for compressive strength values for Tiva Canyon Tuff. Table 14 shows there is a very wide range of compressive strength data. The compressive strengths determined from this study are much lower than previous test data (125% lower for the high strain rate and 10 MPa confining pressure). Also, the suggested compressive strength values are much higher than the compressive strength values determined in this

study.

The compressive strength difference may be due to several factors. The samples may have been damaged by excavation, thus lowering the compressive strength. Also, the samples of TCw tuff which were obtained for this study were basically outcrop samples, whereas specimens which were previously tested were from depths ranging from 26.7 meters to 64.8 meters (Price, 1982). Thus, the samples used in this study may have been stressed from the removal of overburden and weakened by weathering processes.

Table 14. Compressive Strength Comparison for Tiva Canyon Tuff (after Olsson and Jones*, 1980 and Lin et. al**., 1993).

Confining Pressure (MPa)	Average Compressive Strength (MPa)		Previous Test Data* (strain rate = 10^{-4} s^{-1})	Suggested Values (MPa)**
	strain rate: 10^{-5} s^{-1}	strain rate: 10^{-4} s^{-1}		
10	SET 1: 154.61	SET 3: 180.84	406 MPa	no suggested values
	SET 2: 154.90	NO DATA		
5	SET 1: 122.01	NO DATA	NO DATA	no suggested values
	SET 2: 102.00	NO DATA		
0.1	SET 1: 83.14	NO DATA	7.03 & 364 MPa	161 ± 63
	SET 2: 72.00	NO DATA		

One other type of compressive strength comparison which can be

used is to compare the compressive strength - porosity relationship from this study and other studies. Figure 28 shows a plot of the compressive strengths of specimens from SET 2 tested at a confining pressure of 0.1 MPa versus the specimen porosity. A best fit line is plotted through this data and compared with a best fit line through similar data for tuffs from the Nevada tests tested at the same conditions. As shown by Figure 28, the data from this study shows a similar trend as the trend shown by Price et. al. (1994). However, the data presented by Price et. al. (1994) includes not only Tiva Canyon Tuff, but other tuffs as well.

Young's Modulus Comparison

Data from this study, test data from Olsson and Jones (1980) and suggested values of Young's Modulus for Tiva Canyon Tuff and TCw are presented in Table 15.

Table 15 shows that previous testing of Tiva Canyon Tuff specimens has produced large variations in Young's Modulus values. None of the specimens tested for this study came near to the Young's Modulus values determined by previous testing. This difference may be explained by the differences in the specimens used in each study. However, the suggested values of Young's Modulus are close to the values obtained by testing SET 1 specimens. Specimens from SET 2 have a Young's

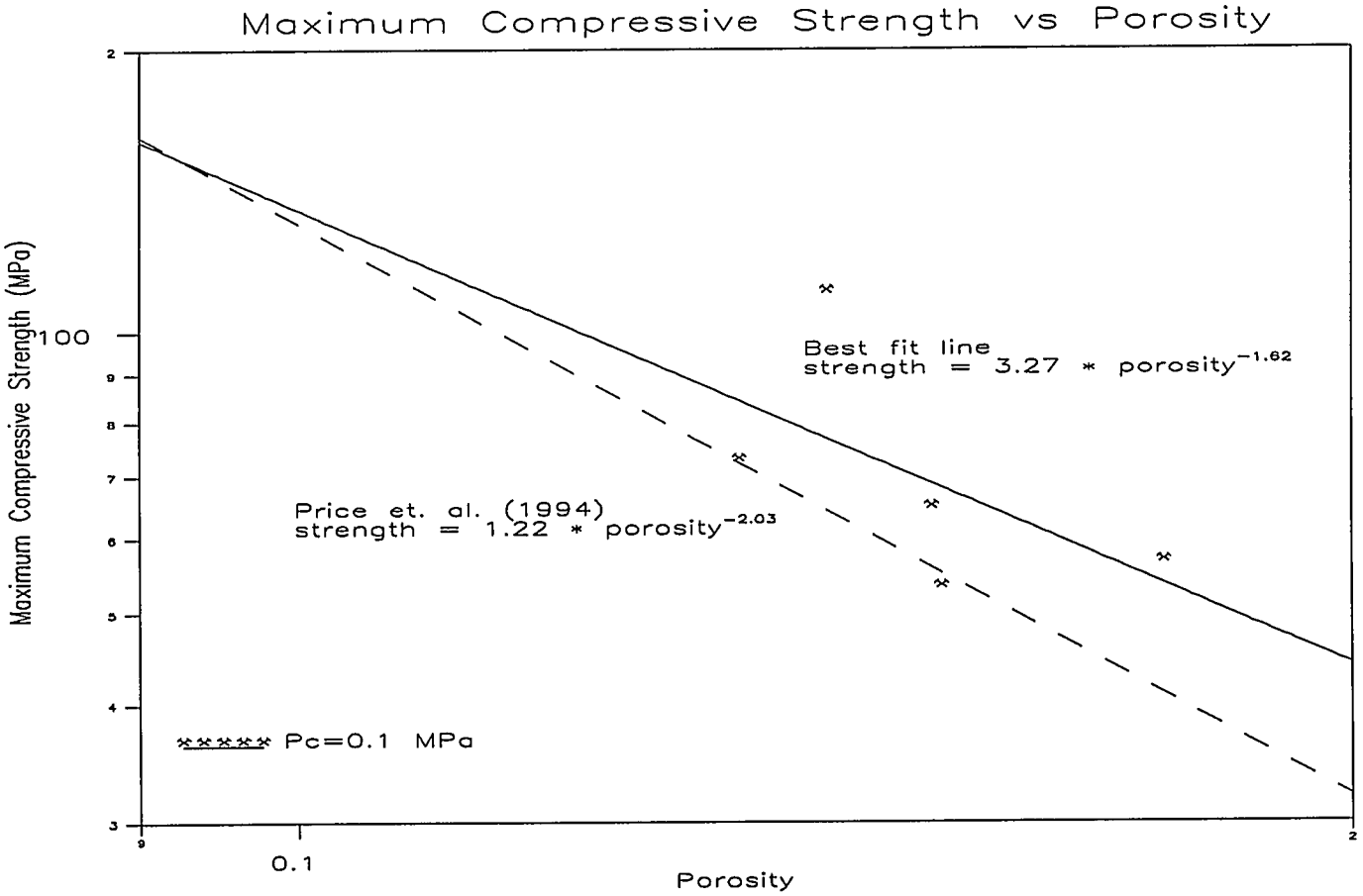

Figure 28. Best Fit Line - Compressive Strength vs Porosity, SET 2 (Specimens Tested at a Confining Pressure of 0.1 MPa).

Modulus value well below the suggested value.

Table 15. Young's Modulus Comparison for Tiva Canyon Tuff (after Price*, 1982 and Lin et. al**., 1993).

Confining Pressure (MPa)	Average Young's Modulus (GPa) strain rate: 10^{-5} s^{-1}	strain rate: 10^{-4} s^{-1}	Previous Test Data* (strain rate = 10^{-4} s^{-1})	Suggested Values (GPa)**
10	SET 1: 24.60	SET 3: 19.15	43.9 GPa	no suggested values
	SET 2: 15.48	NO DATA		
5	SET 1: 22.12	NO DATA	NO DATA	no suggested values
	SET 2: 12.39	NO DATA		
0.1	SET 1: 23.41	NO DATA	.41 & 57.5 GPa	19.9±3.0
	SET 2: 11.26	NO DATA		

A comparison can also be made with the Young's Modulus - porosity relationship from tuffs from the Nevada Test Site and the tuffs tested in this study. Figure 29 shows the variation of Young's Modulus with porosity for SET 2 specimens tested at a confining pressure of 0.1 MPa and the same variation of other tuffs from the Nevada Test Site tested by Price et. al. (1994). Both sets of specimens were tested under similar conditions. It is obvious that the Young's Modulus values determined for the study by Price et. al. (1994) were much higher than the modulus

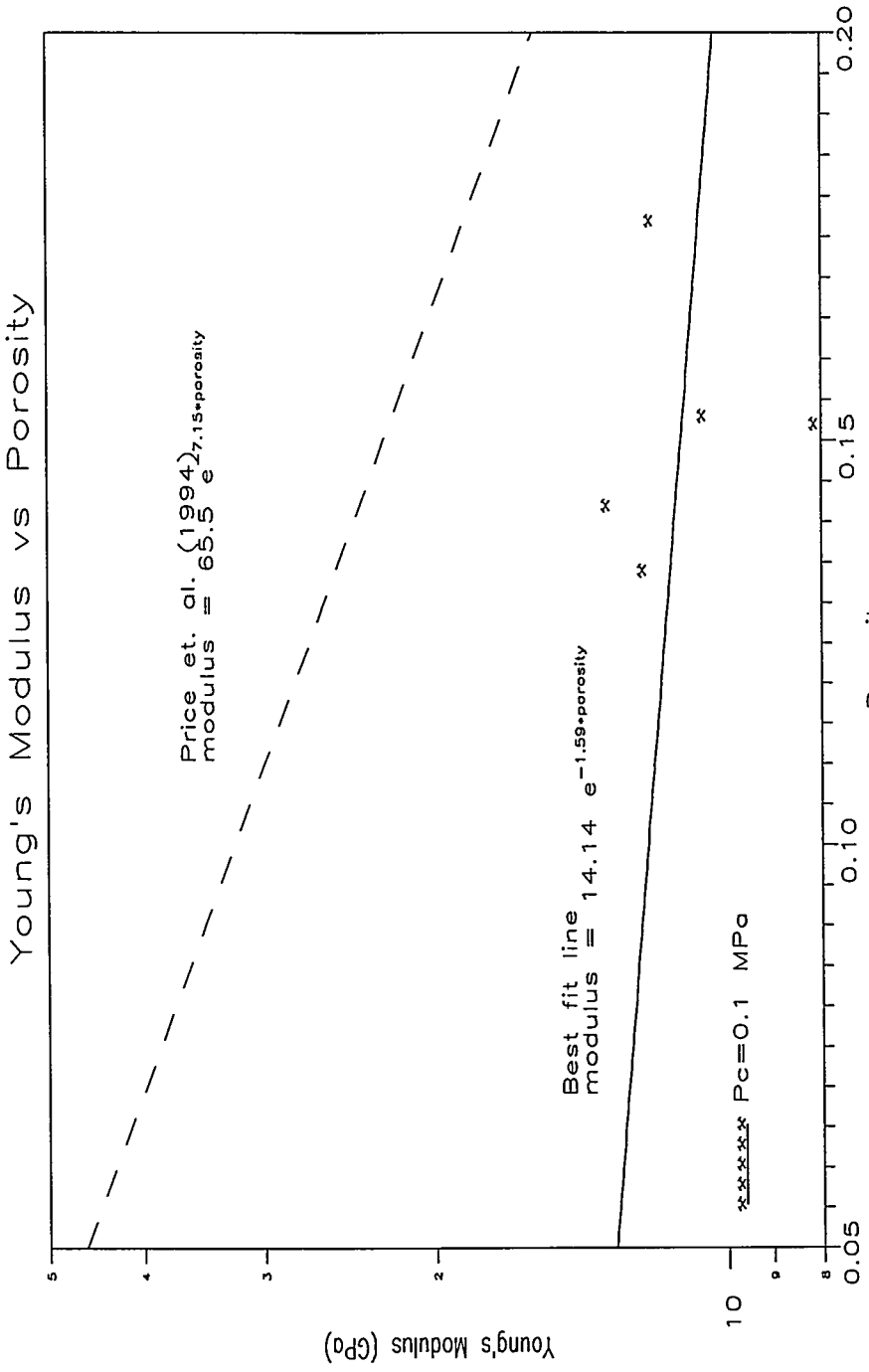

Figure 29. Best Fit Line - Young's Modulus vs Porosity, SET 2 (Specimens Tested at a Confining Pressure of 0.1 MPa).

values determined for this study. However, the same general trend is observed, decreasing Young's Modulus with increasing porosity.

Mohr - Coulomb Strength Parameters Comparison

Table 16 compares the Mohr - Coulomb strength parameters determined by this study with Mohr - Coulomb strength parameters from previous studies and the suggested values the Mohr - Coulomb strength parameters.

Table 16. Comparison of Mohr - Coulomb Strength Parameters

Hudyma (1994)				Olsson and Jones (1980)		Suggested Values (Lin et. al., 1993)	
Data Set	Specimen Orientation	ϕ (deg.)	cohesion (MPa)	ϕ (deg.)	cohesion (MPa)	ϕ (deg.)	cohesion (MPa)
SET 1	Perpendicular	49.3	15.78	68	28.1	68	28.1
	Parallel	48.9	15.53				
SET 2	Perpendicular	49.6	10.89				
	Parallel	53.2	10.85				

Table 16 shows that the suggested values and values from previous testing are much higher than the Mohr - Coulomb strength parameters determined in this study. The angle of internal friction value determined by Olsson and Jones (1980) may be higher since they tested their specimens at higher strain rates, which result in higher compressive strengths. However, the specimens which were tested for this study at

the strain rates used by Olsson and Jones (1980) had far lower compressive strength values than those obtained in their study.

CONCLUSIONS

Several conclusions on the compressive strength and Young's Modulus of specimens from the thermo - mechanical unit TCw can be drawn from the triaxial testing performed for this study.

- There is a large variation in compressive strengths and Young's Moduli of specimens from the thermo - mechanical unit TCw.
- Generally, there is an increase in compressive strength with an increase in confining pressure.
- An increase in confining pressure raises Young's Moduli for specimens cored parallel to the lithophysal cavities but has no effect on the Young's Moduli for specimens cored perpendicular to the lithophysal cavities.
- Generally, saturation lowers the average compressive strengths of TCw specimens.
- Saturation lowers the average Young's Modulus values of TCw specimens.
- Saturation lowers the cohesion of TCw specimens, but has no appreciable effect on the angle of internal friction of the specimens.
- An increase in strain rate generally increases the compressive strengths of TCw specimens.
- An increase in strain rate generally decreases the Young's Moduli of

TCw specimens.

- TCw specimens show no indication of an average compressive strength anisotropy.
- TCw specimens show an indication of an average Young's Modulus anisotropy.
- An increase in porosity generally lowers the compressive strength of TCw specimens.
- An increase in porosity generally lowers the Young's Moduli of TCw specimens.
- Comparisons with previous data show that the data from this study is generally lower than the strengths and Young's Modulus values from previous studies and lower than the suggested values. This difference may most probably due to excavation damage and a shallower rock specimen than the rock specimens used in the previous studies.

REFERENCES

ASTM (American Society for Testing and Materials), 1985. Standard Practice for Preparing Rock Core Specimens and Determining Dimensional and Shape Tolerances, Standard Test Method, Reapproved 1991, ASTM D 4543-85, Philadelphia, Penn.

Boyd, P. J., R. J. Martin III, and R. H. Price, 1994. An Experimental Comparison of Laboratory Techniques in Determining Bulk Properties of Tuffaceous Rocks, SAND92-0119, Sandia National Laboratories, Albuquerque, New Mexico.

Brown, E.T. (editor), 1981. Rock Characterization Testing and Monitoring - ISRM Suggested Methods, Pergamon Press, U.S.A., 211 p.

DOE, 1988. Site Characterization Plan: Yucca Mountain Site, Nevada Research and Development Area, Nevada, Volume 1, Part A.

Donath, F. A., J. T. Holder, and L. S. Fruth, 1988. *Simultaneous Hydraulic/Physical Parameter Measurement on Rock Specimens Subjected to Triaxial Conditions*, in Advanced Triaxial Testing of Soil and Rock, *ASTM STP 977*, R. T. Donaghe, R. C. Chaney, and M. L. Silver (editors), American Society for Testing and Materials, Philadelphia, pp. 143 - 154.

Dyskin, A. V., L. N. Germanovich, A. R. Ingraffea, and R. L. Salganik, 1994. Fundamentals of Rock Fracture Mechanics: Short Course, Austin, Texas, 500 p.

Franklin, F. A., and M. B. Dusseault, 1989. Rock Engineering, McGraw-Hill Publishing Company, New York, 600 p.

Fox, K. F., R. W. Spengler, and W. B. Myers, 1990. *Geologic Framework and Cenozoic Evolution of the Yucca Mountain Area, Nevada*, in International Symposium on Unique Underground Structures, Vol 2, CSM Press, pp 56-1 - 56-18.

Goodman, R. E., 1989. Introduction to Rock Mechanics: Second Edition, John Wiley & Sons, New York, 562 p.

Griggs, D., 1967. *Hydrolytic Weakening of Quartz and Other Silicates*, The Geophysical Journal of the Royal Astronomical Society, Vol. 4, No. 14, pp 19 - 31.

Judd, William R., 1963. *Rock Stress, Rock Mechanics, and Research* in State of Stress in the Earth's Crust, William R. Judd (editor), American Elsevier Publishing Company, Inc., 732 p.

Kwasniewski, Marek A., 1993. *Mechanical Behavior of Anisotropic Rocks* in Comprehensive Rock Engineering: Principles, Practice and Projects, Volume 1, Hudson, J. A. (editor in chief), Pergamon Press, New York, 752 p.

Lin, M., M. P. Hardy, and S. J. Bauer, 1993. Rock Mass Mechanical Property Estimations for the Yucca Mountain Site Characterization Project, SAND92-0450, Sandia National Laboratories, Albuquerque, New Mexico.

Martin, R.J., R.H. Price, P.J. Boyd, and J.S. Noel, 1993. *The Influence of Strain Rate and Sample Inhomogeneity on the Moduli and Strength of Welded Tuff* in Rock Mechanics in the 1990's - Pre-print proceedings 34th U.S. Symposium on Rock Mechanics, Bezalel Haimson (editor), Geological Engineering Program, University of Wisconsin - Madison, Madison, U.S.A., Volume II, 780 p.

Martin III, R. J., R. H. Price, P. J. Boyd, and R. W. Haupt, 1992. Anisotropy of the Topopah Spring Member Tuff, SAND91-0894, Sandia National Laboratories, Albuquerque, New Mexico.

Nelson, P. H., and L. A. Anderson, 1992. *Physical Properties of Ash Flow Tuff From Yucca Mountain, Nevada*, Journal of Geophysical Research, Vol. 97, No. B5, pp. 6823 - 6841.

Nimick, F.B., R.H. Price, R.G. Van Buskirk, and J.R. Goodell, 1985, Uniaxial and Triaxial Compression Test Series on Topopah Spring Tuff From USW G-4, Yucca Mountain, Nevada, SAND84-1101, Sandia National Laboratories, Albuquerque, New Mexico.

Olsson, W. A., and A. K. Jones, 1980. Rock Mechanics Properties of Volcanic Tuffs From the Nevada Test Site, SAND80-1453, Sandia National Laboratories, Albuquerque, New Mexico.

Price, R.H., P.J. Boyd, J.S. Noel, and R.J. Martin, 1994. *Relationship Between Static and Dynamic Rock Properties in Welded and Nonwelded Tuff* in Rock Mechanics: Models and Measurements Challenges from Industry, P.P. Nelson and S.E. Laubach (editors), A.A. Balkema, Netherlands, 1994.

Price, R.H., R.J. Martin, P.J. Boyd, and J.S. Noel, 1993. *Mechanical and Bulk Properties in Support of ESF Design Issues* in High Level Radioactive Waste Management - Proceedings of the Fifth International Conference, American Society of Civil Engineers, U.S.A., Volume 4, 2815 p.

Price, R.H., J.R. Connolly, and K. Keil, 1987. Petrologic and Mechanical Properties of Outcrop Samples of the Welded, Devitrified Topopah Spring Member of the Paintbrush Tuff, SAND86-1131, Sandia National Laboratories, Albuquerque, New Mexico.

Price, R.H., F.B. Nimick, J.R. Connolly, K. Keil, B.M. Schwartz, and S.J. Spence, 1985. Preliminary Characterization of Petrologic, Bulk, and Mechanical Properties of a Lithophysal Zone Within the Topopah Spring Member of the Paintbrush Tuff, SAND84-0860, Sandia National Laboratories, Albuquerque, New Mexico.

Price, R. H., 1983. Analysis of Rock Mechanics Properties of Volcanic Tuff Units from Yucca Mountain, Nevada Test Site, SAND82-1315, Sandia National Laboratories, Albuquerque, New Mexico.

R.S. Carmichael (editor), 1989. Practical Handbook of Physical Properties of Rocks and Minerals, CRC Press, Inc., U.S.A., 741 p.

Scott, R. B., R. W. Spengler, A. R. Lappin, and M. P. Chornack, 1983. *Geologic Character of Tuffs in the Unsaturated Zone at Yucca Mountain, Southern Nevada*, in Role of the Unsaturated Zone in Radioactive and Hazardous Waste Disposal, J. W. Mercer, P. S. C. Rao, and I. W. Marine (editors), Ann Arbor Science Publishers, Ann Arbor, Michigan, pp. 289 - 335.

Scott, R. B. and J. Bonk, 1984. Preliminary Geologic Map of Yucca Mountain, Nye County, Nevada, With Geologic Sections, USGS-OFR-84-494, Open-File Report, U. S. Geological Survey.

Swolfs, H., 1971. *Chemical Effects of Pore Fluids on Rock Properties*, in Underground Waste Management and Environmental Implications, T. D. Cook (editor), The American Association of Petroleum Geologists, Tulsa, Oklahoma, pp. 224 - 234.

Tillerson, J. R., and F. B. Nimick, 1984. Geoengineering Properties of Potential Repository Units at Yucca Mountain, Southern Nevada, SAND84-0221, Sandia National Laboratories, Albuquerque, New Mexico.

Wilder, D. G., 1993. Preliminary Near-Field Environment Report Volume II: Scientific Overview of Near-Field Environment and Phenomena, UCRL\Lr-107476 Vol 2, Lawrence Livermore National Laboratory, Livermore, California.

APPENDIX - Test Data

SPECIMEN DIMENSIONS AND WEIGHTS

Specimen Number - Orientation	Specimen Dimensions (inches)		Specimen Weights (grams)	
	Length	Diameter	Dry	Saturated
726A - PER	5.072	2.114	629.3	
726B - PER	4.488	2.115	548.4	
726C - PER	5.231	2.113	648.3	687.3
726D - PAR	4.311	2.115	539.9	
727A - PER	4.459	2.121	553.9	
728B - PAR	4.523	2.125	568.6	
727C - PAR	4.014	2.121	488.7	523.3
729C - PER	4.909	2.124	619.2	
729D - PER	4.742	2.122	602.9	
729E - PER	4.745	2.123	624.4	
729F - PAR	4.790	2.123	590.6	
729G - PAR	4.783	2.123	602.3	636.4
729H - PAR	4.903	2.120	610.1	
730A - PAR	4.580	2.116	546.7	
730B - PAR	4.345	2.118	513.8	
730C - PAR	4.484	2.117	557.8	
730D - PER	4.439	2.115	538.5	
730E - PER	4.499	2.121	548.4	588.3
731A - PAR	4.602	2.120	561.9	602.2
734B - PER	4.601	2.121	572.7	
734D - PAR	4.597	2.120	559.3	
735C - PAR	4.695	2.112	560.7	604.3
736A - PER	4.290	2.122	529.0	
736B - PAR	4.743	2.122	571.3	
738B - PAR	4.087	2.122	511.1	
737B - PAR	4.711	2.123		
739A - PER	4.892	2.124	620.7	

Specimen Number - Orientation	Specimen Dimensions (inches)		Specimen Weights (grams)	
	Length	Diameter	Dry	Saturated
741A - PER	4.825	2.123	603.4	639.6
742A - PAR	4.766	2.120	561.7	
742B - PAR	4.825	2.123	571.7	621.3
742C - PAR	4.882	2.124	575.8	
743A - PER	4.581	2.114	562.7	
743B - PER	4.536	2.119	561.5	
746A - PER	4.168	2.118	522.9	
746C - PAR	4.980	2.113	617.2	
747A - PER	4.868	2.125	609.5	647.1
747B - PER	4.616	2.125	554.0	
747C - PER	4.667	2.122	582.1	618.3
749B - PAR	4.652	2.121	570.0	609.0
749C - PAR	4.120	2.119	499.5	535.8
749E - PER	4.715	2.121	591.8	
750A - PAR	4.278	2.119	587.9	
750B - PAR	4.721	2.120	578.8	620.0
750C - PAR	4.824	2.120	591.3	
750D - PAR	4.842	2.120	604.4	640.7
750E - PER	4.860	2.123	585.5	
750G - PER	4.931	2.121	580.3	632.2
750K - PAR	4.337	2.115	534.7	570.1

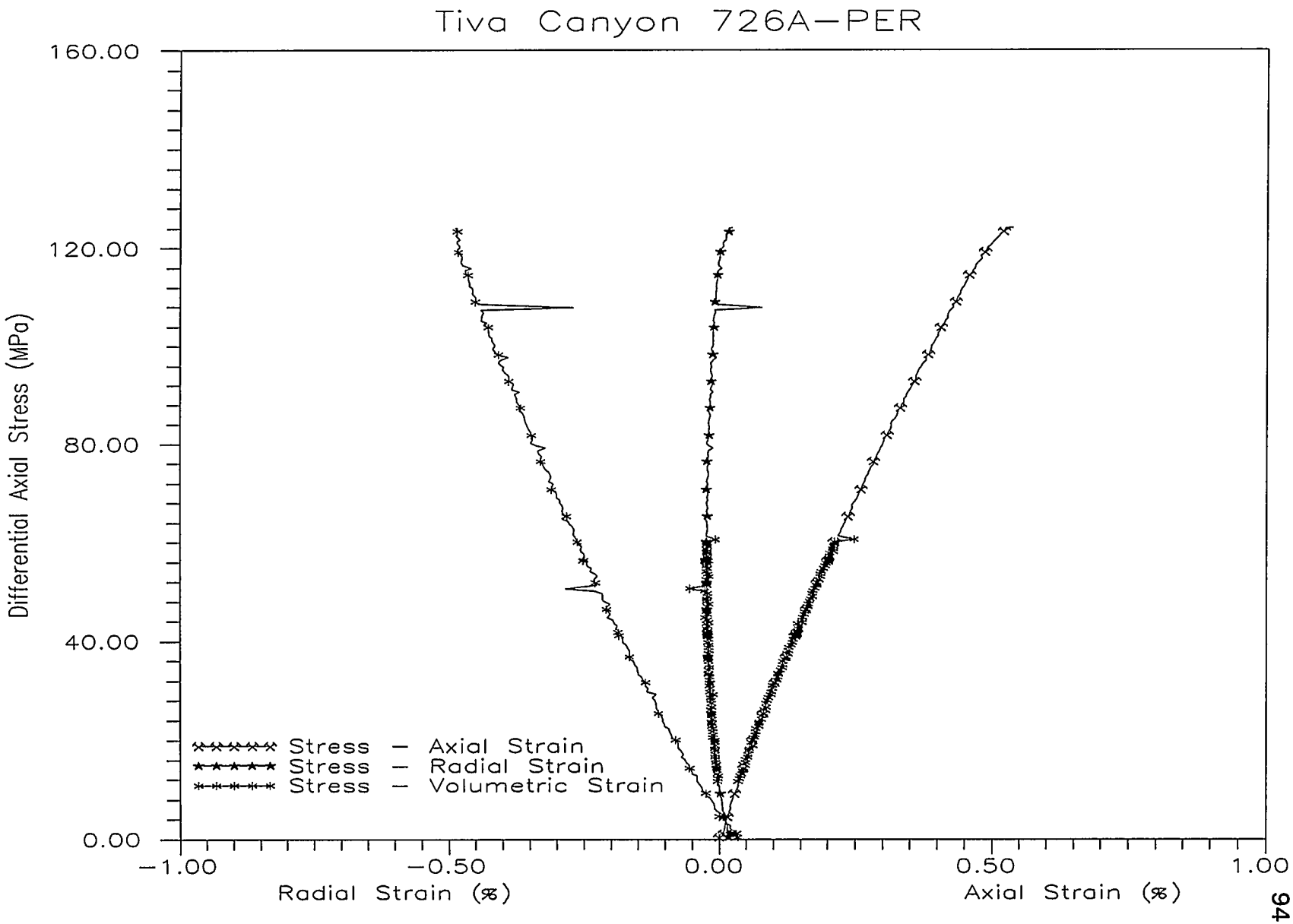
Tiva Canyon 726A—PER
160.00
120.00
80.00
40.00
0.00
Differential Axial Stress (MPa)
Stress — Axial Strain
Stress — Radial Strain
Stress — Volumetric Strain
−1.00
−0.50
0.00
0.50
1.00
Radial Strain (%)
Axial Strain (%)

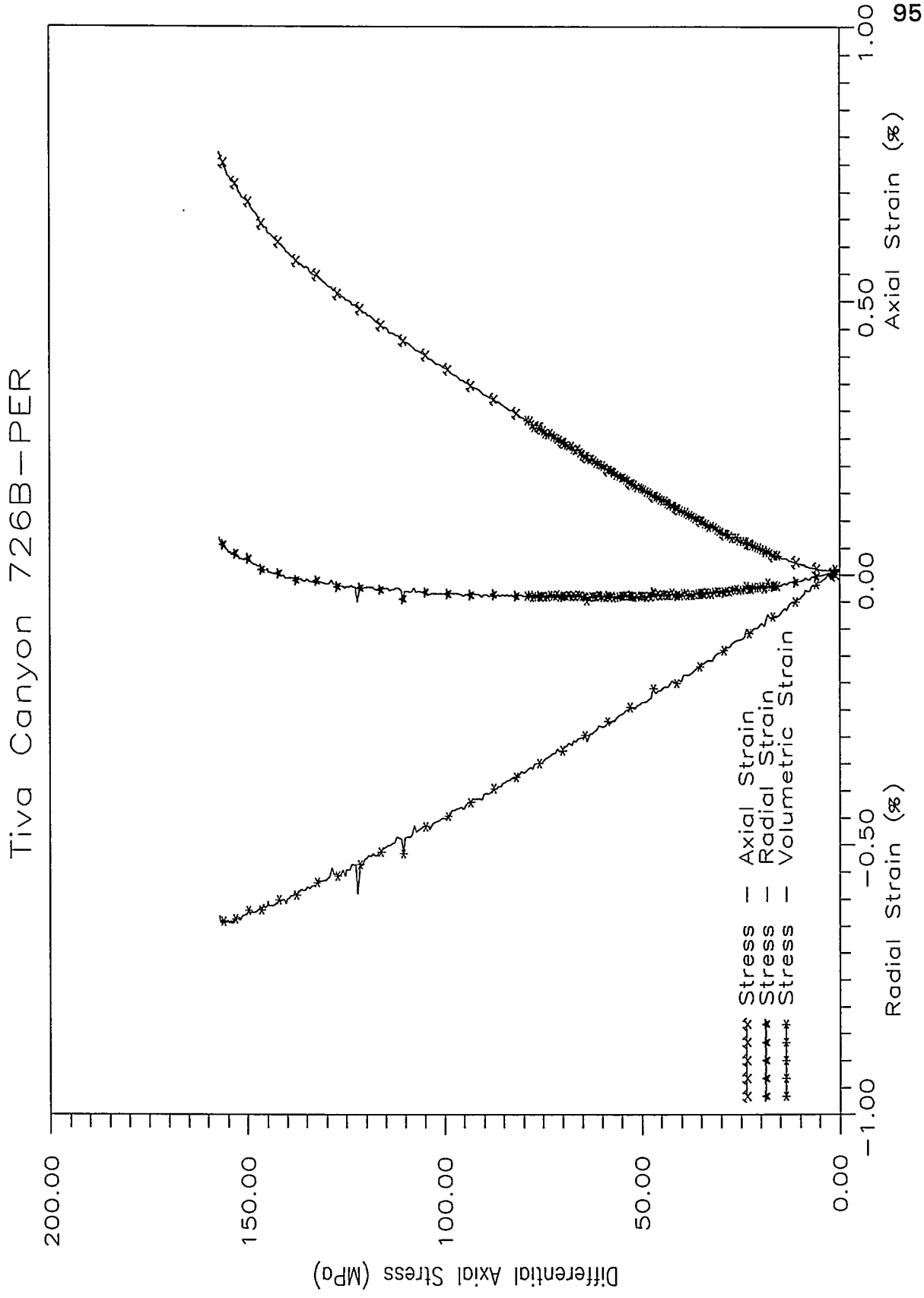
Tiva Canyon 726B-PER
Differential Axial Stress (MPa)
200.00
150.00
100.00
50.00
0.00
-1.00
-0.50
0.00
0.50
1.00
Radial Strain (%)
Axial Strain (%)
Stress -- Axial Strain
Stress -- Radial Strain
Stress -- Volumetric Strain

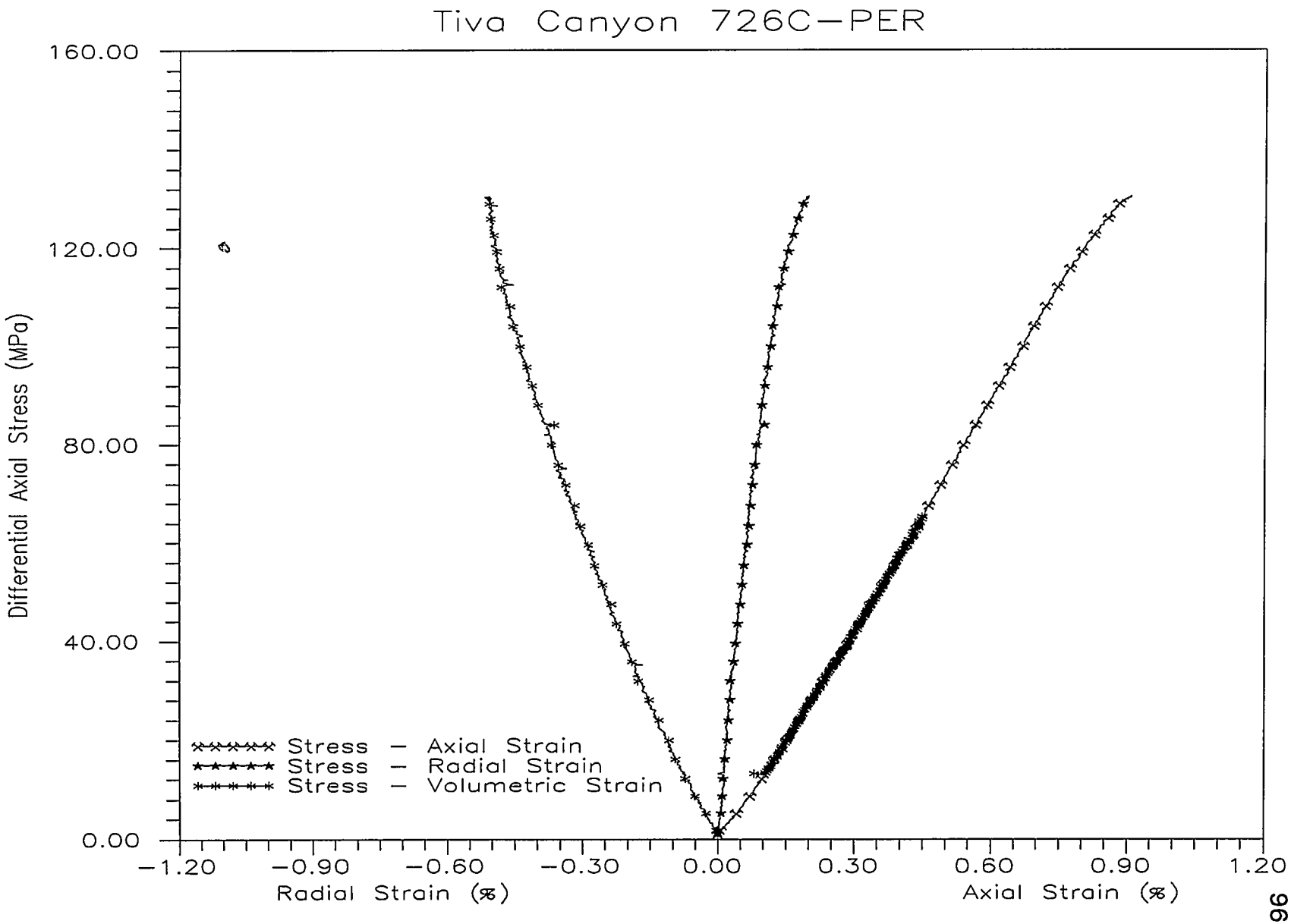
Tiva Canyon 726C—PER
160.00
120.00
80.00
40.00
0.00
Differential Axial Stress (MPa)
Stress — Axial Strain
Stress — Radial Strain
Stress — Volumetric Strain
−1.20
−0.90
−0.60
−0.30
0.00
0.30
0.60
0.90
1.20
Radial Strain (%)
Axial Strain (%)

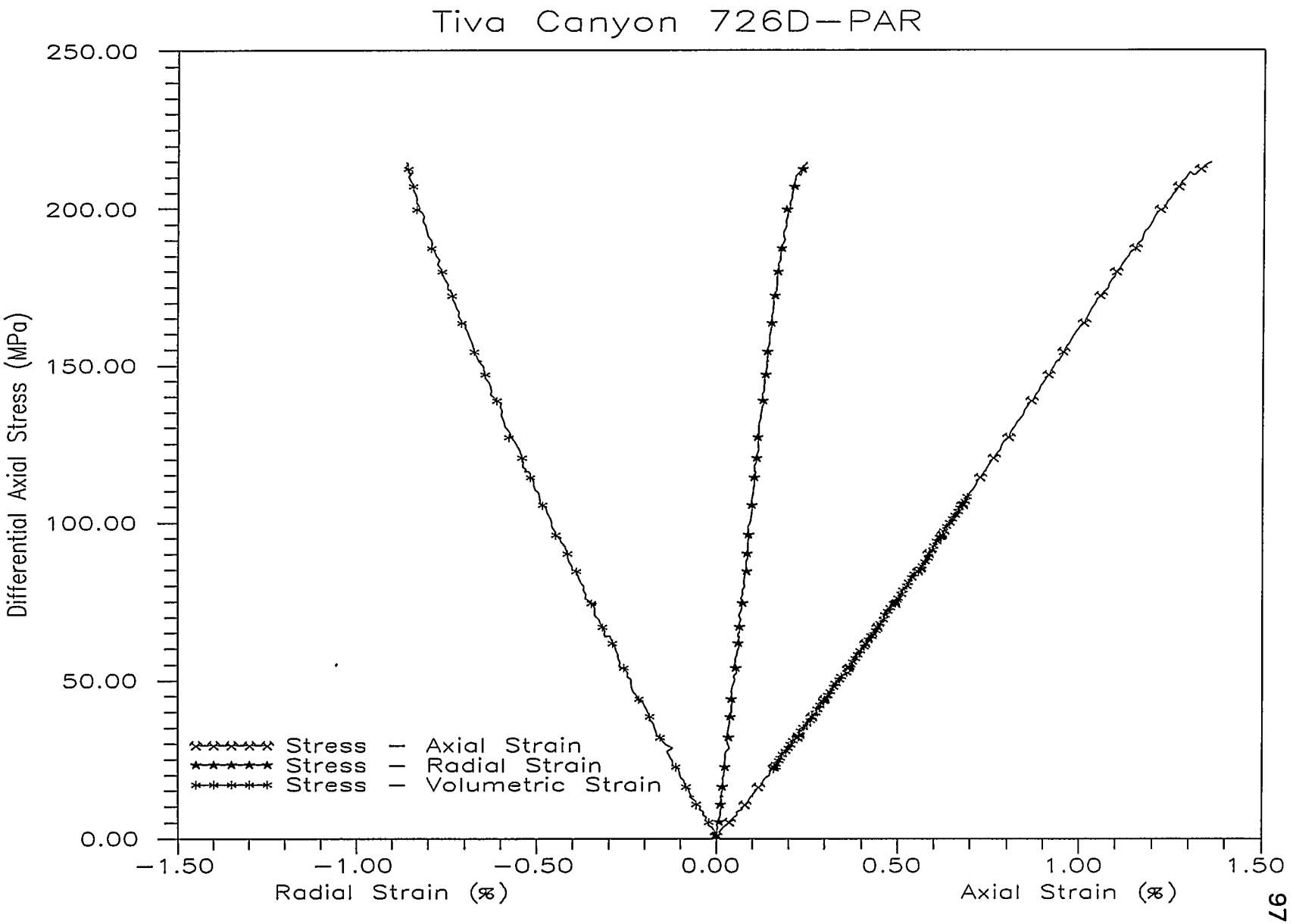
Tiva Canyon 726D—PAR
250.00
200.00
150.00
100.00
50.00
0.00
Differential Axial Stress (MPa)
Stress — Axial Strain
Stress — Radial Strain
Stress — Volumetric Strain
−1.50
−1.00
−0.50
0.00
0.50
1.00
1.50
Radial Strain (%)
Axial Strain (%)

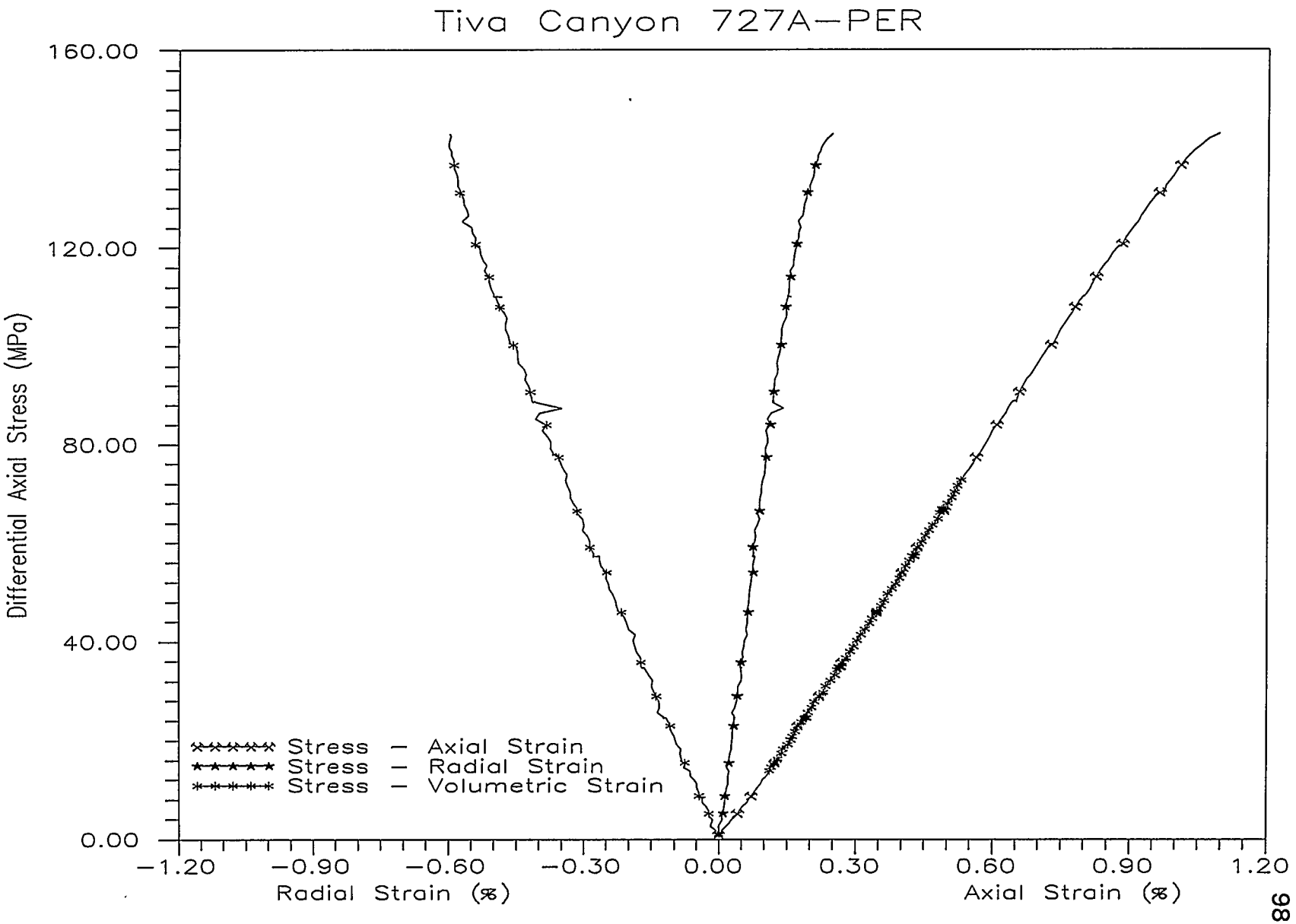
Tiva Canyon 727A—PER
160.00
120.00
80.00
40.00
0.00
Differential Axial Stress (MPa)
Stress — Axial Strain
Stress — Radial Strain
Stress — Volumetric Strain
−1.20
−0.90
−0.60
−0.30
0.00
0.30
0.60
0.90
1.20
Radial Strain (%)
Axial Strain (%)

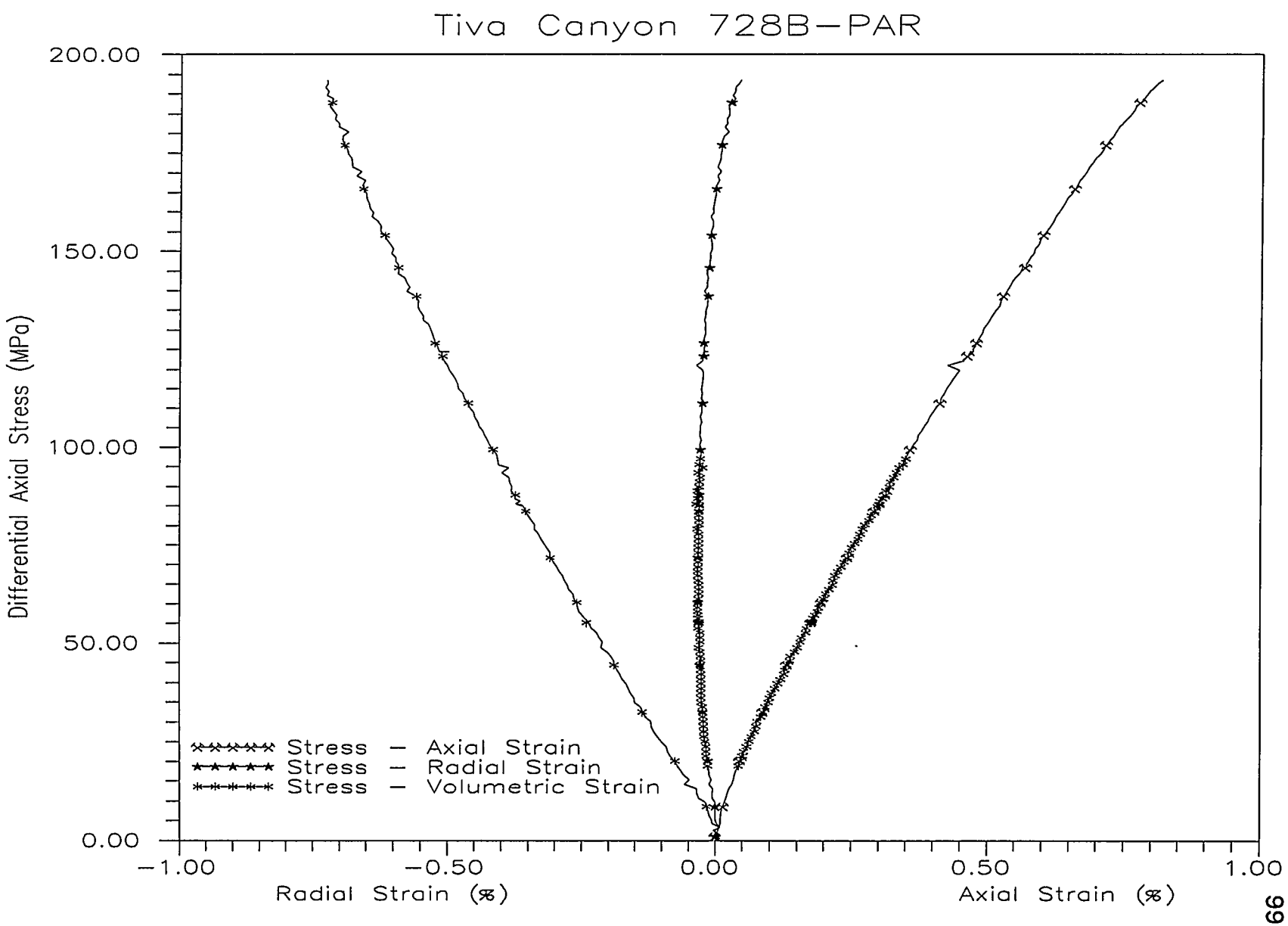
Tiva Canyon 728B—PAR
200.00
150.00
100.00
50.00
0.00
Differential Axial Stress (MPa)
Stress — Axial Strain
Stress — Radial Strain
Stress — Volumetric Strain
−1.00
−0.50
0.00
0.50
1.00
Radial Strain (%)
Axial Strain (%)

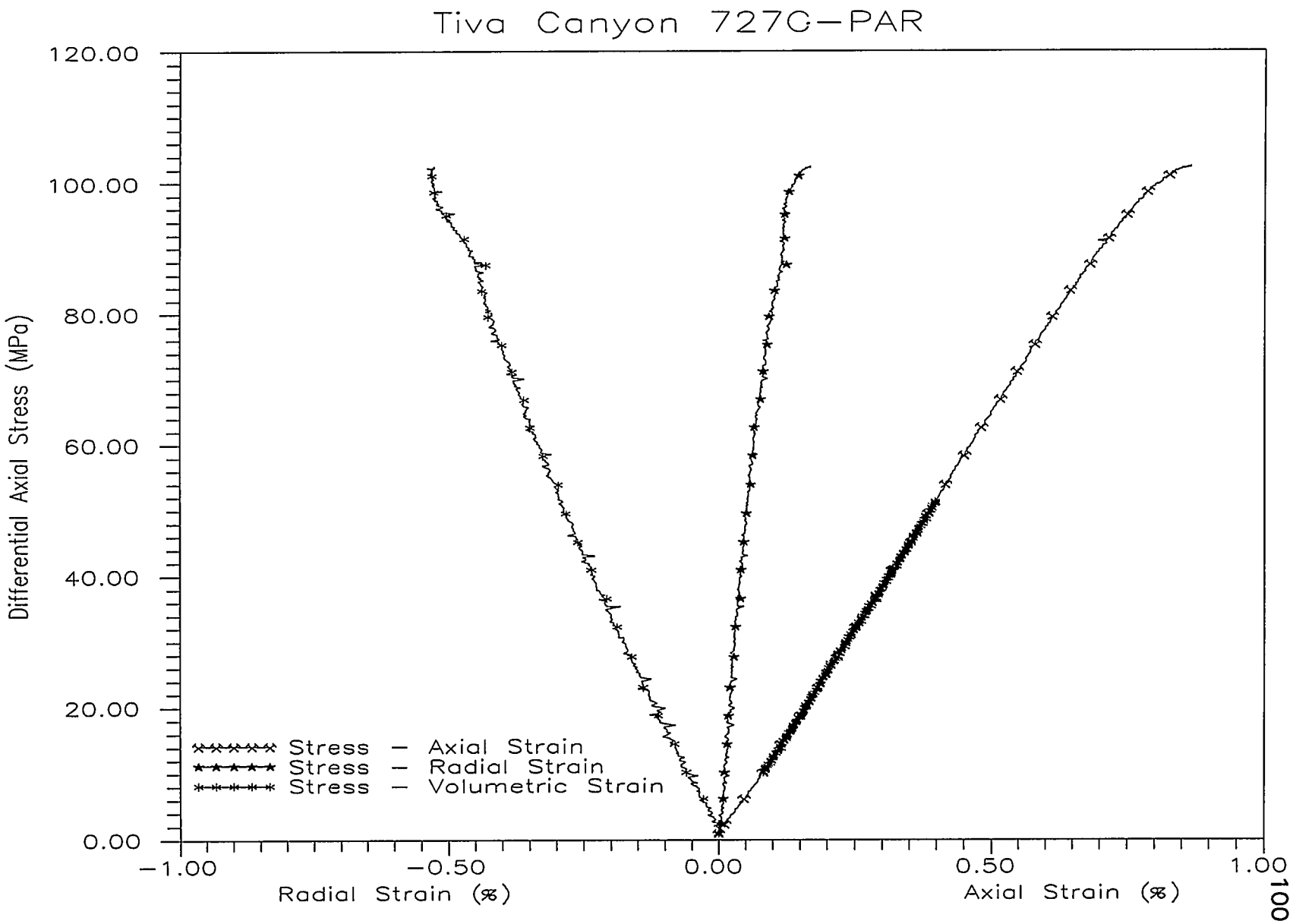
Tiva Canyon 727C—PAR
120.00
100.00
80.00
60.00
40.00
20.00
0.00
Differential Axial Stress (MPa)
Stress — Axial Strain
Stress — Radial Strain
Stress — Volumetric Strain
−1.00
−0.50
0.00
0.50
1.00
Radial Strain (%)
Axial Strain (%)
100

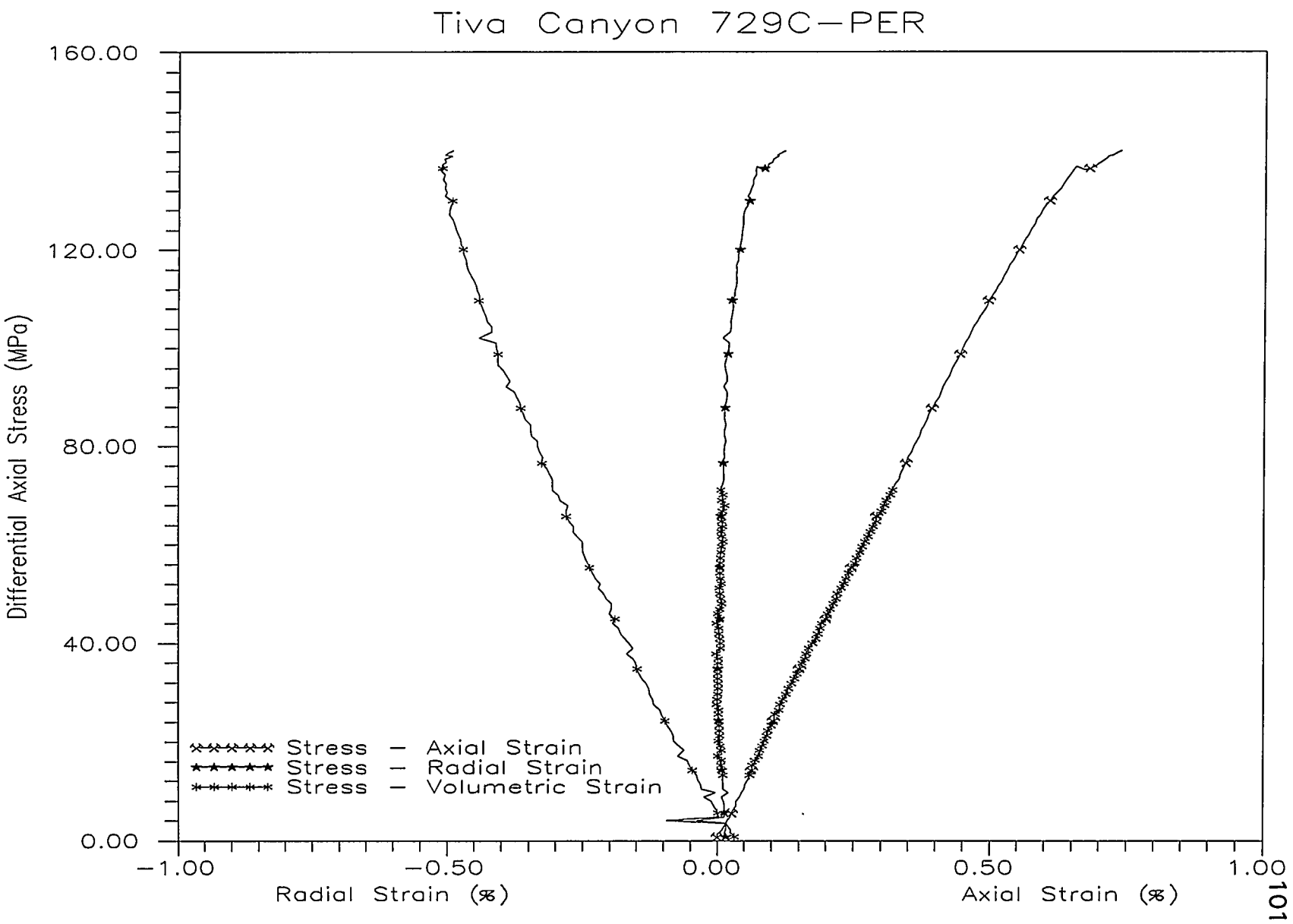
Tiva Canyon 729C—PER
160.00
120.00
80.00
40.00
0.00
Differential Axial Stress (MPa)
Stress — Axial Strain
Stress — Radial Strain
Stress — Volumetric Strain
−1.00
−0.50
0.00
0.50
1.00
Radial Strain (%)
Axial Strain (%)

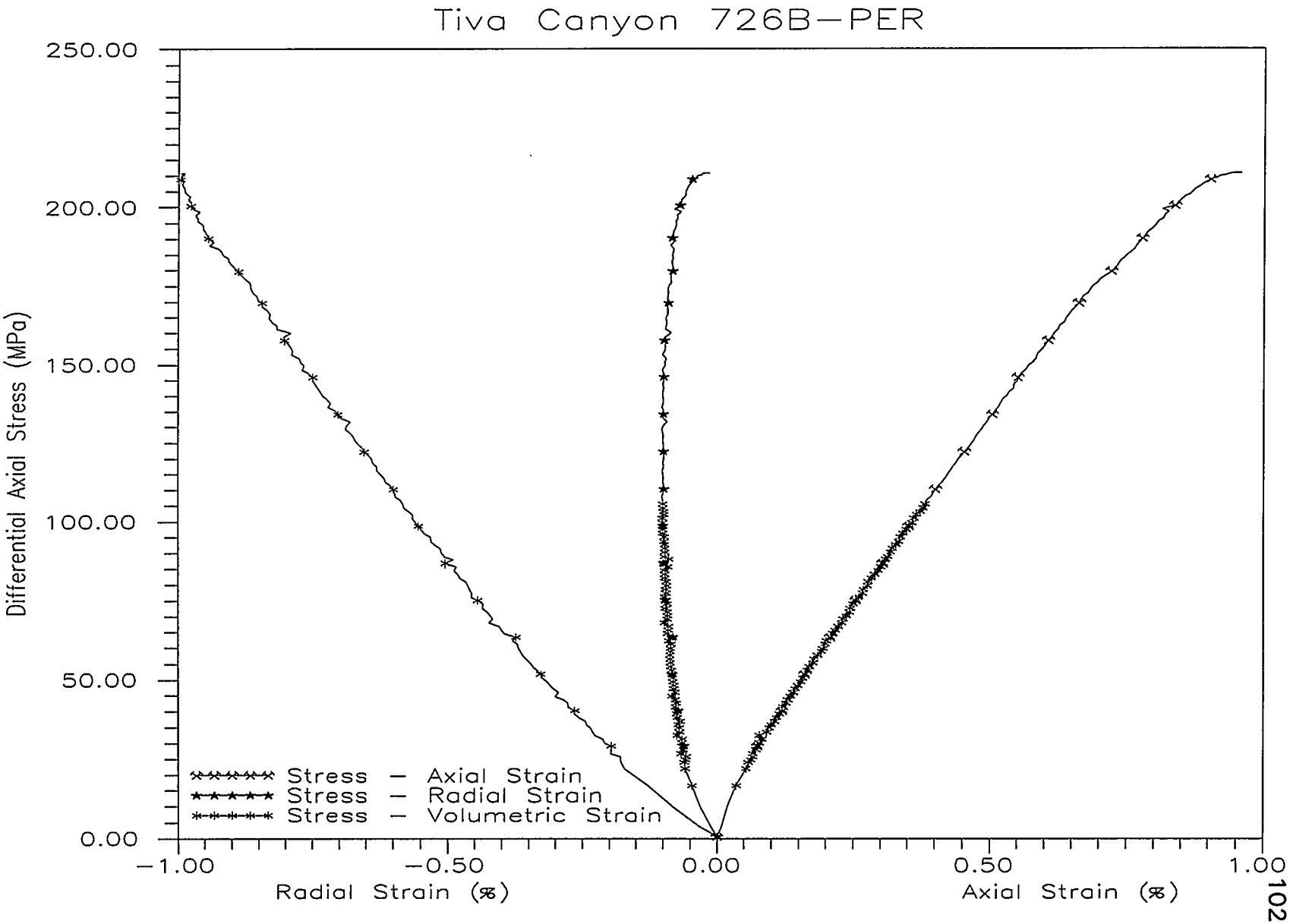
Tiva Canyon 726B—PER
250.00
200.00
150.00
100.00
50.00
0.00
Differential Axial Stress (MPa)
Stress — Axial Strain
Stress — Radial Strain
Stress — Volumetric Strain
−1.00
−0.50
0.00
0.50
1.00
Radial Strain (%)
Axial Strain (%)

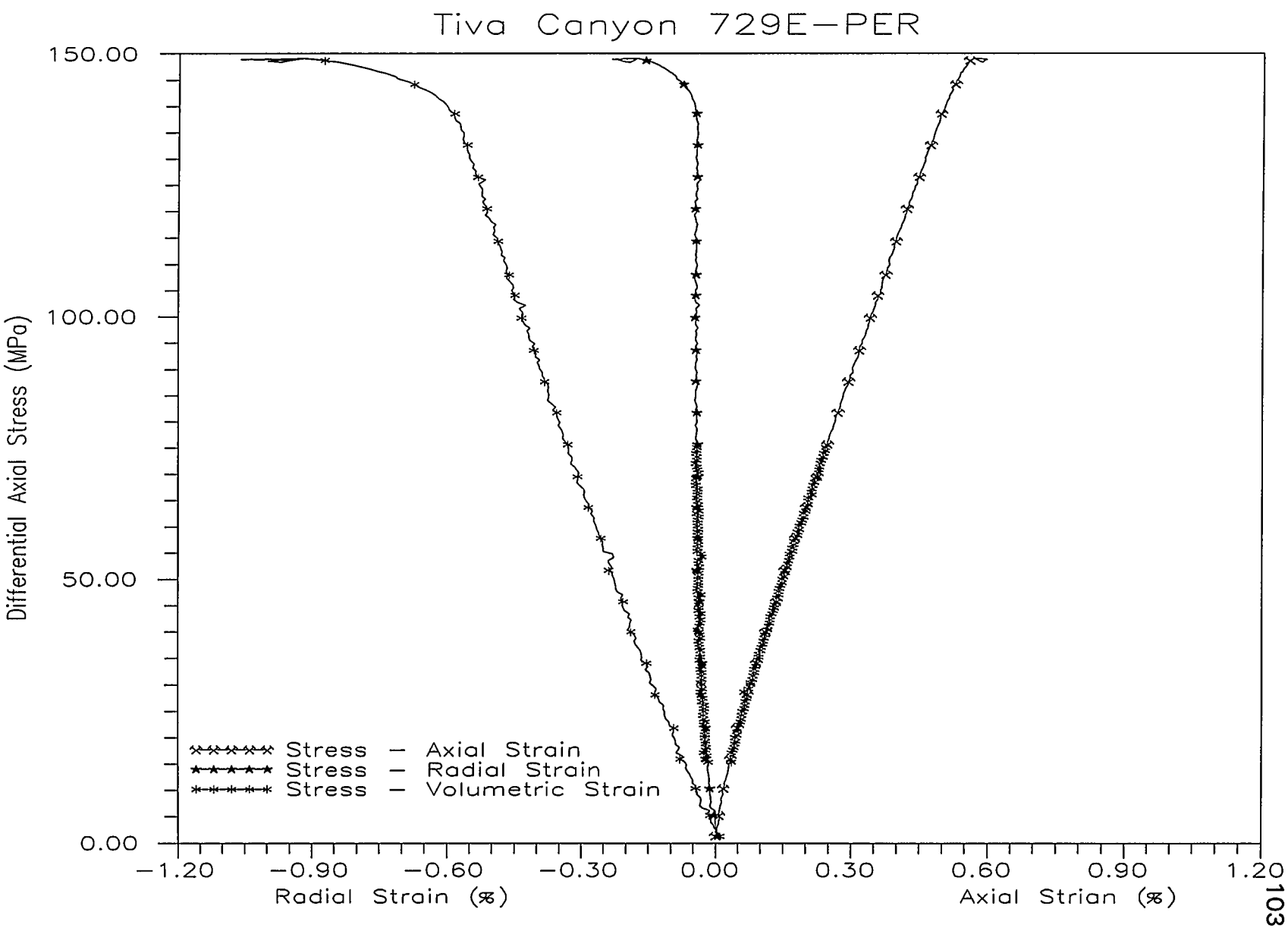
Tiva Canyon 729E—PER
150.00
100.00
50.00
0.00
Differential Axial Stress (MPa)
Stress — Axial Strain
Stress — Radial Strain
Stress — Volumetric Strain
−1.20
−0.90
−0.60
−0.30
0.00
0.30
0.60
0.90
1.20
Radial Strain (%)
Axial Strian (%)

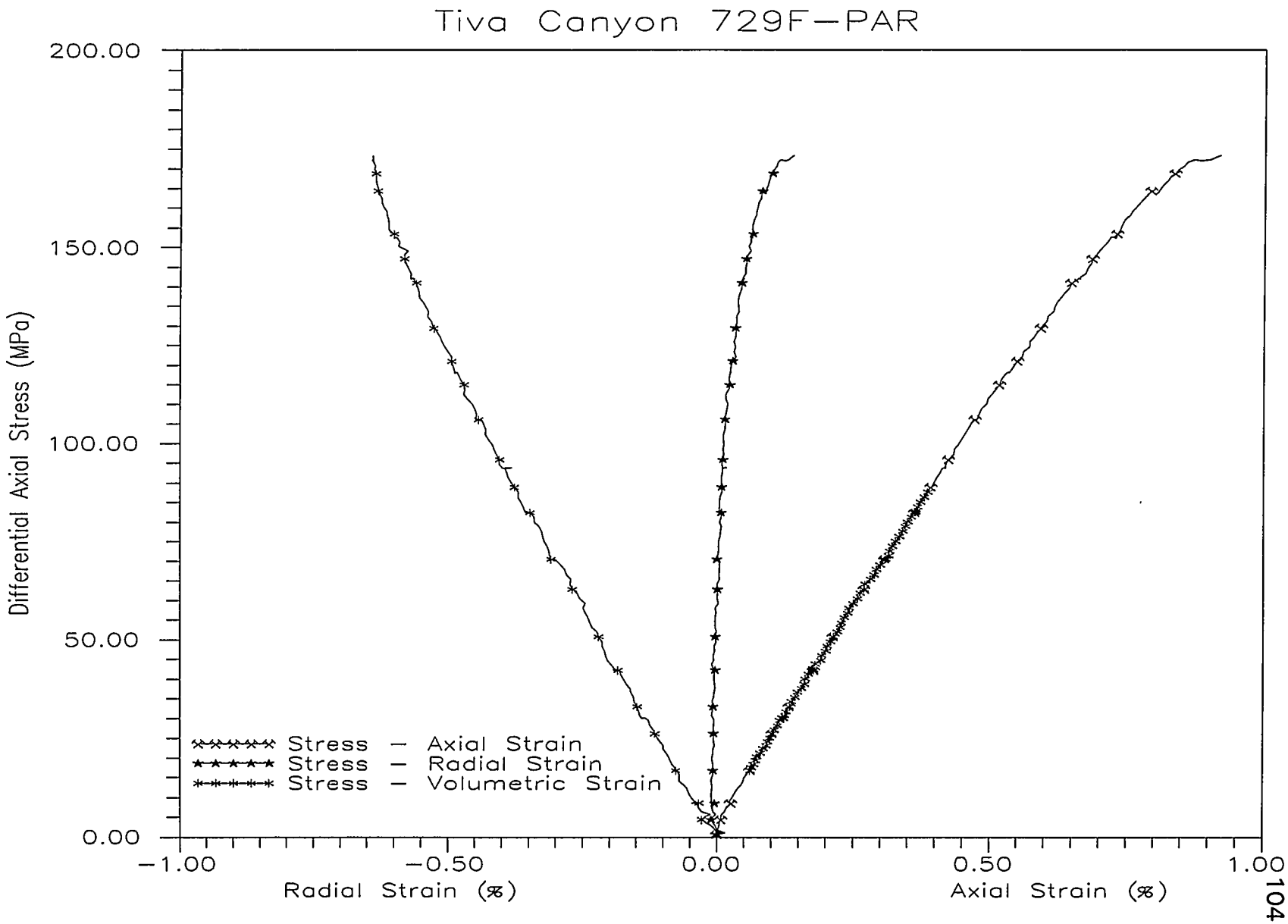
Tiva Canyon 729F—PAR
200.00
150.00
100.00
50.00
0.00
Differential Axial Stress (MPa)
Stress — Axial Strain
Stress — Radial Strain
Stress — Volumetric Strain
−1.00
−0.50
0.00
0.50
1.00
Radial Strain (%)
Axial Strain (%)

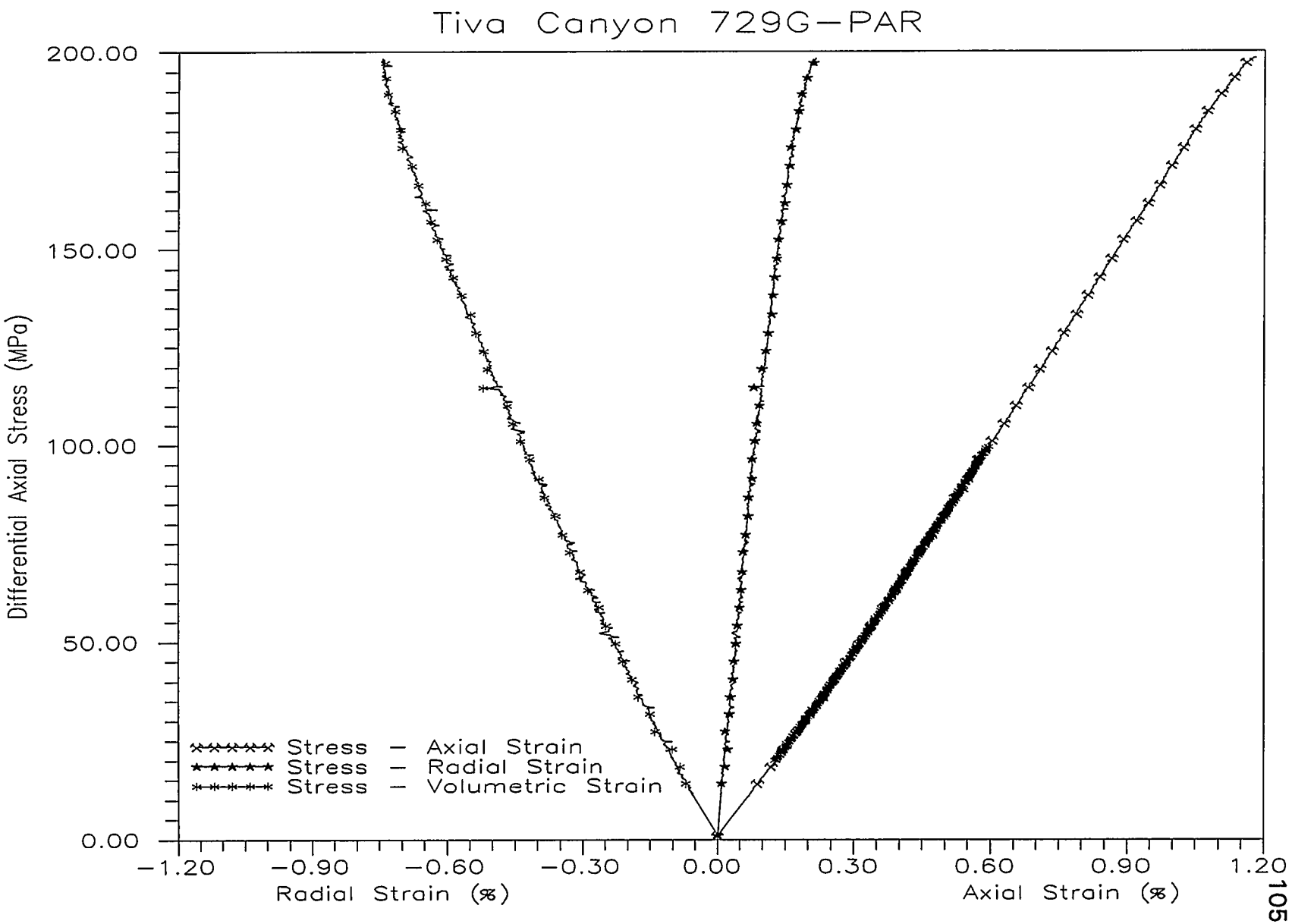
Tiva Canyon 729G—PAR
200.00
150.00
100.00
50.00
0.00
Differential Axial Stress (MPa)
Stress — Axial Strain
Stress — Radial Strain
Stress — Volumetric Strain
−1.20
−0.90
−0.60
−0.30
0.00
0.30
0.60
0.90
1.20
Radial Strain (%)
Axial Strain (%)

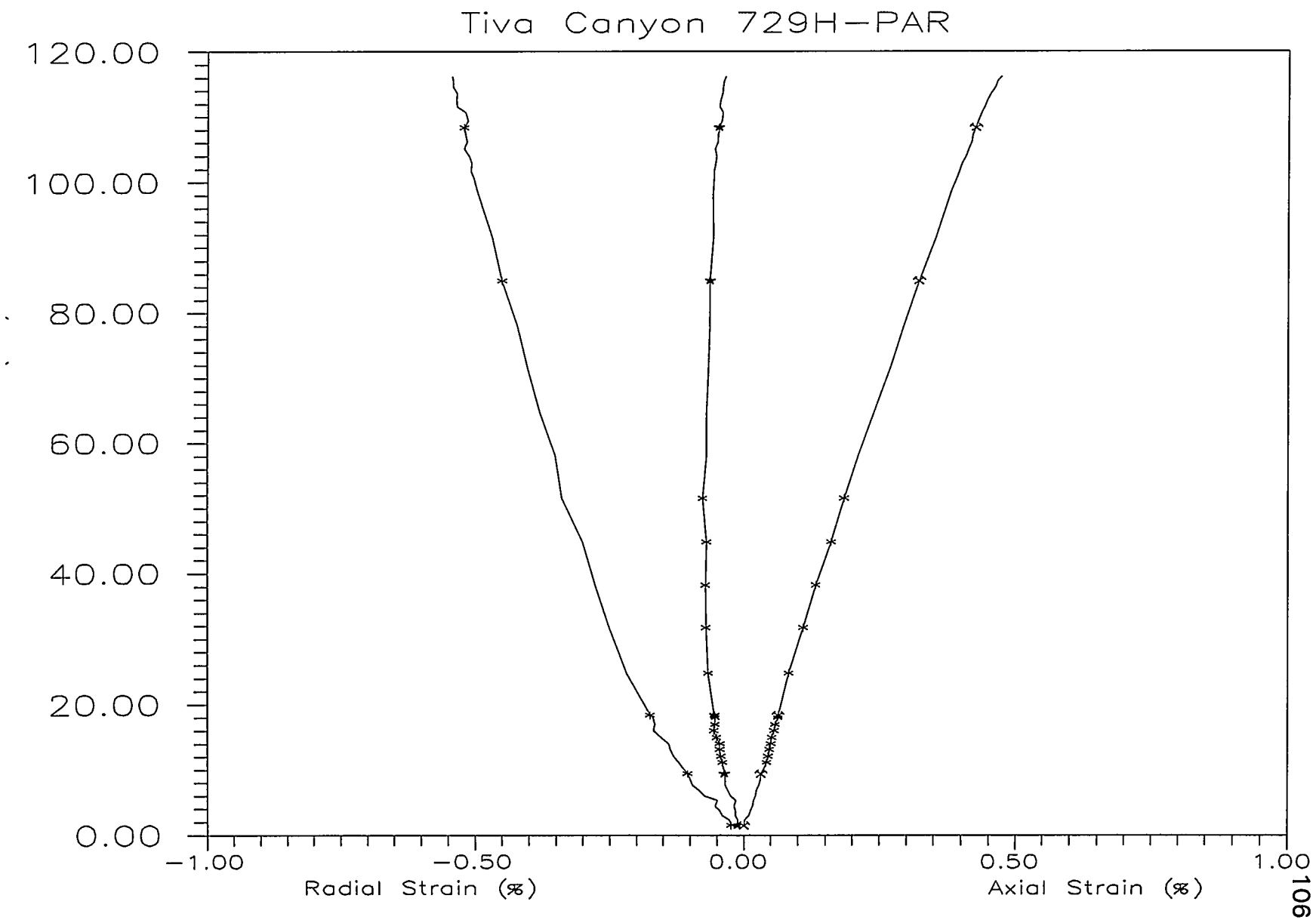
Tiva Canyon 729H-PAR
120.00
100.00
80.00
60.00
40.00
20.00
0.00
-1.00
-0.50
0.00
0.50
1.00
Radial Strain (%)
Axial Strain (%)
106

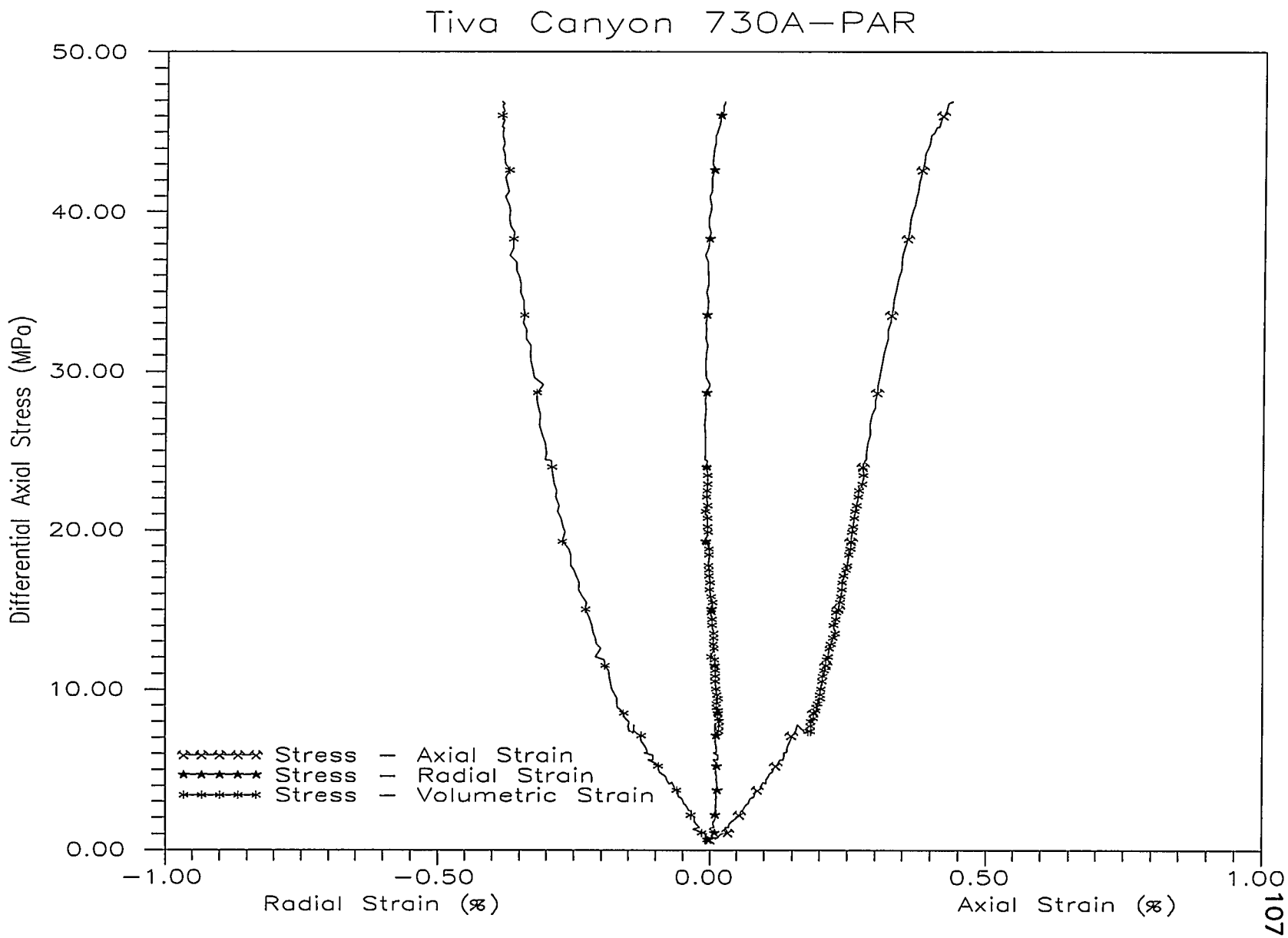
Tiva Canyon 730A—PAR
50.00
40.00
30.00
20.00
10.00
0.00
Differential Axial Stress (MPa)
Stress — Axial Strain
Stress — Radial Strain
Stress — Volumetric Strain
−1.00
−0.50
0.00
0.50
1.00
Radial Strain (%)
Axial Strain (%)
107

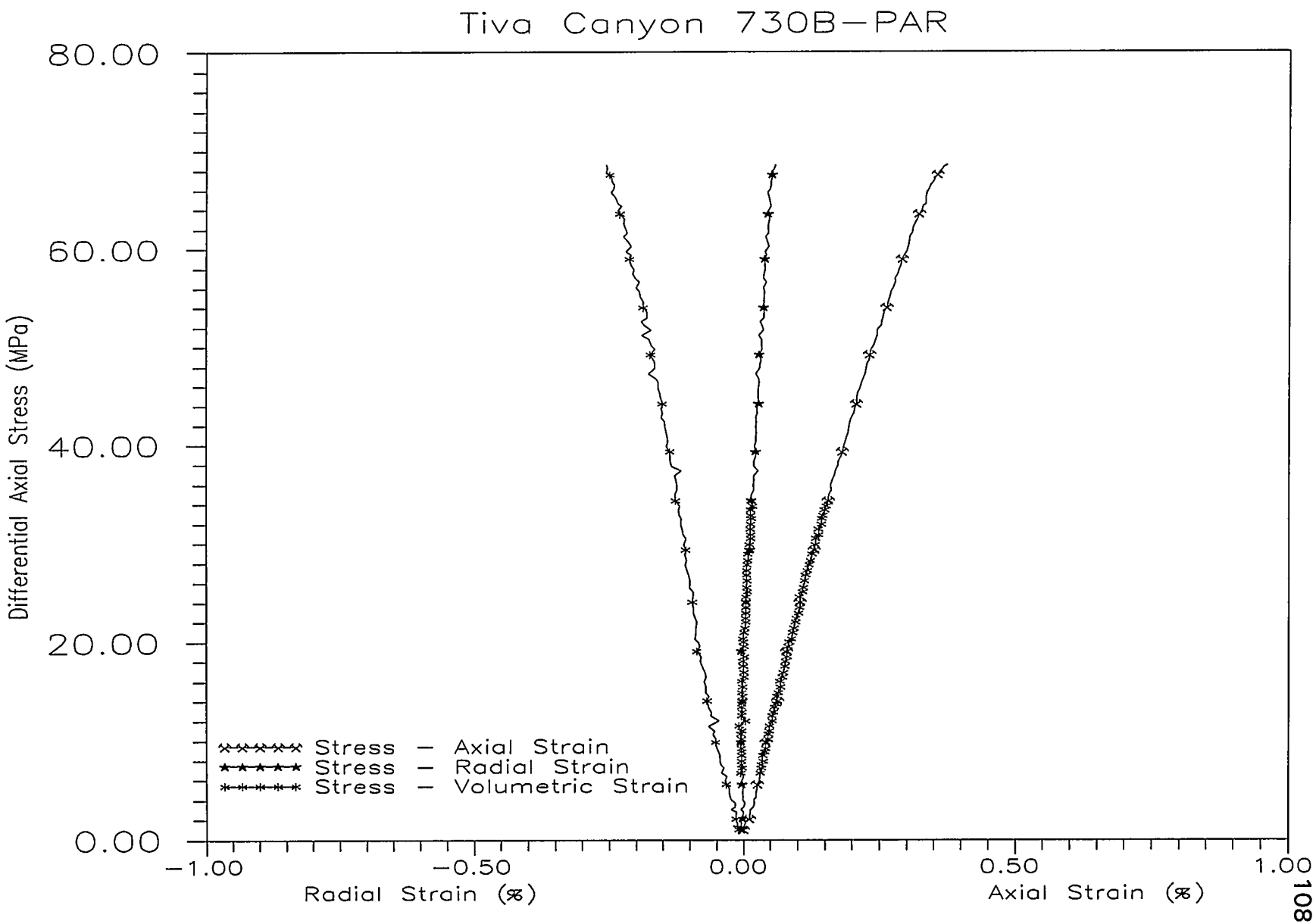
Tiva Canyon 730B—PAR
80.00
60.00
40.00
20.00
0.00
Differential Axial Stress (MPa)
Stress — Axial Strain
Stress — Radial Strain
Stress — Volumetric Strain
−1.00
−0.50
0.00
0.50
1.00
Radial Strain (%)
Axial Strain (%)

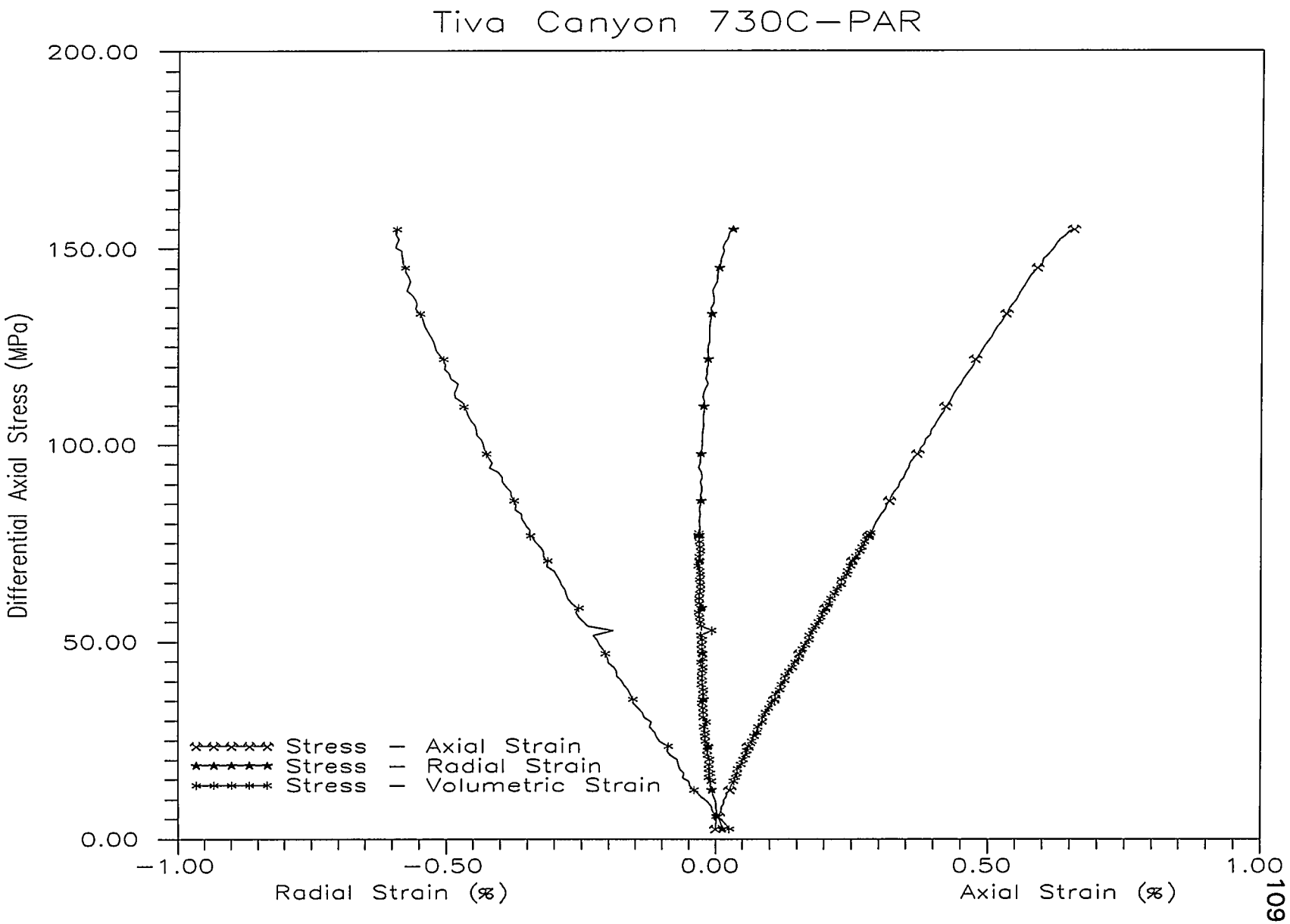
Tiva Canyon 730C—PAR
200.00
150.00
100.00
50.00
0.00
Differential Axial Stress (MPa)
Stress — Axial Strain
Stress — Radial Strain
Stress — Volumetric Strain
−1.00
−0.50
0.00
0.50
1.00
Radial Strain (%)
Axial Strain (%)

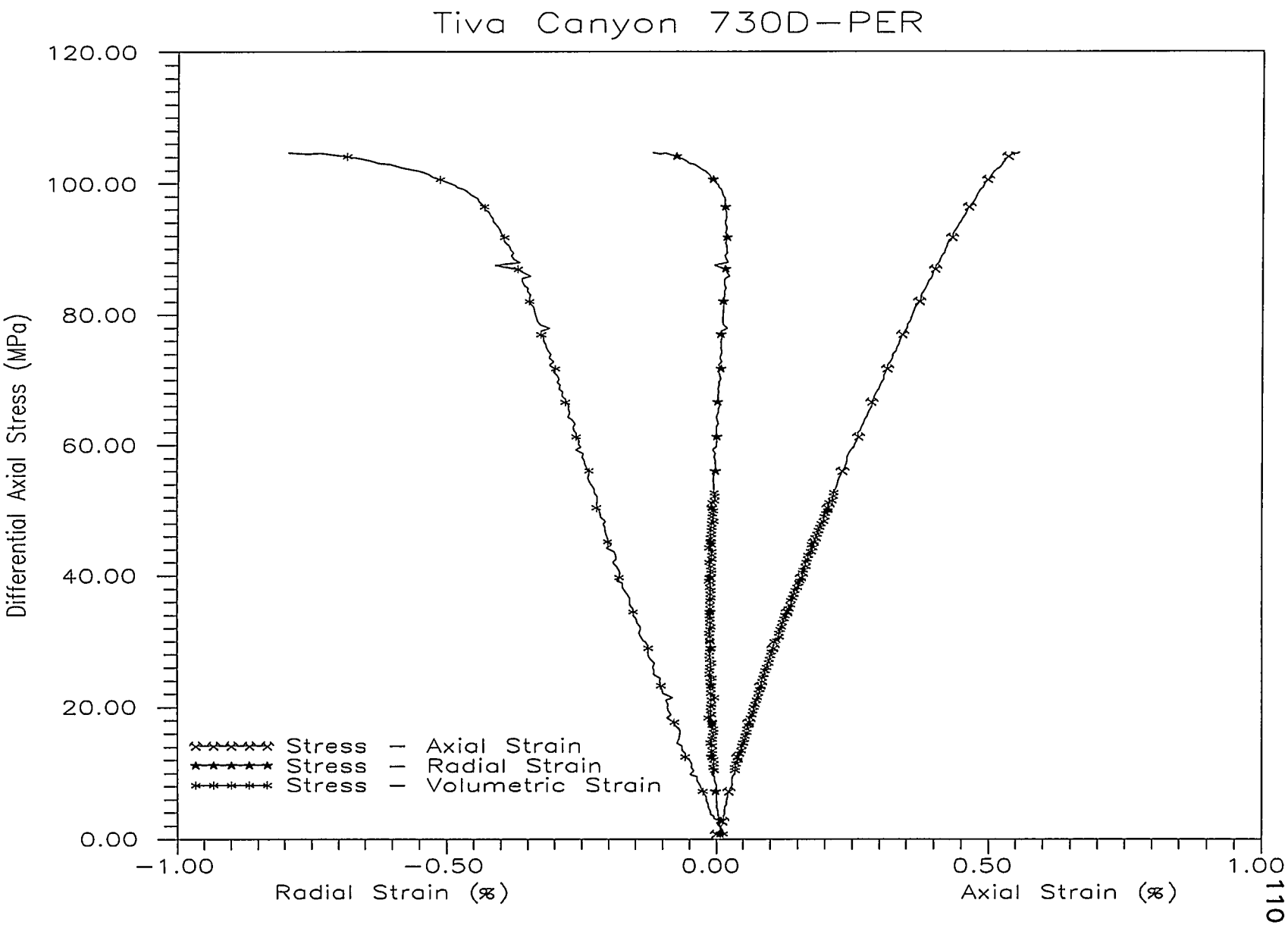
Tiva Canyon 730D—PER
120.00
100.00
80.00
60.00
40.00
20.00
0.00
Differential Axial Stress (MPa)
Stress — Axial Strain
Stress — Radial Strain
Stress — Volumetric Strain
−1.00
−0.50
0.00
0.50
1.00
Radial Strain (%)
Axial Strain (%)

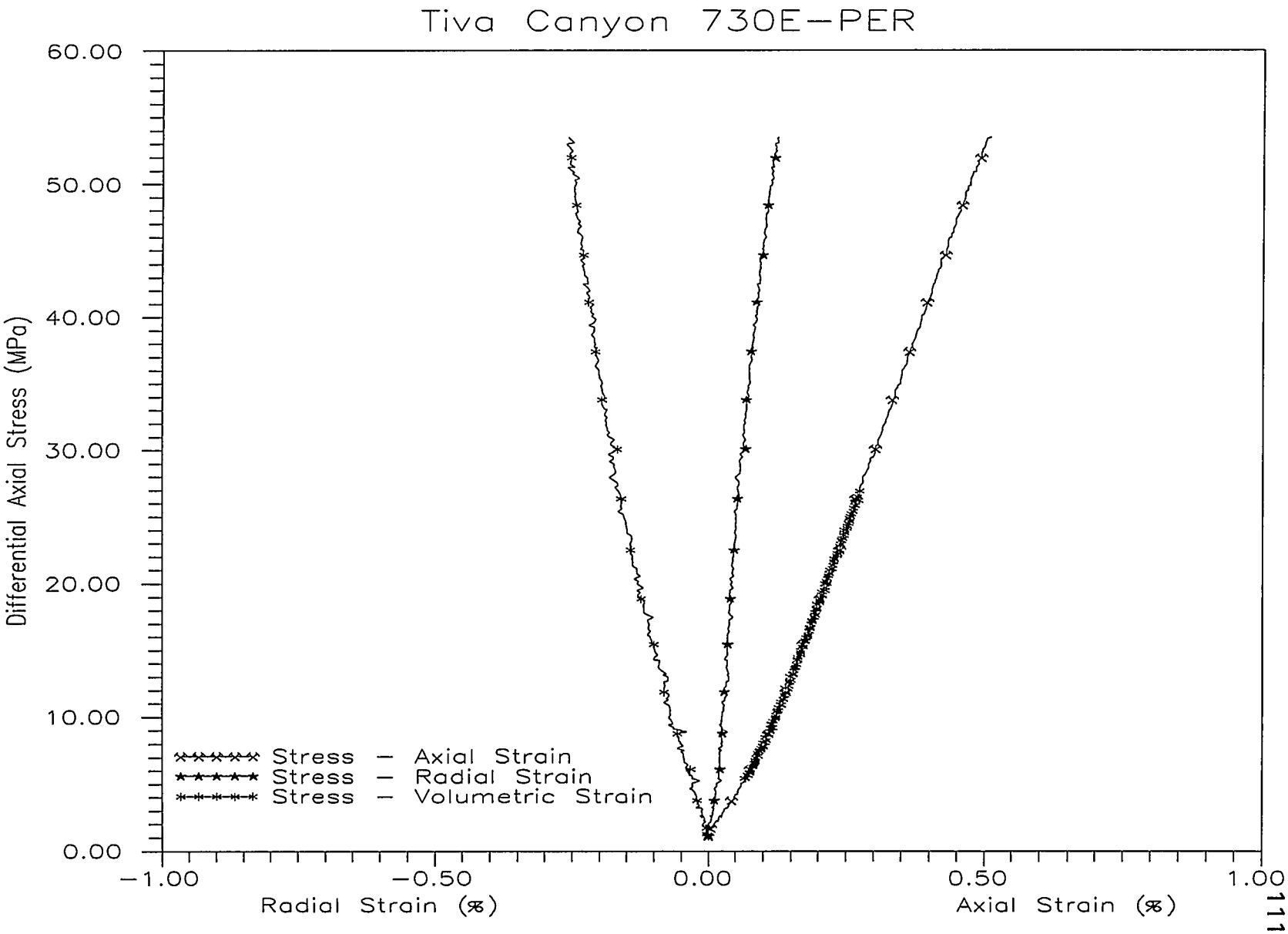
Tiva Canyon 730E-PER
60.00
50.00
40.00
30.00
20.00
10.00
0.00
Differential Axial Stress (MPa)
Stress - Axial Strain
Stress - Radial Strain
Stress - Volumetric Strain
-1.00
-0.50
0.00
0.50
1.00
Radial Strain (%)
Axial Strain (%)

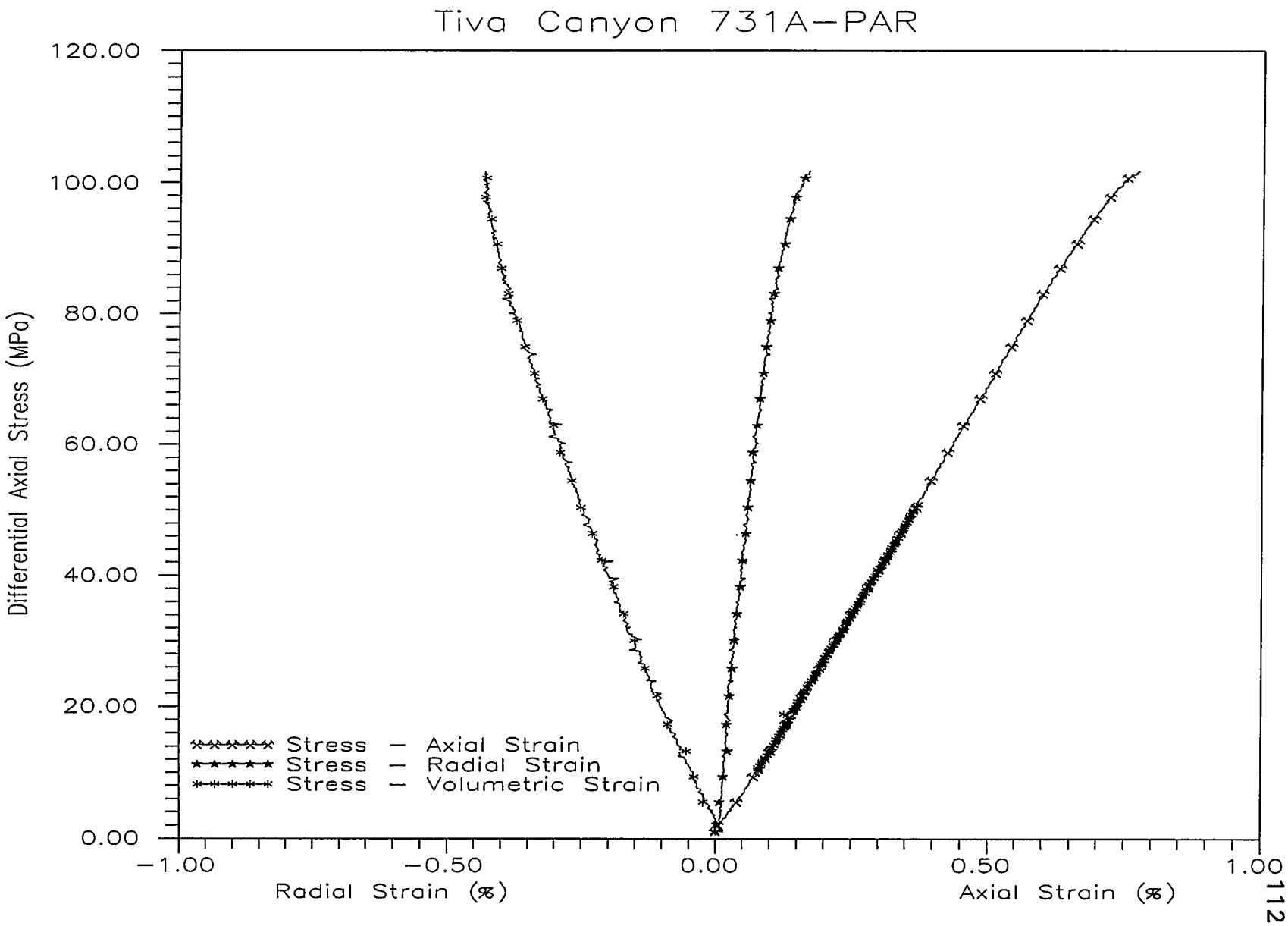
Tiva Canyon 731A—PAR
120.00
100.00
80.00
60.00
40.00
20.00
0.00
Differential Axial Stress (MPa)
Stress — Axial Strain
Stress — Radial Strain
Stress — Volumetric Strain
−1.00
−0.50
0.00
0.50
1.00
Radial Strain (%)
Axial Strain (%)

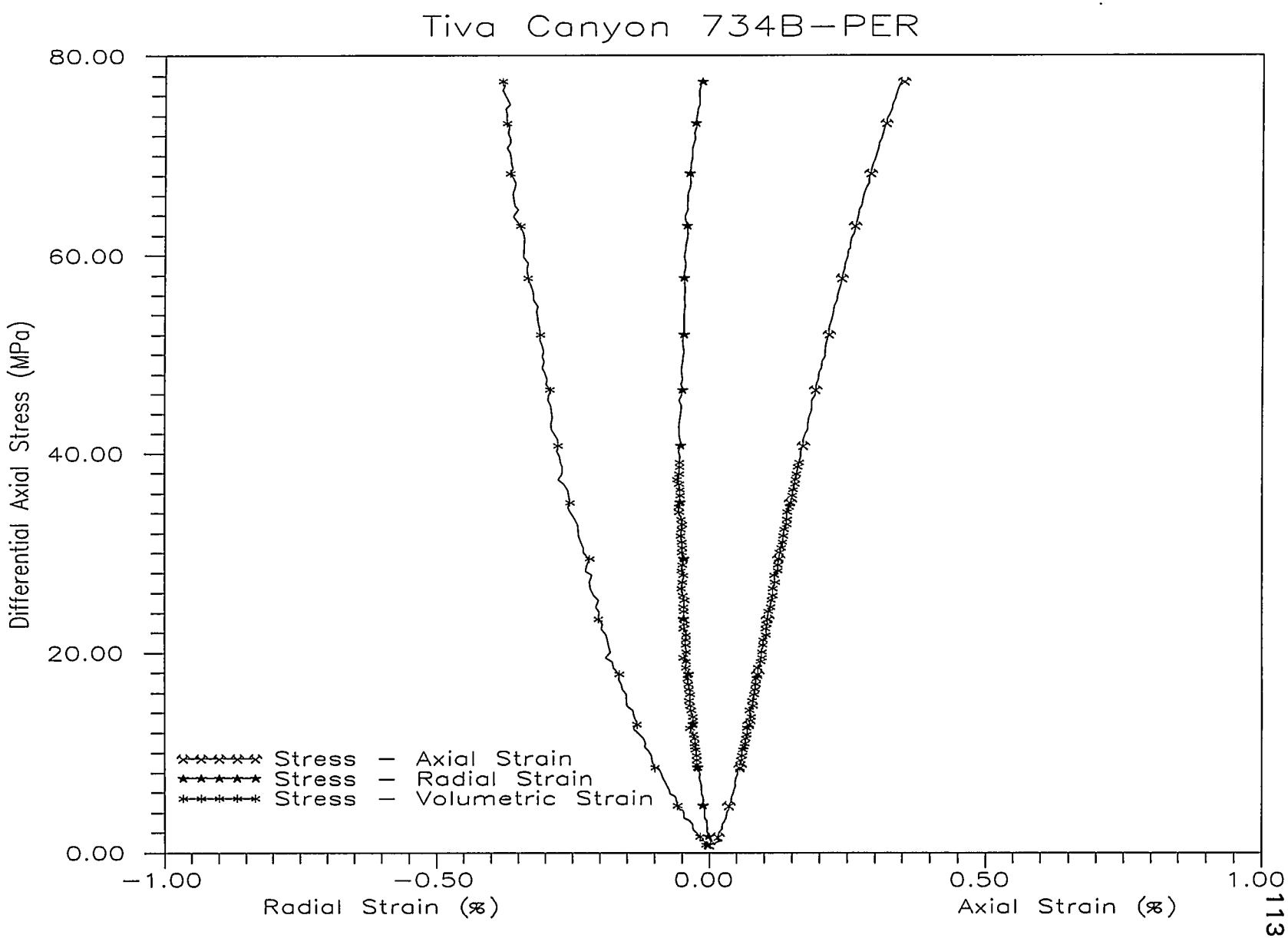
Tiva Canyon 734B—PER
80.00
60.00
40.00
20.00
0.00
Differential Axial Stress (MPa)
Stress — Axial Strain
Stress — Radial Strain
Stress — Volumetric Strain
−1.00
−0.50
0.00
0.50
1.00
Radial Strain (%)
Axial Strain (%)

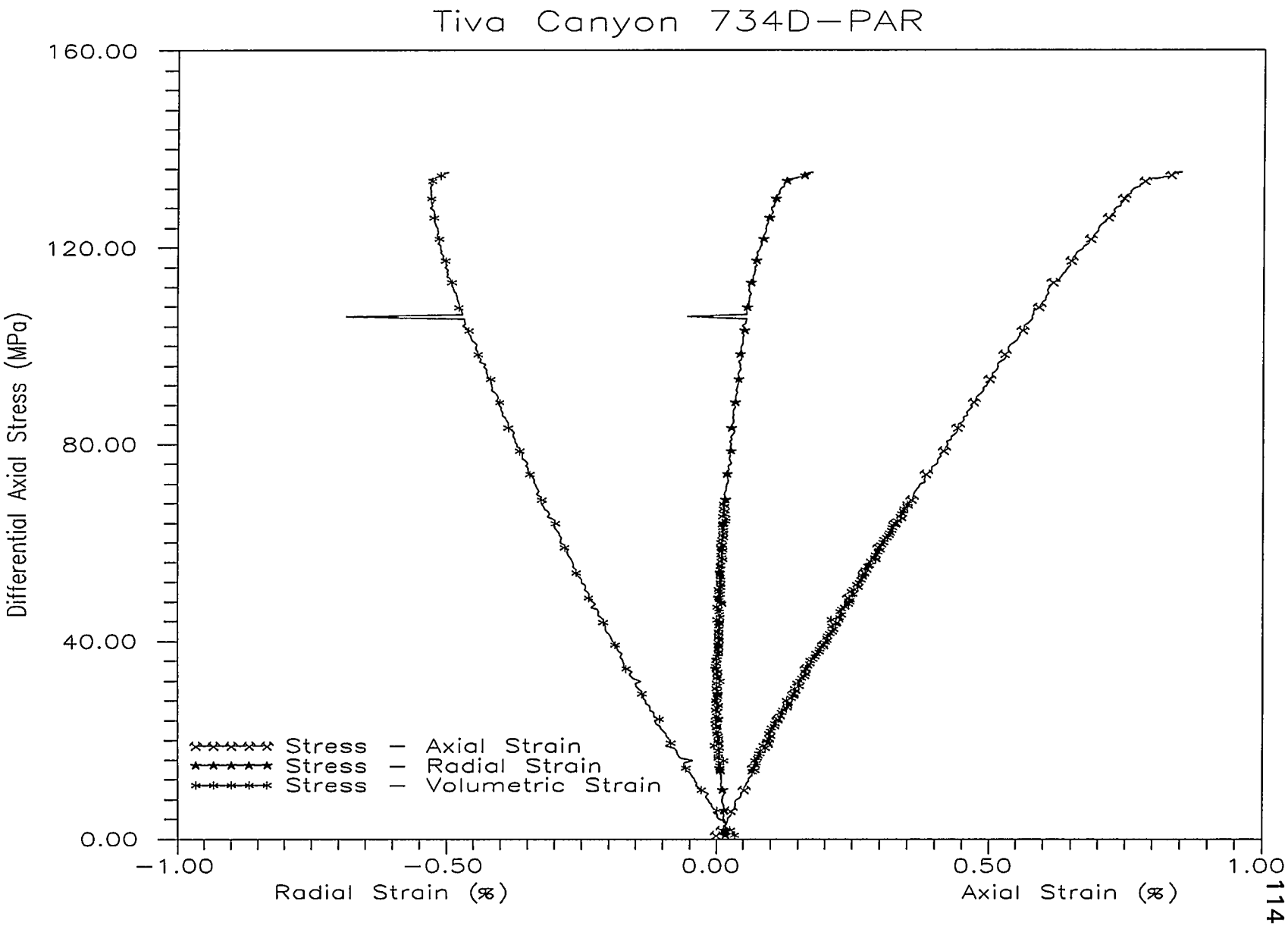
Tiva Canyon 734D—PAR
160.00
120.00
80.00
40.00
0.00
Differential Axial Stress (MPa)
Stress — Axial Strain
Stress — Radial Strain
Stress — Volumetric Strain
−1.00
−0.50
0.00
0.50
1.00
Radial Strain (%)
Axial Strain (%)

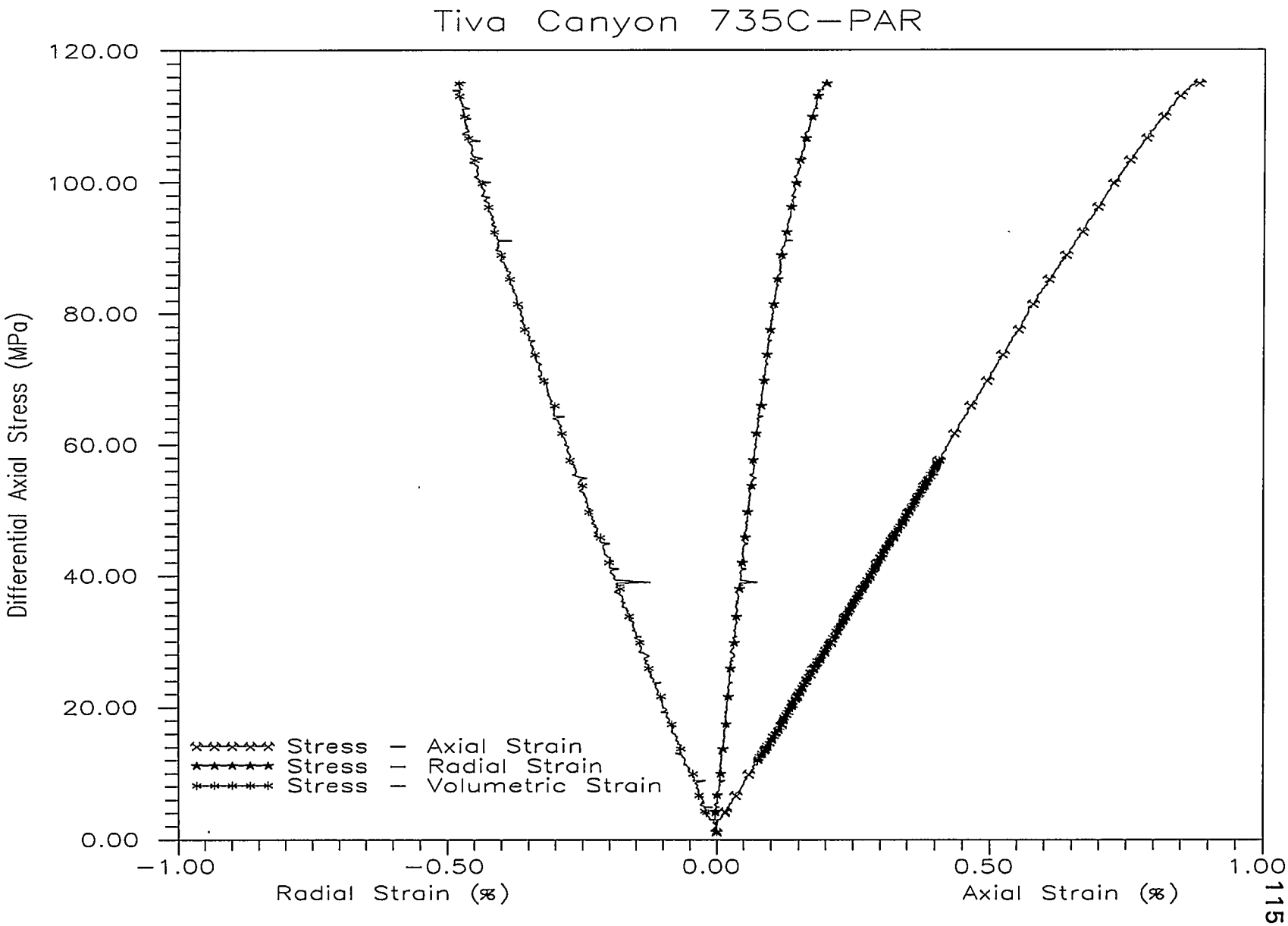
Tiva Canyon 735C—PAR
120.00
100.00
80.00
60.00
40.00
20.00
0.00
Differential Axial Stress (MPa)
Stress — Axial Strain
Stress — Radial Strain
Stress — Volumetric Strain
−1.00
−0.50
0.00
0.50
1.00
Radial Strain (%)
Axial Strain (%)

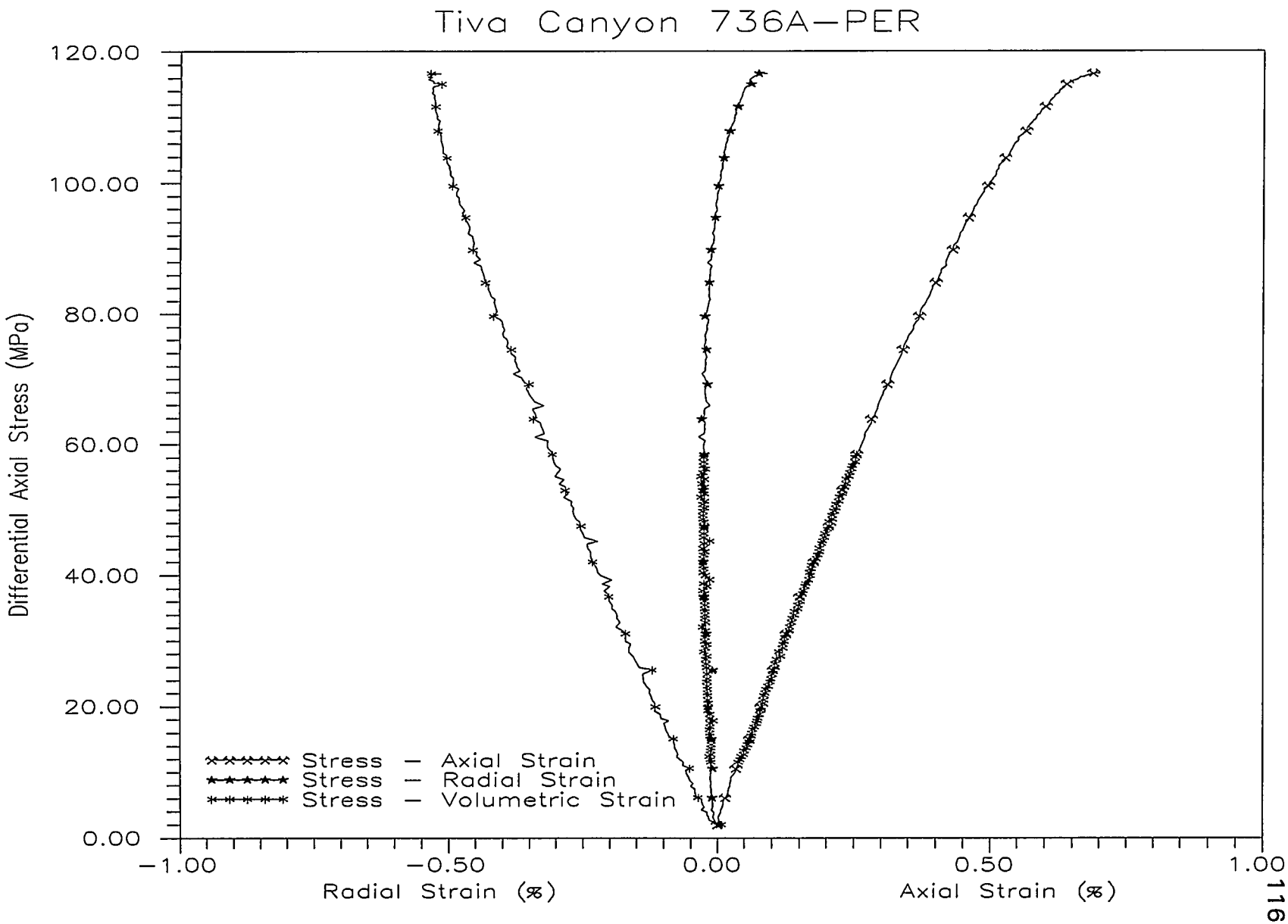
Tiva Canyon 736A—PER
120.00
100.00
80.00
60.00
40.00
20.00
0.00
Differential Axial Stress (MPa)
Stress — Axial Strain
Stress — Radial Strain
Stress — Volumetric Strain
−1.00
−0.50
0.00
0.50
1.00
Radial Strain (%)
Axial Strain (%)

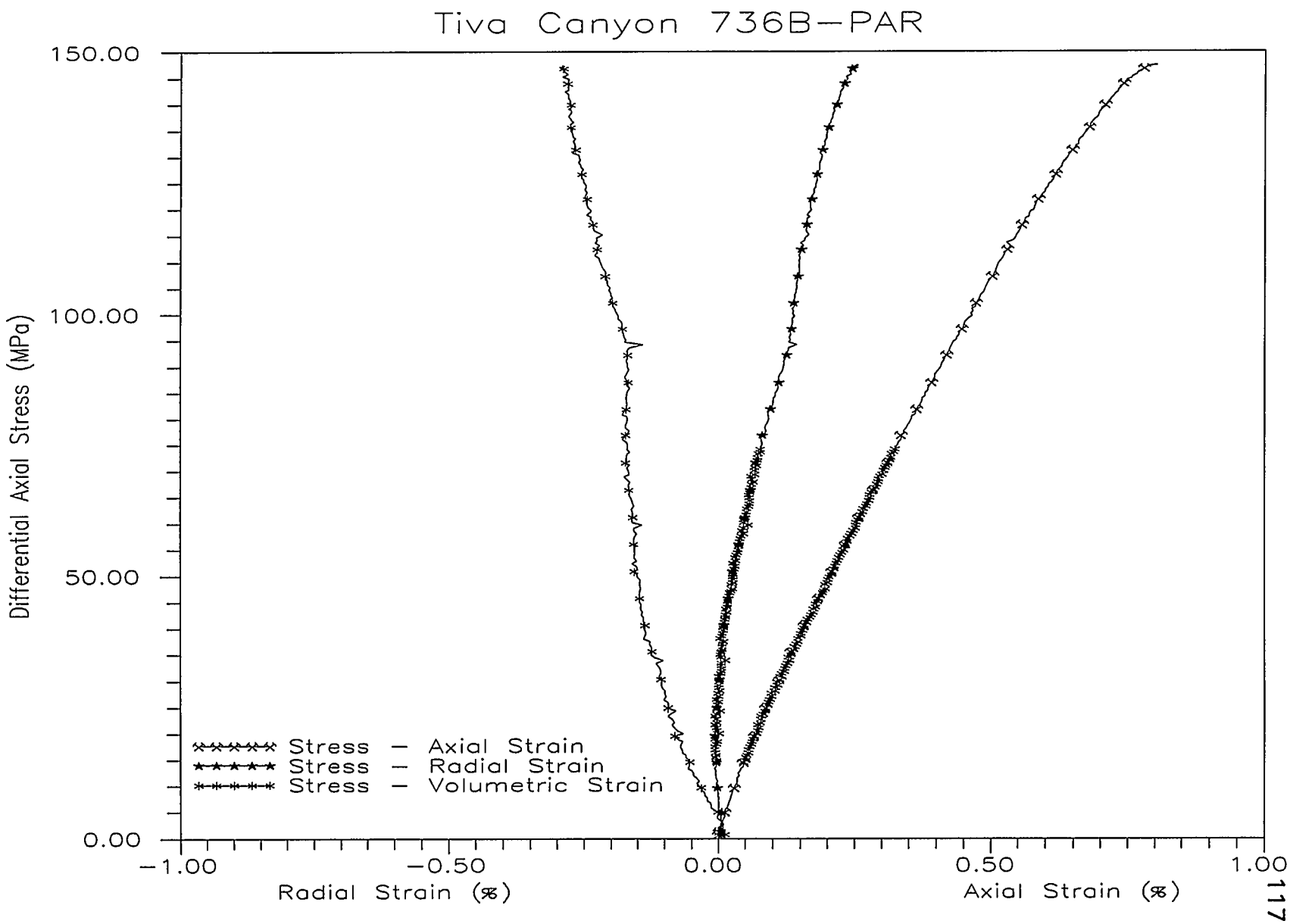
Tiva Canyon 736B—PAR
150.00
100.00
50.00
0.00
Differential Axial Stress (MPa)
Stress — Axial Strain
Stress — Radial Strain
Stress — Volumetric Strain
−1.00
−0.50
0.00
0.50
1.00
Radial Strain (%)
Axial Strain (%)

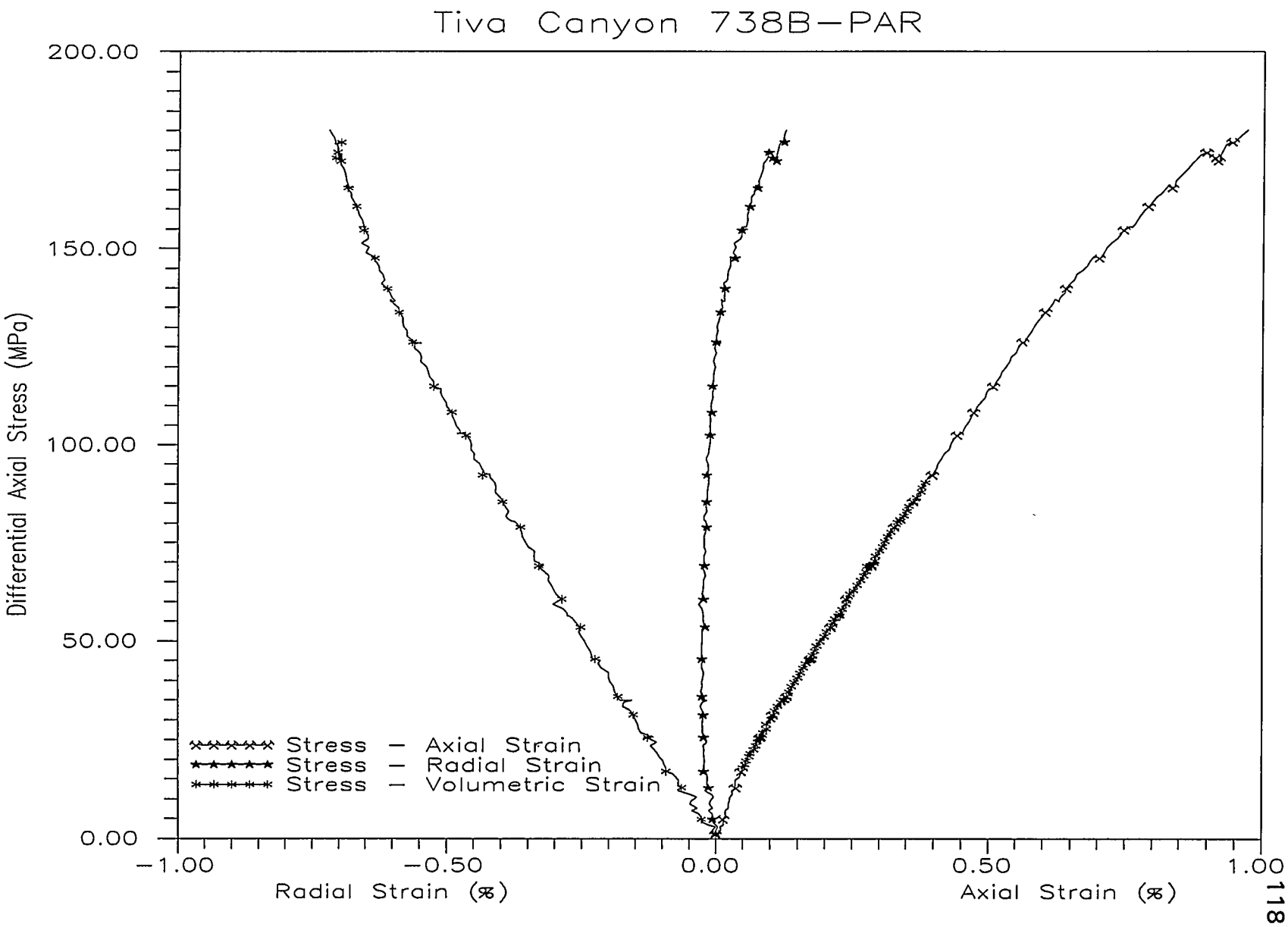
Tiva Canyon 738B—PAR
200.00
150.00
100.00
50.00
0.00
Differential Axial Stress (MPa)
Stress — Axial Strain
Stress — Radial Strain
Stress — Volumetric Strain
−1.00
−0.50
0.00
0.50
1.00
Radial Strain (%)
Axial Strain (%)

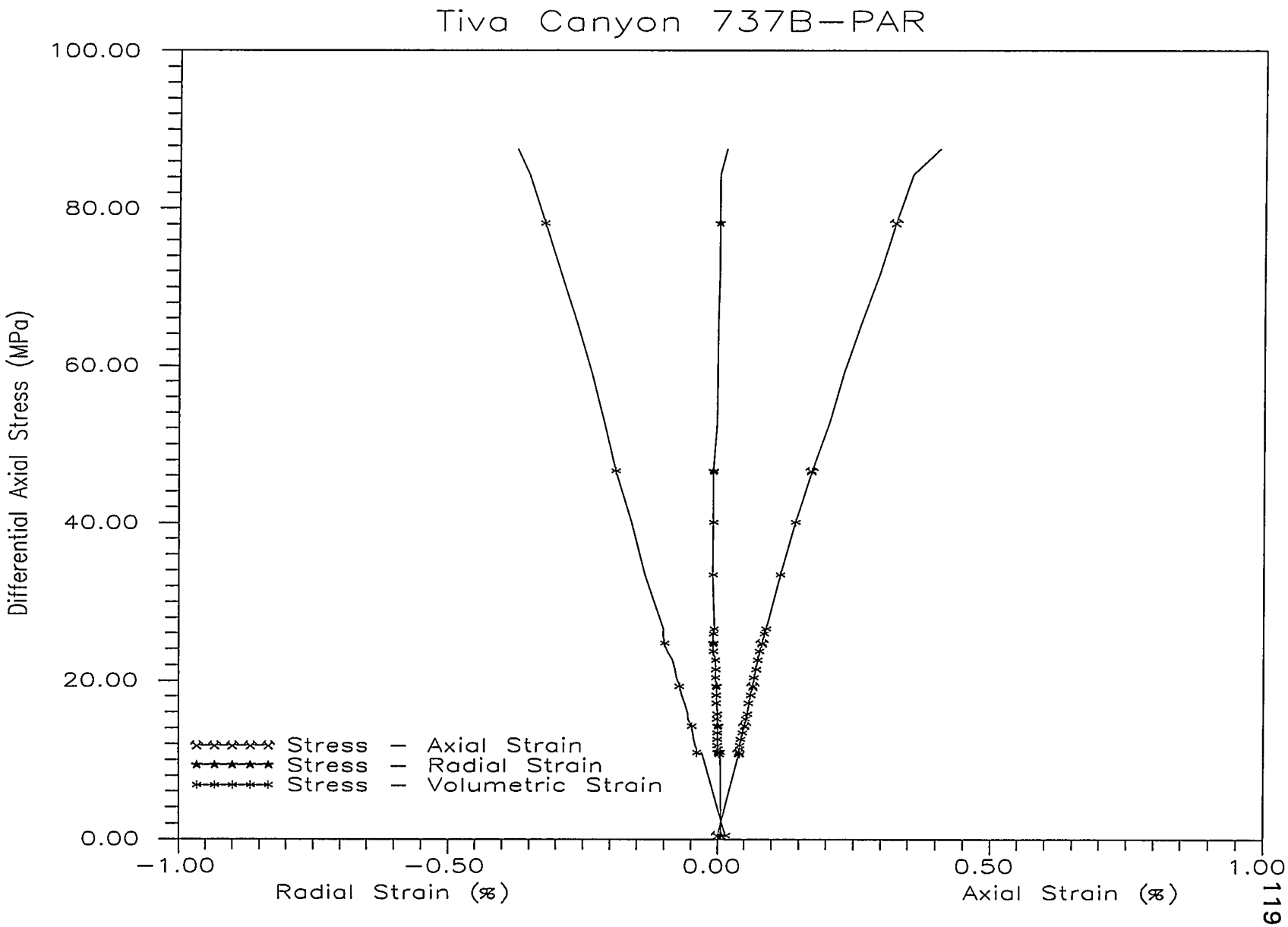
Tiva Canyon 737B-PAR
100.00
80.00
60.00
40.00
20.00
0.00
Differential Axial Stress (MPa)
Stress - Axial Strain
Stress - Radial Strain
Stress - Volumetric Strain
-1.00
-0.50
0.00
0.50
1.00
Radial Strain (%)
Axial Strain (%)

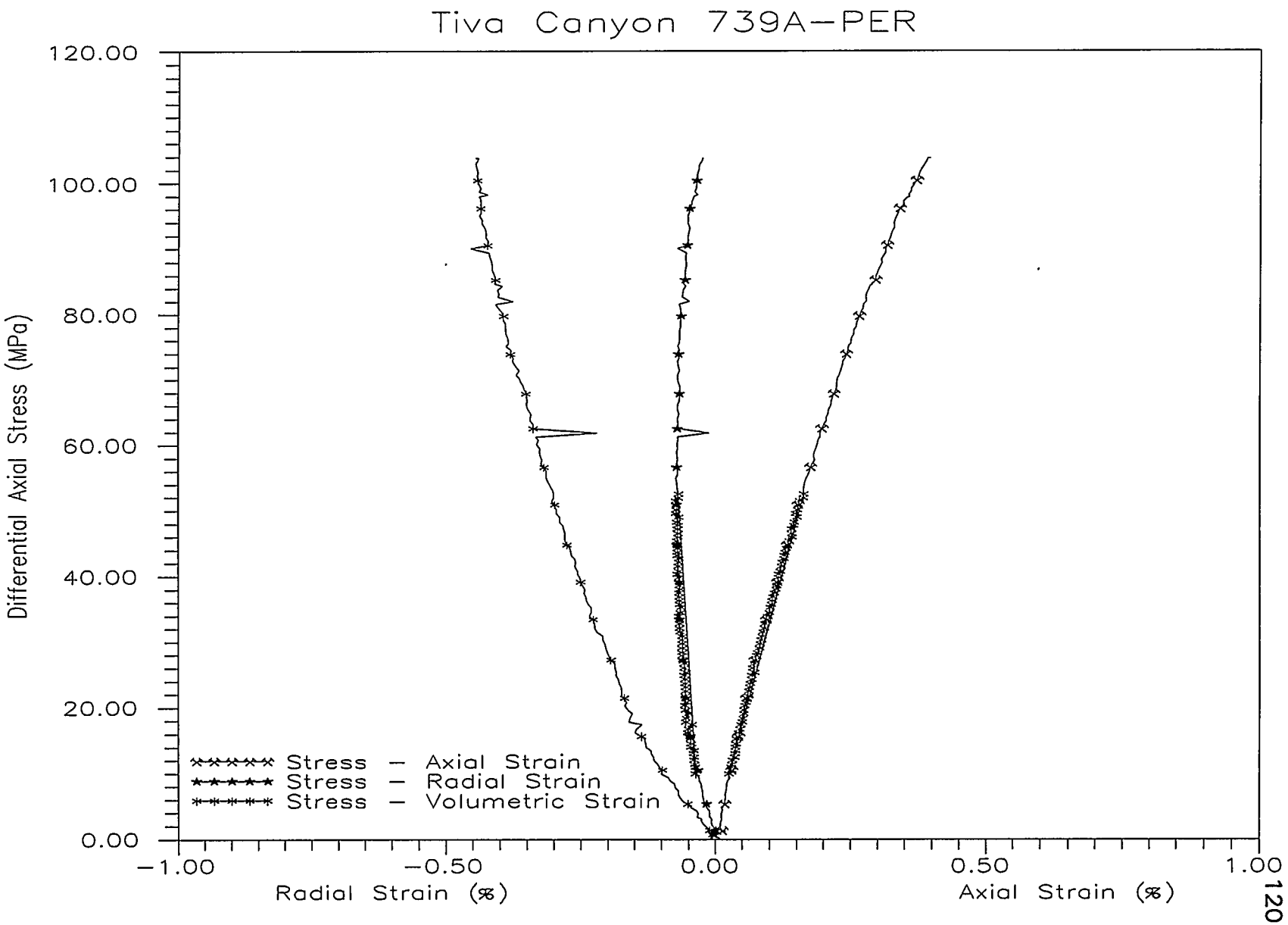
Tiva Canyon 739A-PER
120.00
100.00
80.00
60.00
40.00
20.00
0.00
Differential Axial Stress (MPa)
Stress - Axial Strain
Stress - Radial Strain
Stress - Volumetric Strain
-1.00
-0.50
0.00
0.50
1.00
Radial Strain (%)
Axial Strain (%)
120

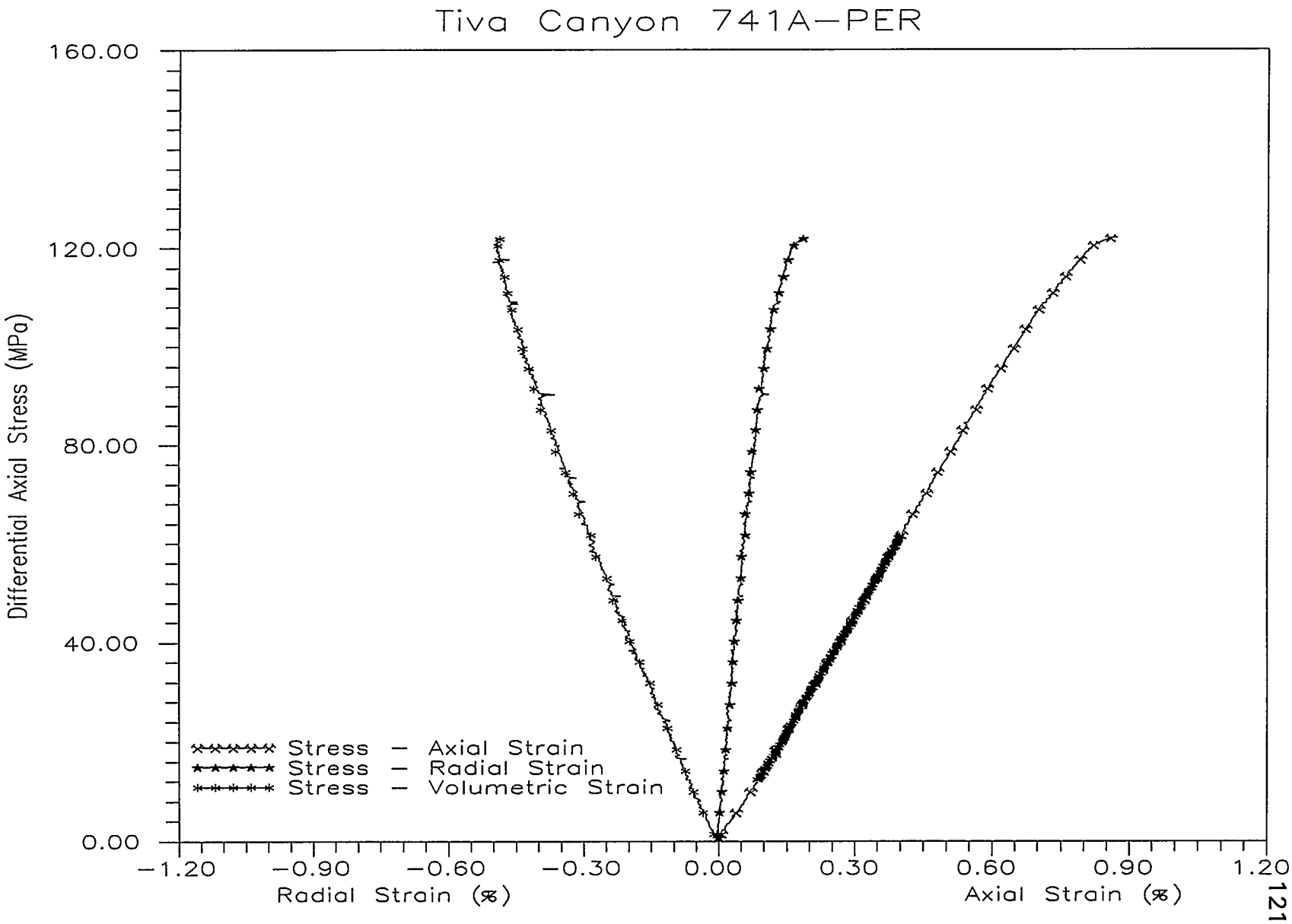
Tiva Canyon 741A—PER
160.00
120.00
80.00
40.00
0.00
Differential Axial Stress (MPa)
Stress — Axial Strain
Stress — Radial Strain
Stress — Volumetric Strain
−1.20
−0.90
−0.60
−0.30
0.00
0.30
0.60
0.90
1.20
Radial Strain (%)
Axial Strain (%)

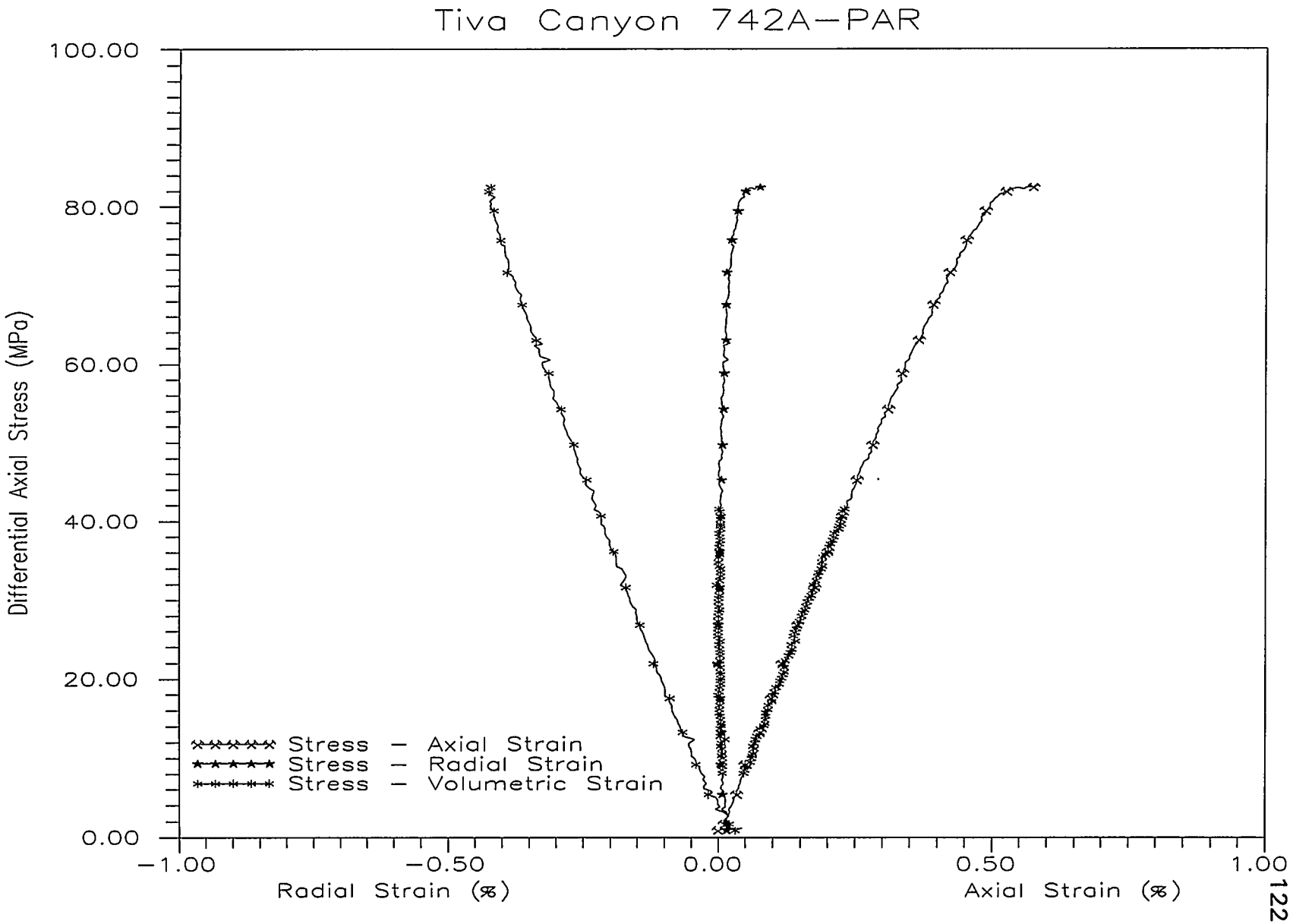
Tiva Canyon 742A-PAR
100.00
80.00
60.00
40.00
20.00
0.00
Differential Axial Stress (MPa)
Stress - Axial Strain
Stress - Radial Strain
Stress - Volumetric Strain
-1.00
-0.50
0.00
0.50
1.00
Radial Strain (%)
Axial Strain (%)

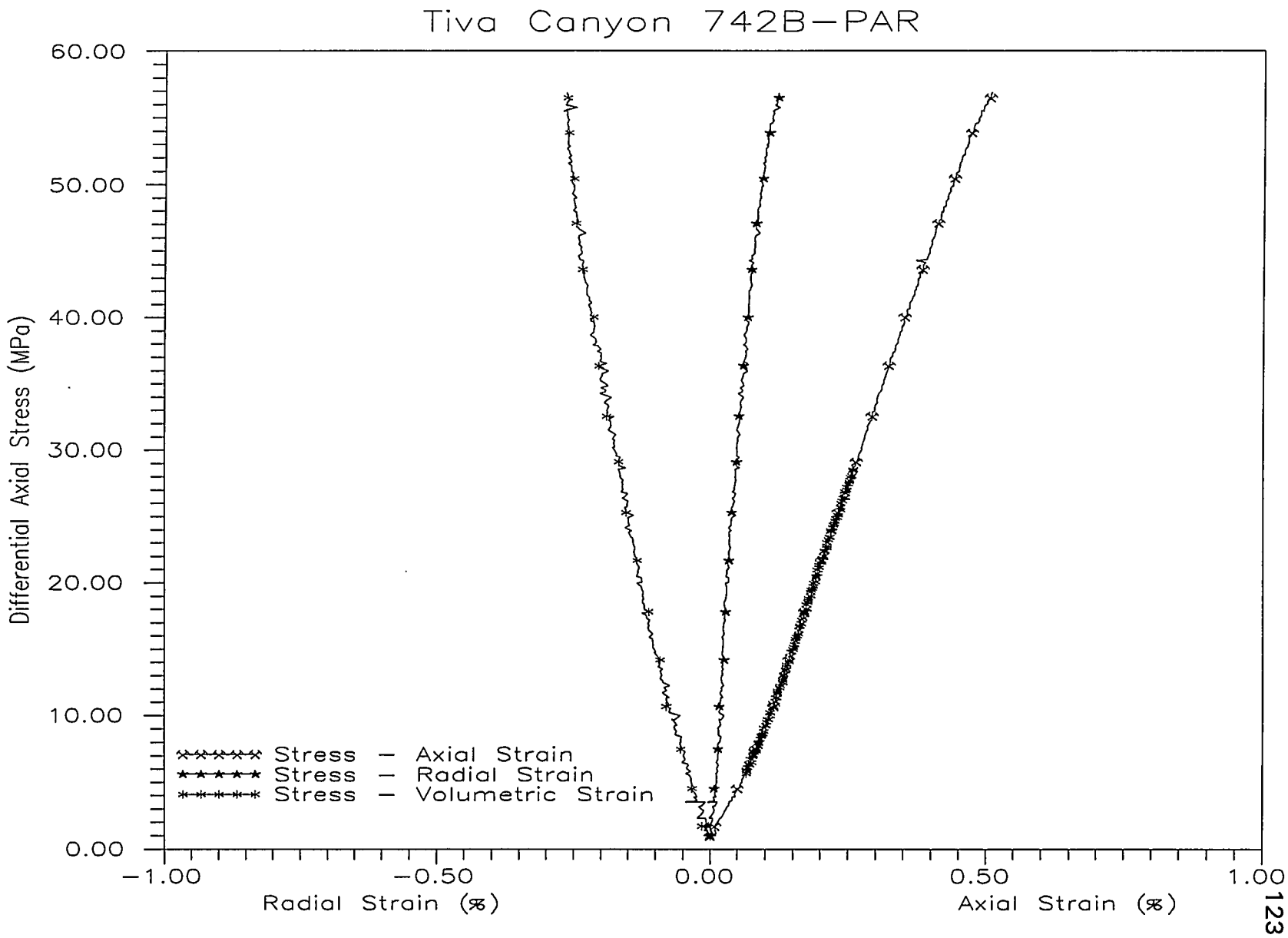
Tiva Canyon 742B—PAR
60.00
50.00
40.00
30.00
20.00
10.00
0.00
Differential Axial Stress (MPa)
Stress — Axial Strain
Stress — Radial Strain
Stress — Volumetric Strain
−1.00
−0.50
0.00
0.50
1.00
Radial Strain (%)
Axial Strain (%)

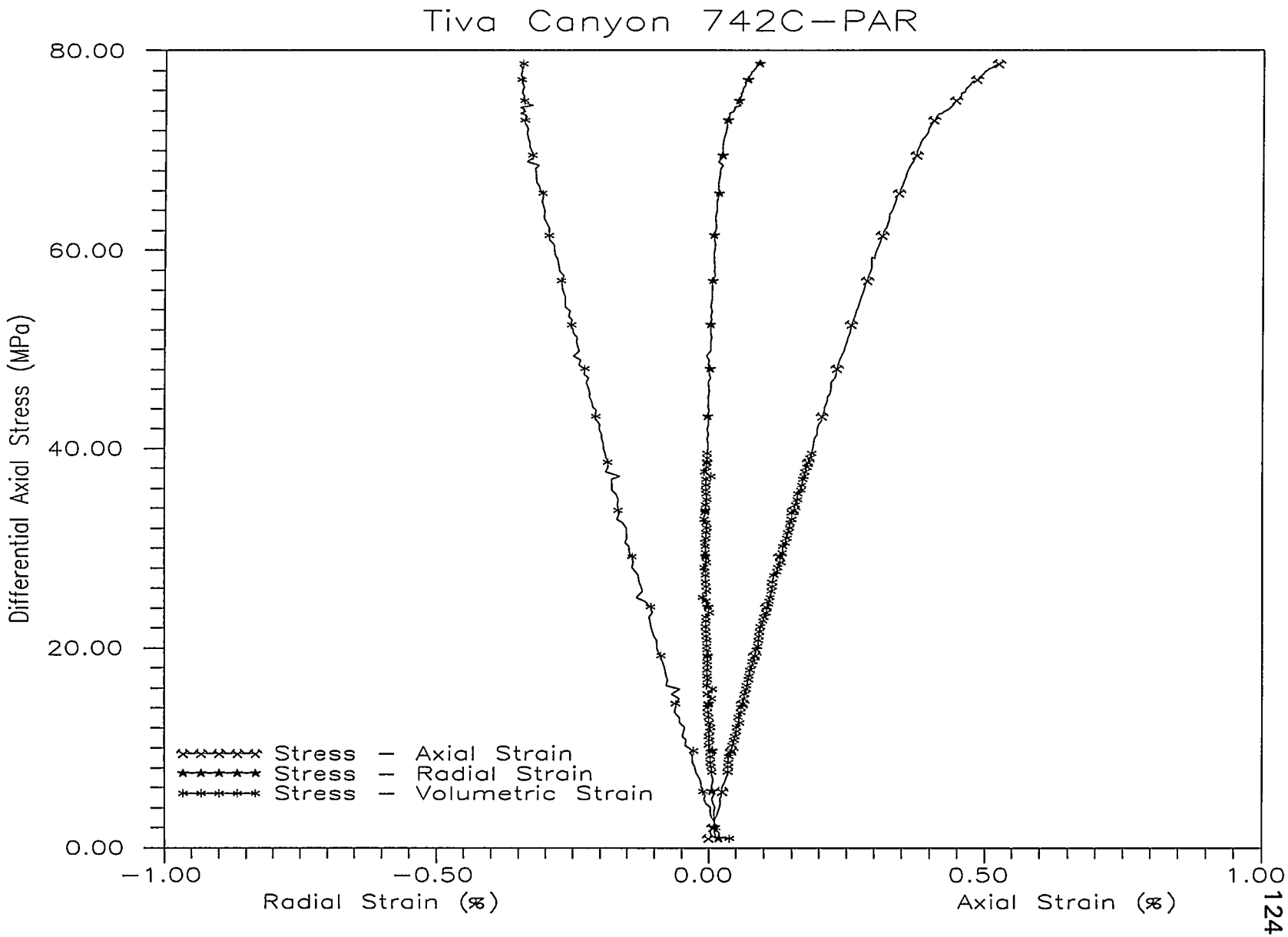
Tiva Canyon 742C-PAR
80.00
60.00
40.00
20.00
0.00
Differential Axial Stress (MPa)
Stress - Axial Strain
Stress - Radial Strain
Stress - Volumetric Strain
-1.00
-0.50
0.00
0.50
1.00
Radial Strain (%)
Axial Strain (%)

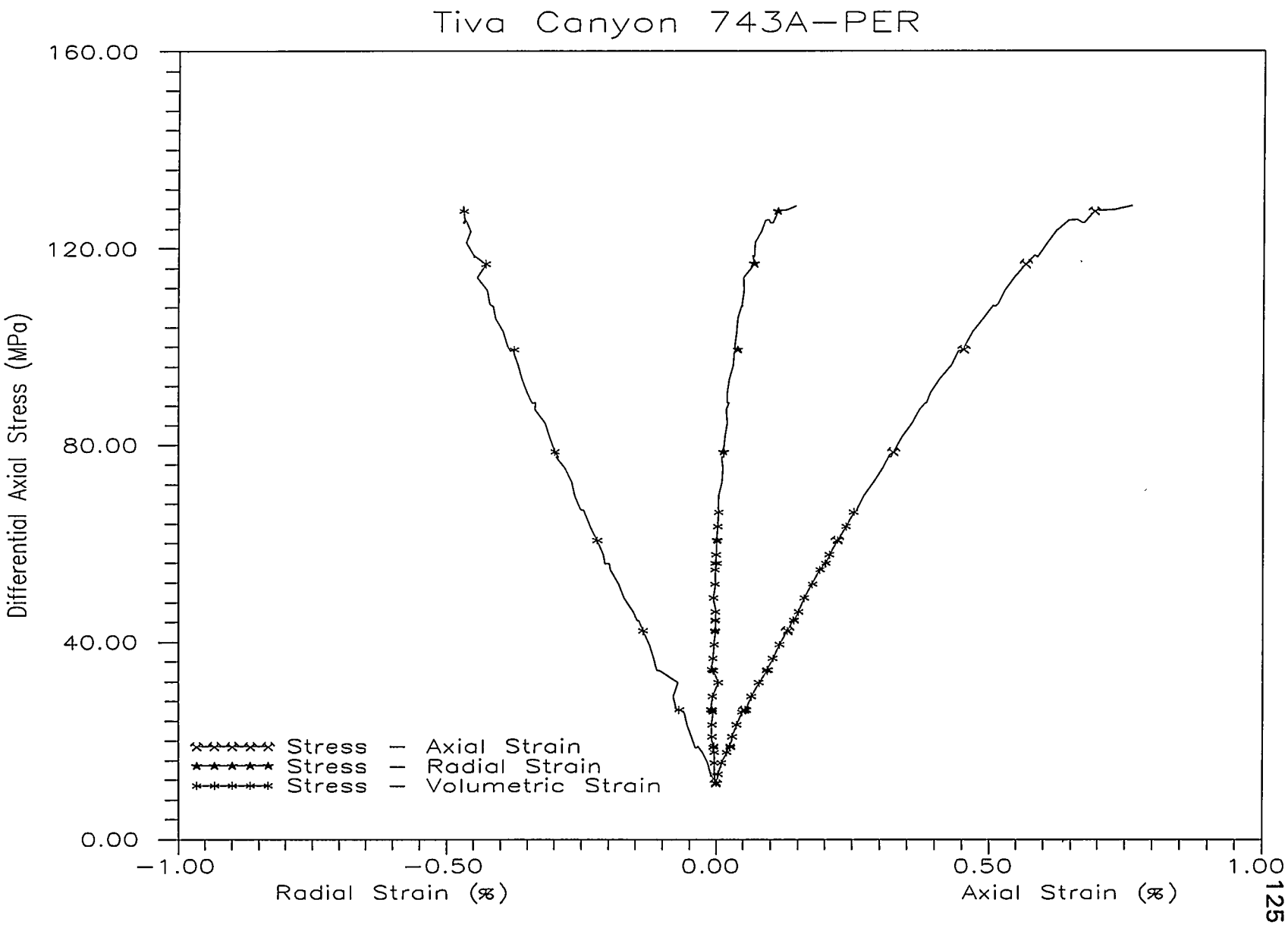
Tiva Canyon 743A—PER
160.00
120.00
80.00
40.00
0.00
Differential Axial Stress (MPa)
Stress — Axial Strain
Stress — Radial Strain
Stress — Volumetric Strain
−1.00
−0.50
0.00
0.50
1.00
Radial Strain (%)
Axial Strain (%)

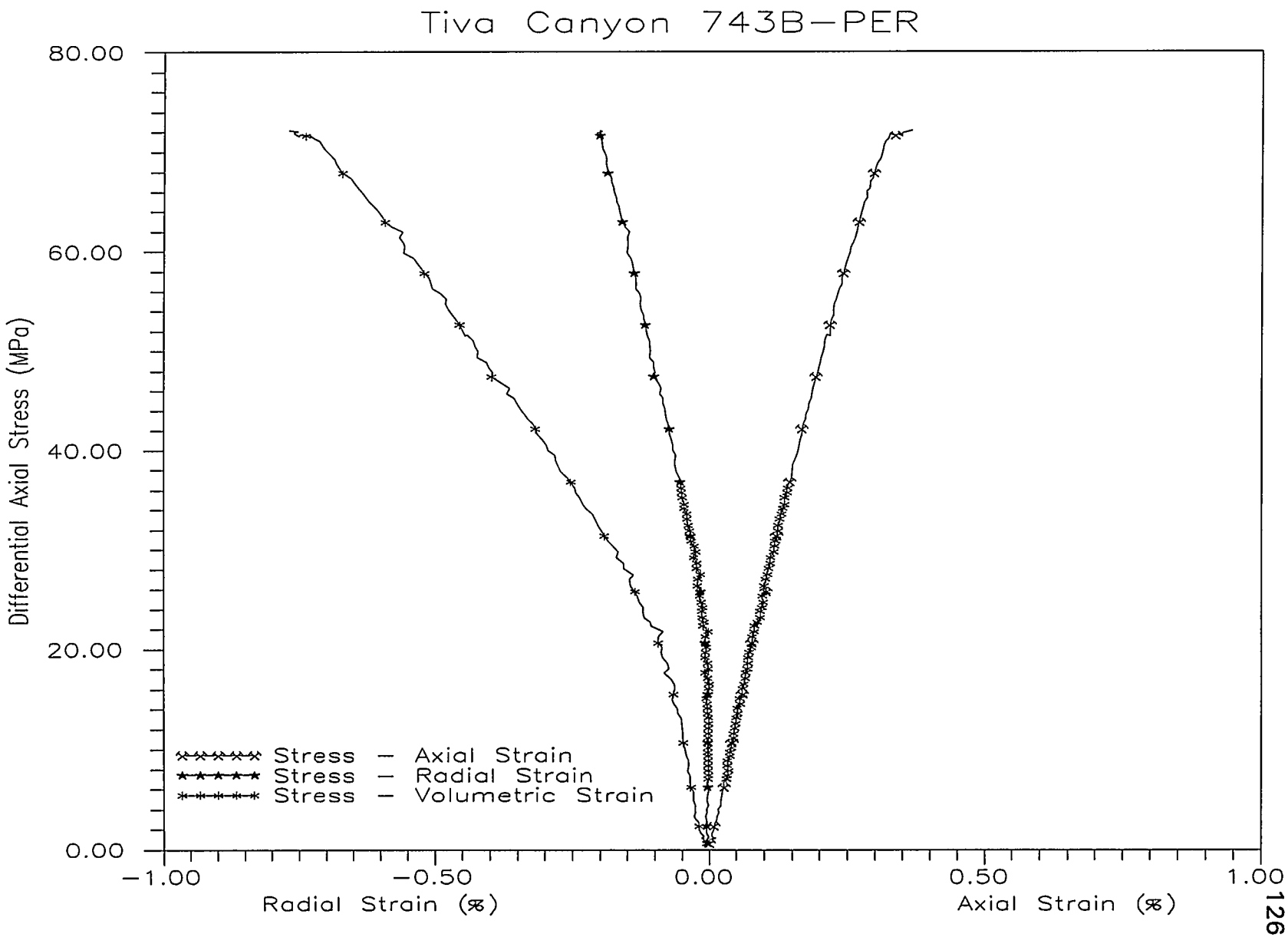
Tiva Canyon 743B—PER
80.00
60.00
40.00
20.00
0.00
Differential Axial Stress (MPa)
Stress — Axial Strain
Stress — Radial Strain
Stress — Volumetric Strain
−1.00
−0.50
0.00
0.50
1.00
Radial Strain (%)
Axial Strain (%)

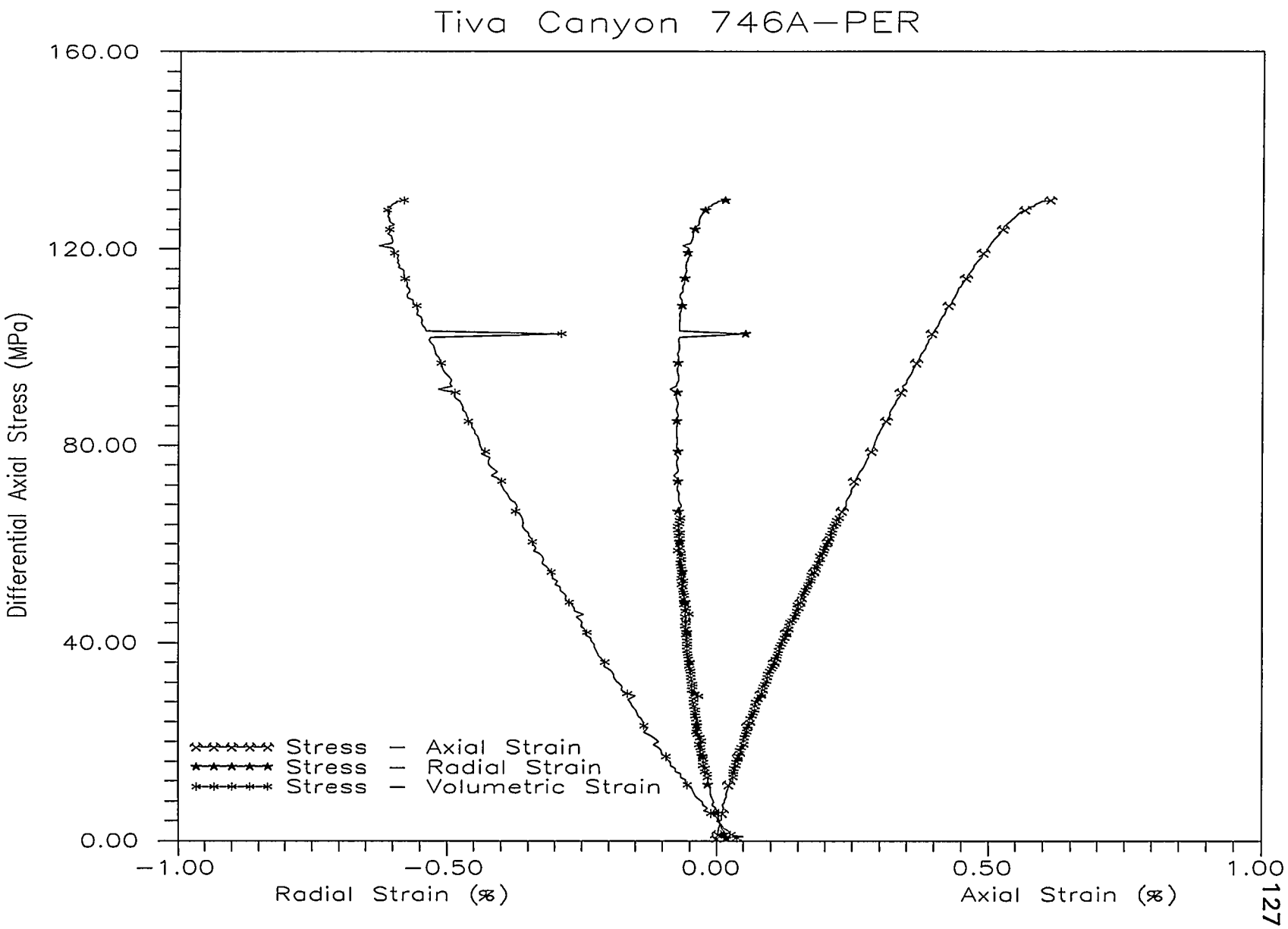
Tiva Canyon 746A—PER
160.00
120.00
80.00
40.00
0.00
Differential Axial Stress (MPa)
Stress — Axial Strain
Stress — Radial Strain
Stress — Volumetric Strain
−1.00
−0.50
0.00
0.50
1.00
Radial Strain (%)
Axial Strain (%)
127

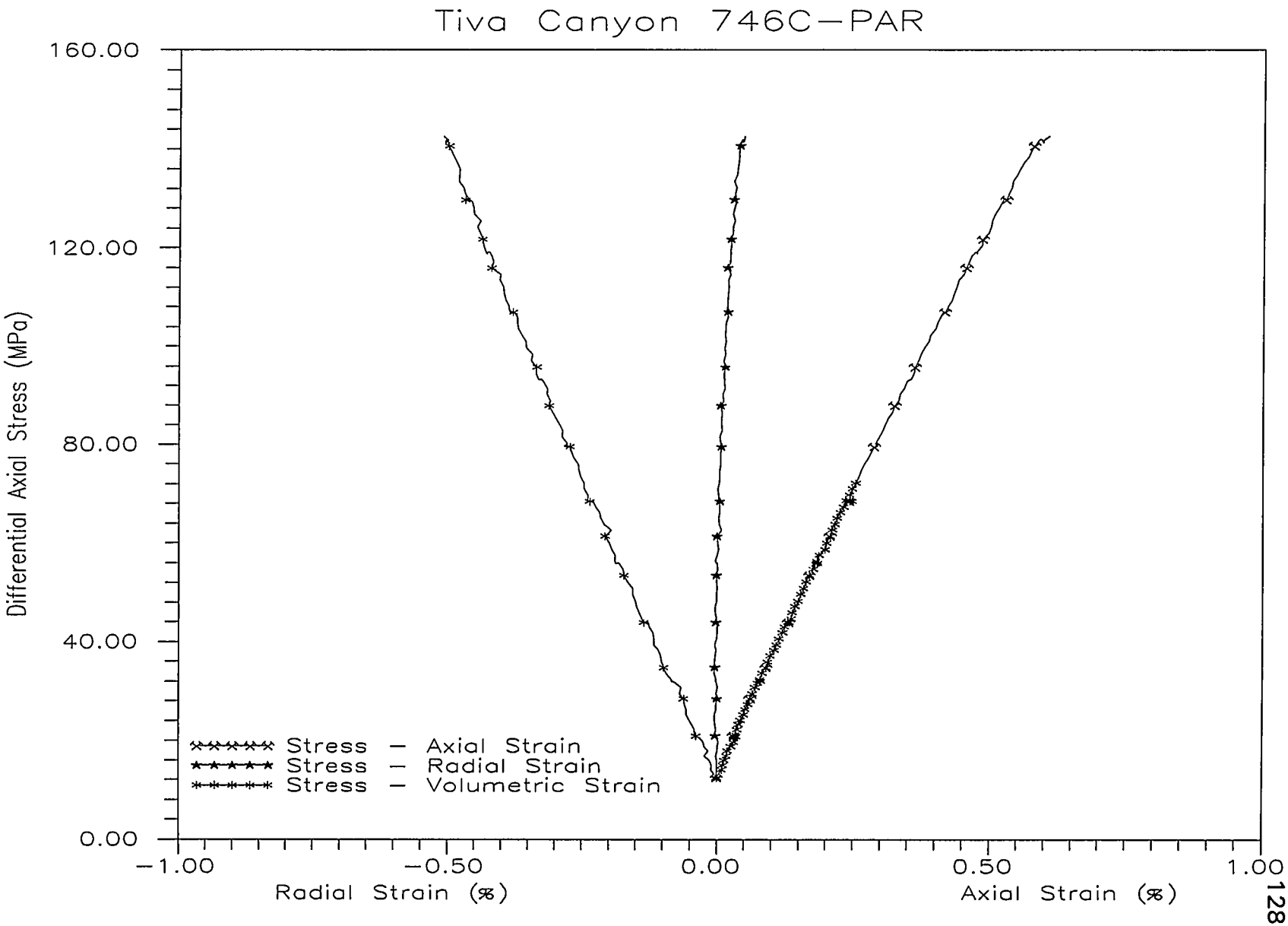
Tiva Canyon 746C—PAR
160.00
120.00
80.00
40.00
0.00
Differential Axial Stress (MPa)
Stress — Axial Strain
Stress — Radial Strain
Stress — Volumetric Strain
−1.00
−0.50
0.00
0.50
1.00
Radial Strain (%)
Axial Strain (%)

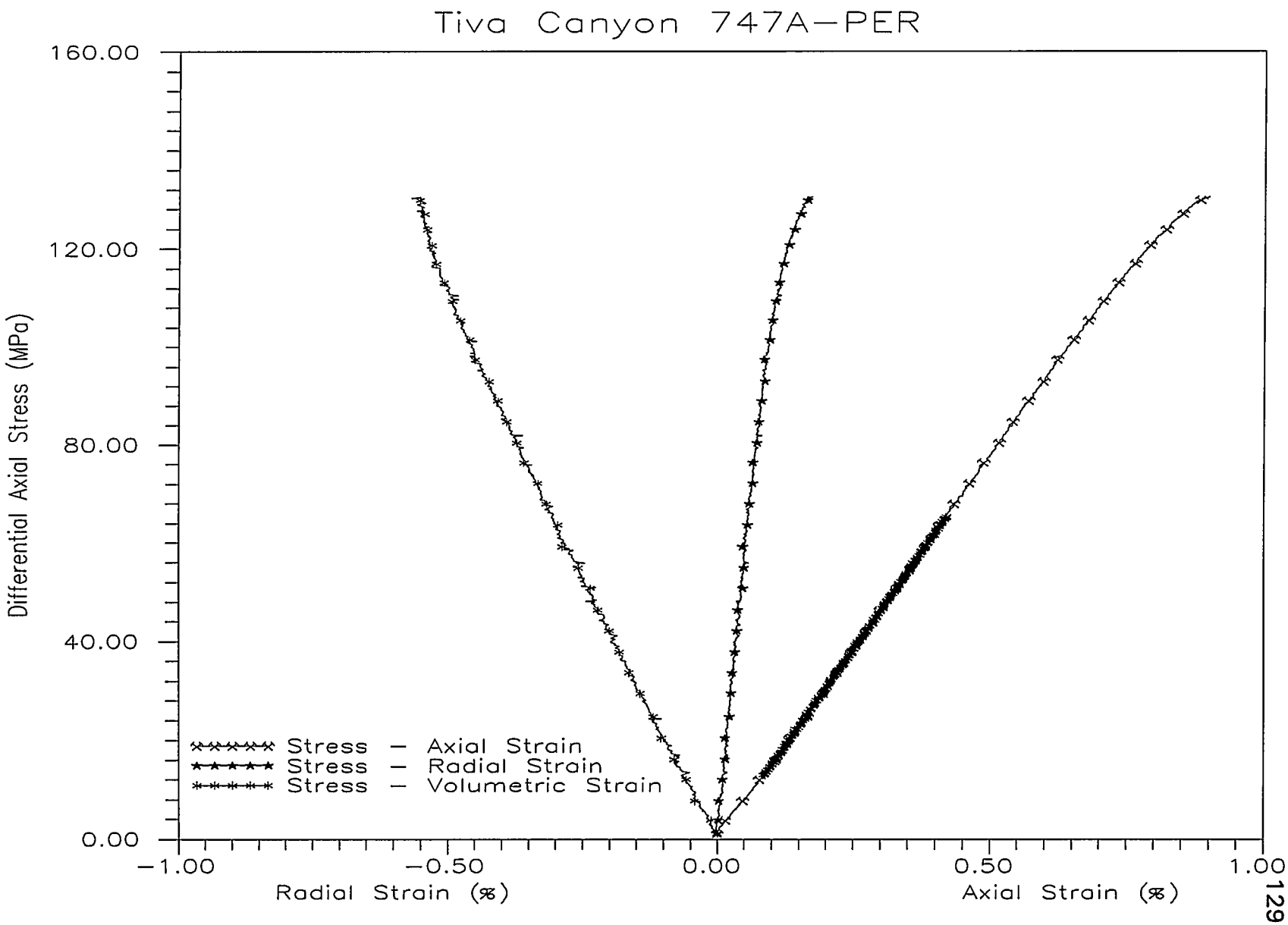
Tiva Canyon 747A—PER
160.00
120.00
80.00
40.00
0.00
Differential Axial Stress (MPa)
Stress — Axial Strain
Stress — Radial Strain
Stress — Volumetric Strain
−1.00
−0.50
0.00
0.50
1.00
Radial Strain (%)
Axial Strain (%)

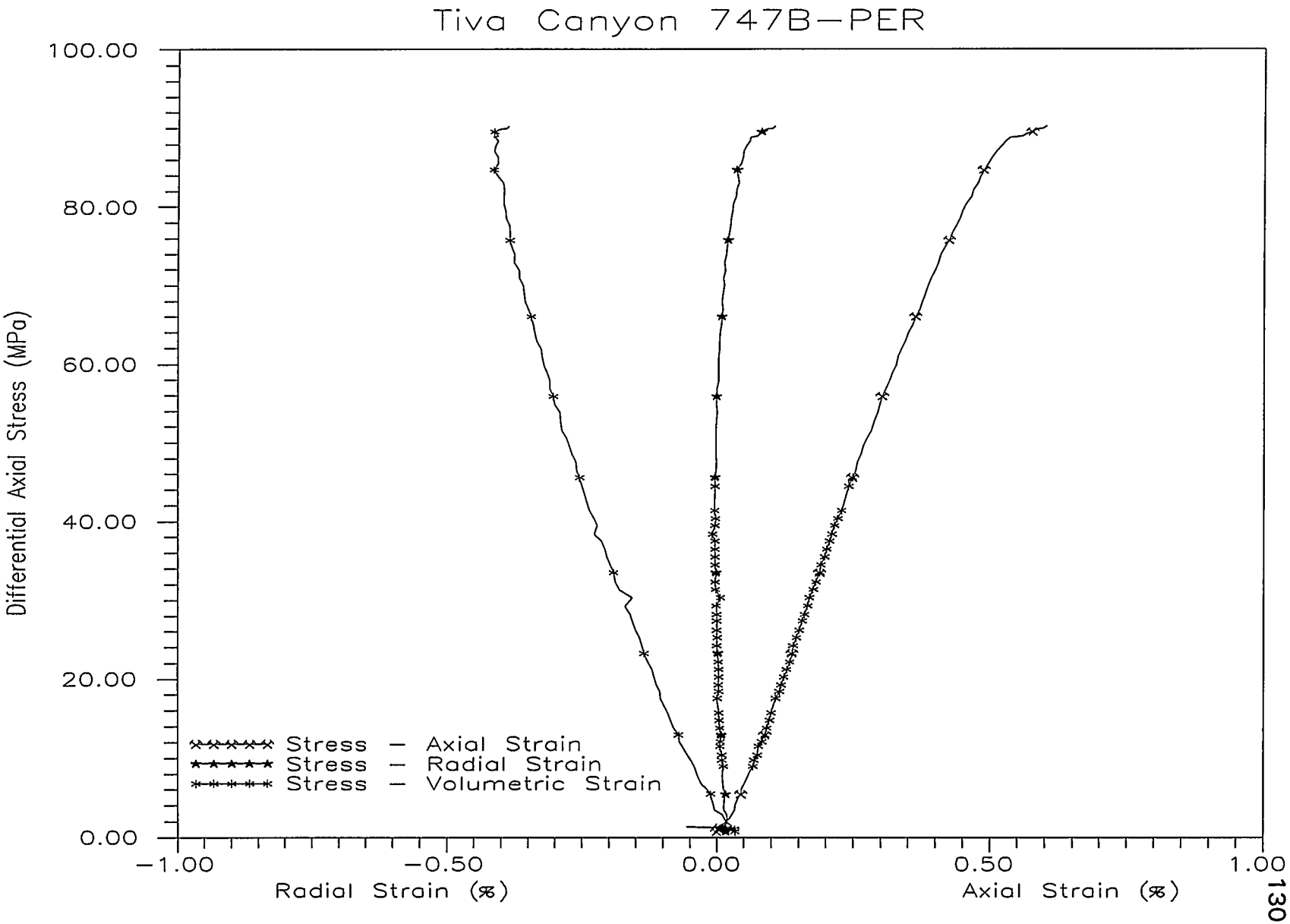
Tiva Canyon 747B—PER
100.00
80.00
60.00
40.00
20.00
0.00
Differential Axial Stress (MPa)
Stress — Axial Strain
Stress — Radial Strain
Stress — Volumetric Strain
−1.00
−0.50
0.00
0.50
1.00
Radial Strain (%)
Axial Strain (%)

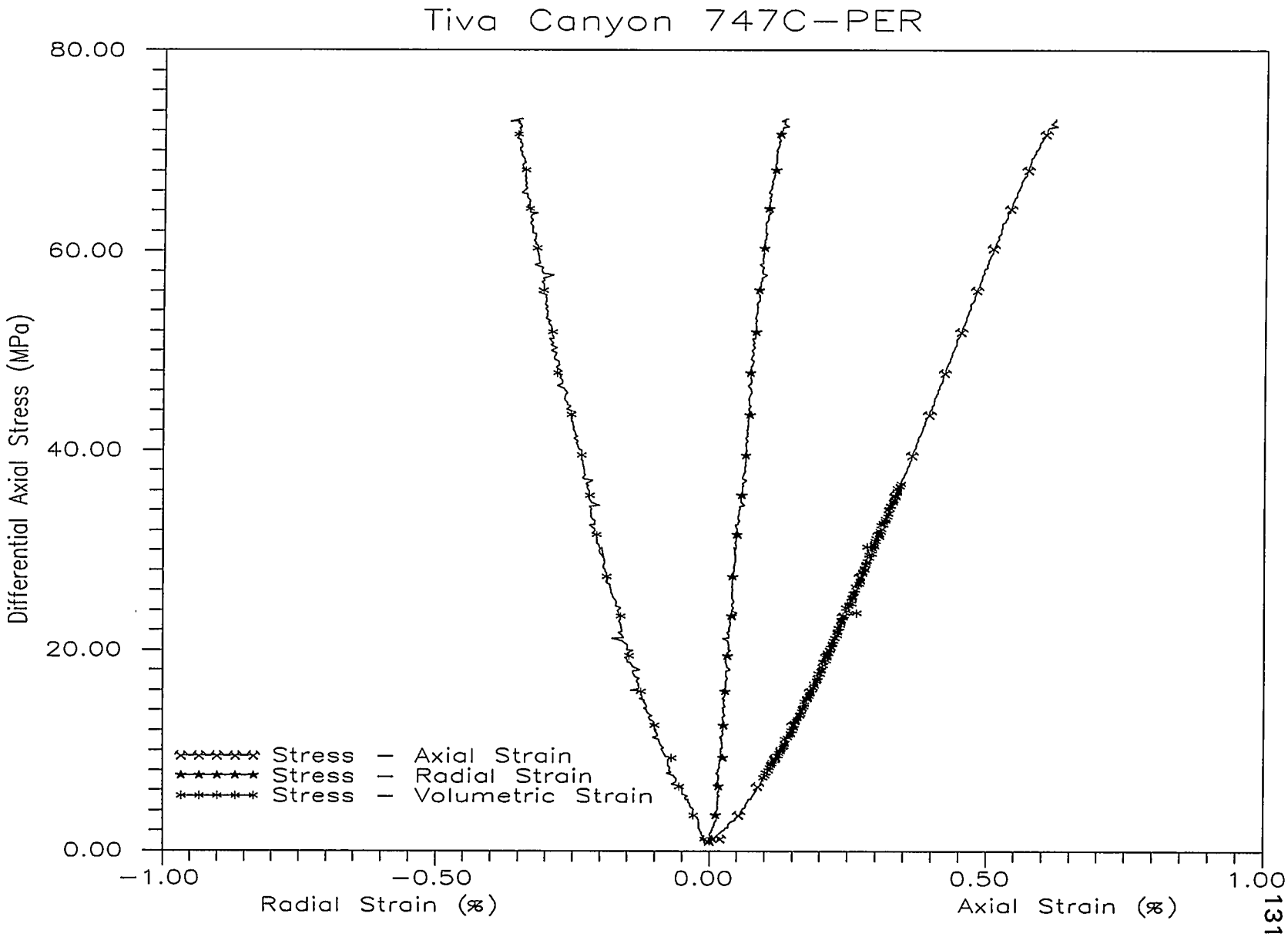
Tiva Canyon 747C-PER
80.00
60.00
40.00
20.00
0.00
Differential Axial Stress (MPa)
Stress - Axial Strain
Stress - Radial Strain
Stress - Volumetric Strain
-1.00
-0.50
0.00
0.50
1.00
Radial Strain (%)
Axial Strain (%)

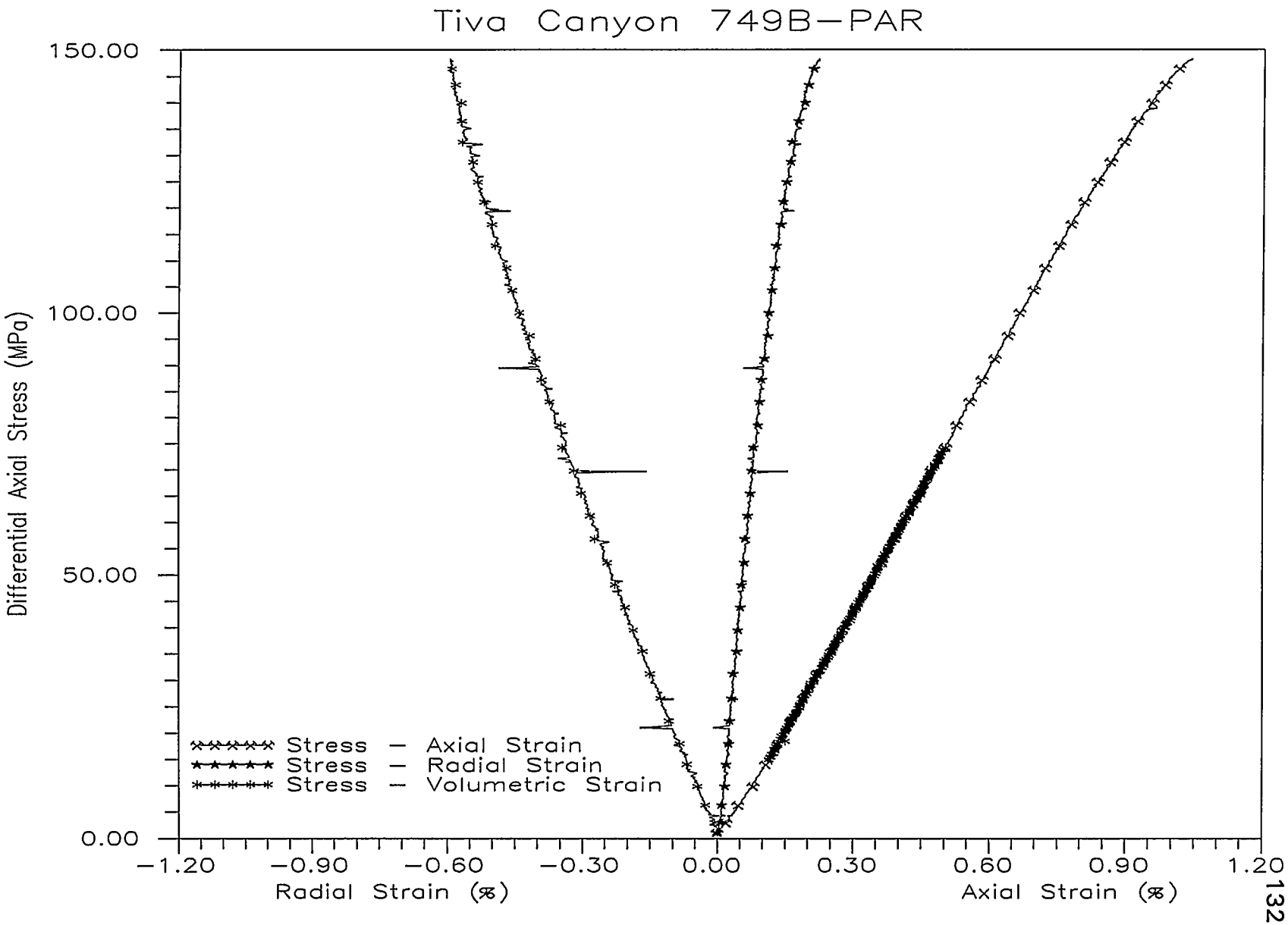
Tiva Canyon 749B—PAR
150.00
100.00
50.00
0.00
Differential Axial Stress (MPa)
Stress — Axial Strain
Stress — Radial Strain
Stress — Volumetric Strain
−1.20
−0.90
−0.60
−0.30
0.00
0.30
0.60
0.90
1.20
Radial Strain (%)
Axial Strain (%)

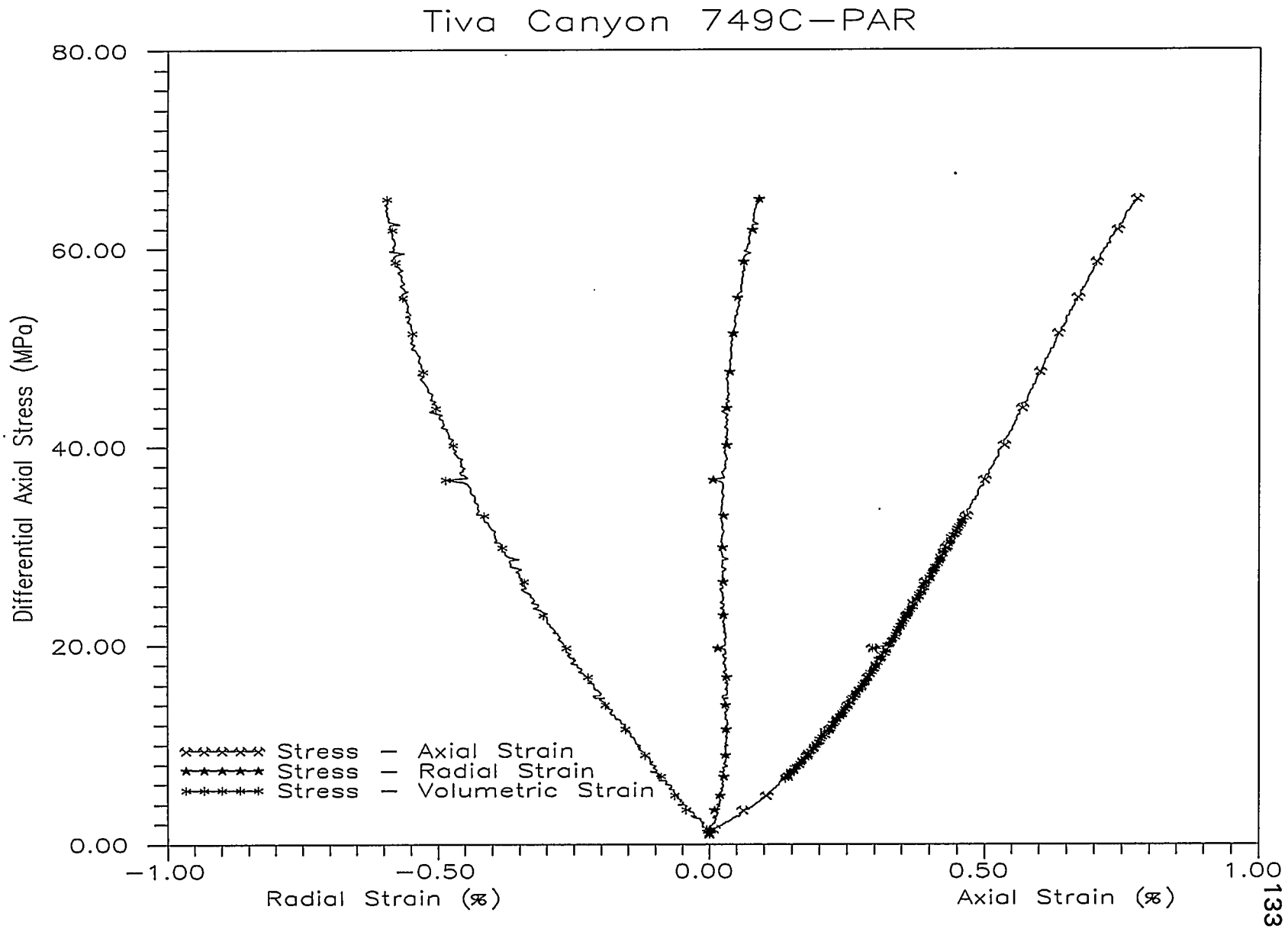
Tiva Canyon 749C—PAR
80.00
60.00
40.00
20.00
0.00
Differential Axial Stress (MPa)
Stress — Axial Strain
Stress — Radial Strain
Stress — Volumetric Strain
−1.00
−0.50
0.00
0.50
1.00
Radial Strain (%)
Axial Strain (%)

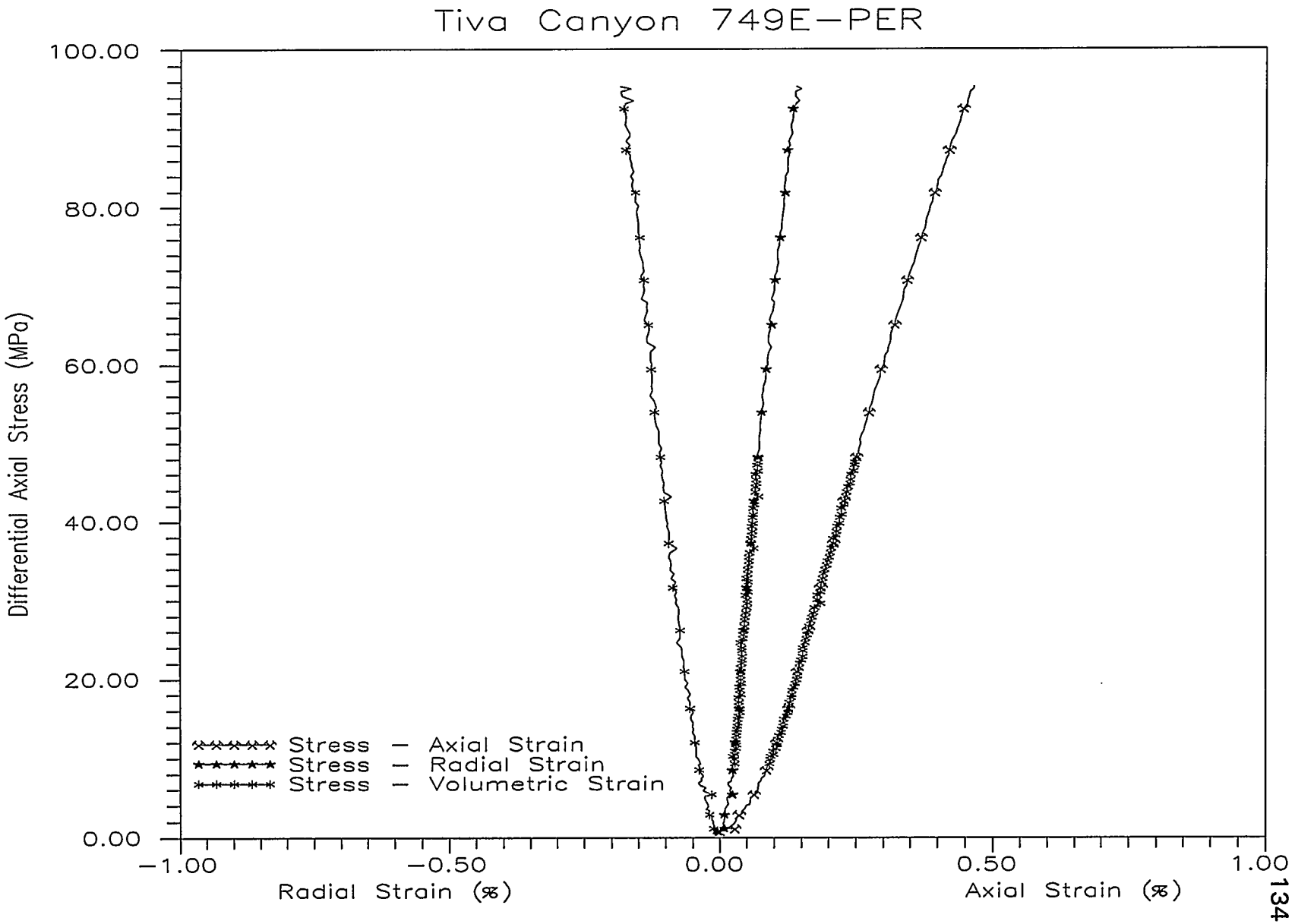
Tiva Canyon 749E-PER
100.00
80.00
60.00
40.00
20.00
0.00
Differential Axial Stress (MPa)
Stress - Axial Strain
Stress - Radial Strain
Stress - Volumetric Strain
-1.00
-0.50
0.00
0.50
1.00
Radial Strain (%)
Axial Strain (%)

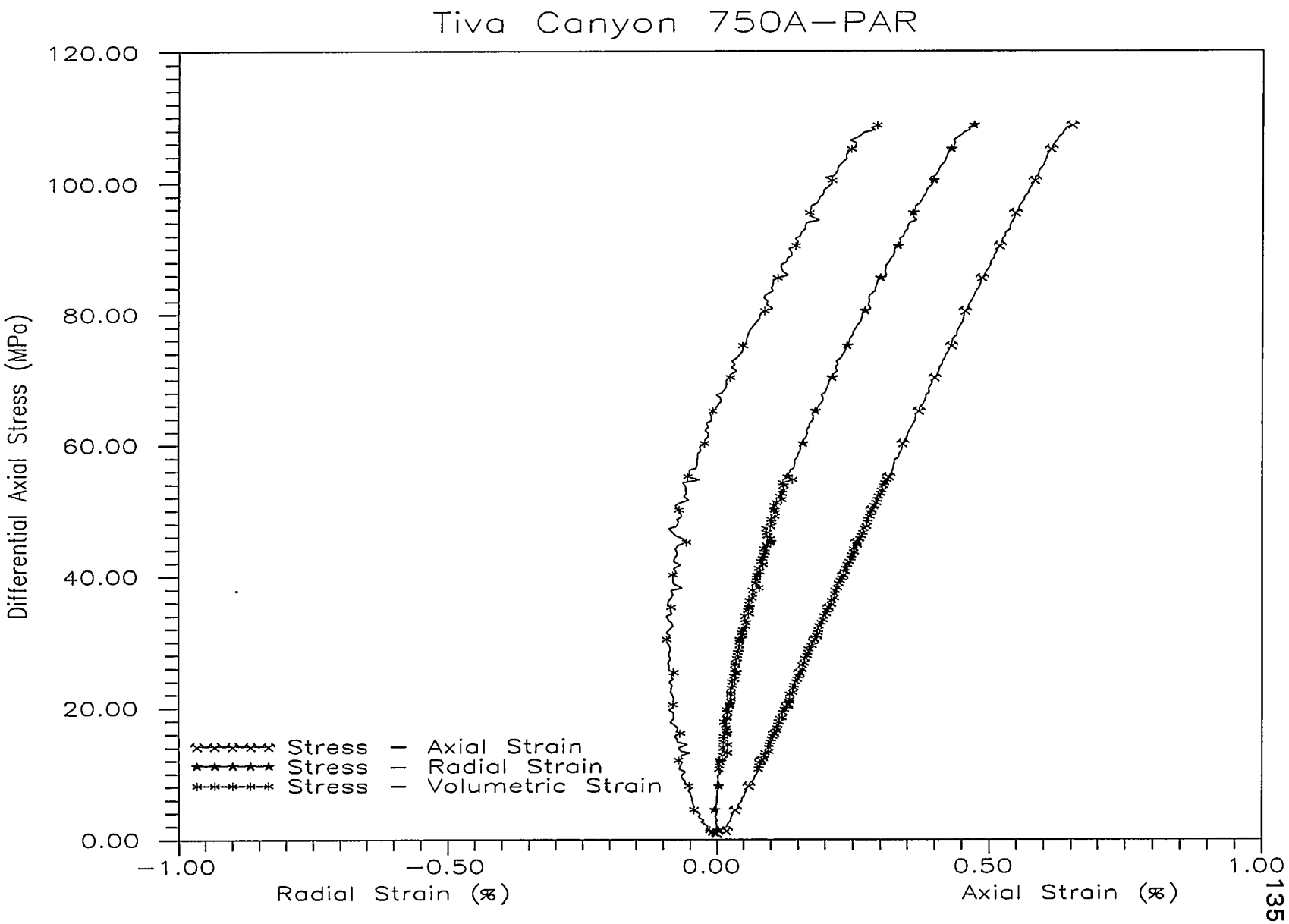
Tiva Canyon 750A—PAR
120.00
100.00
80.00
60.00
40.00
20.00
0.00
Differential Axial Stress (MPa)
Stress — Axial Strain
Stress — Radial Strain
Stress — Volumetric Strain
−1.00
−0.50
0.00
0.50
1.00
Radial Strain (%)
Axial Strain (%)

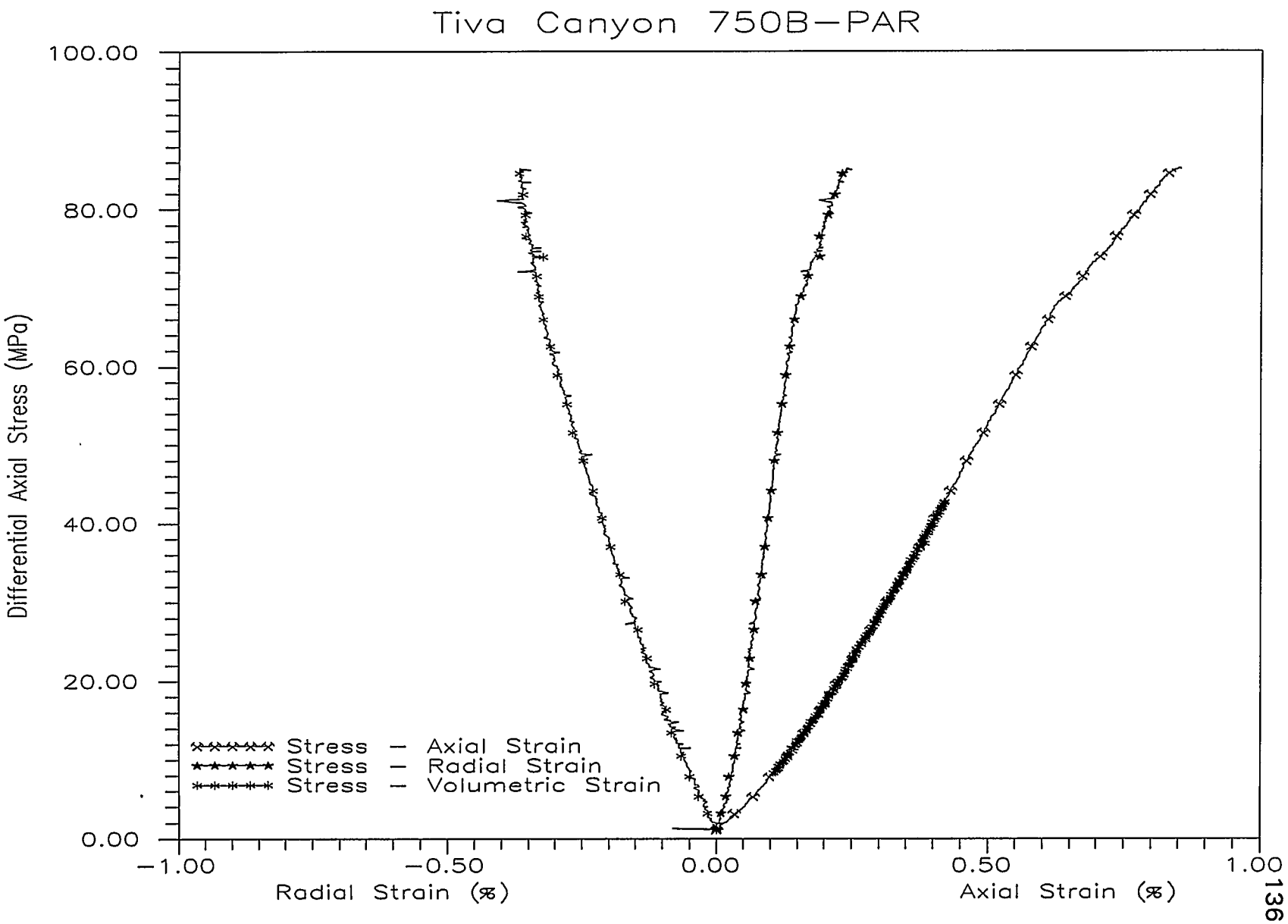
Tiva Canyon 750B—PAR
100.00
80.00
60.00
40.00
20.00
0.00
Differential Axial Stress (MPa)
Stress — Axial Strain
Stress — Radial Strain
Stress — Volumetric Strain
−1.00
−0.50
0.00
0.50
1.00
Radial Strain (%)
Axial Strain (%)

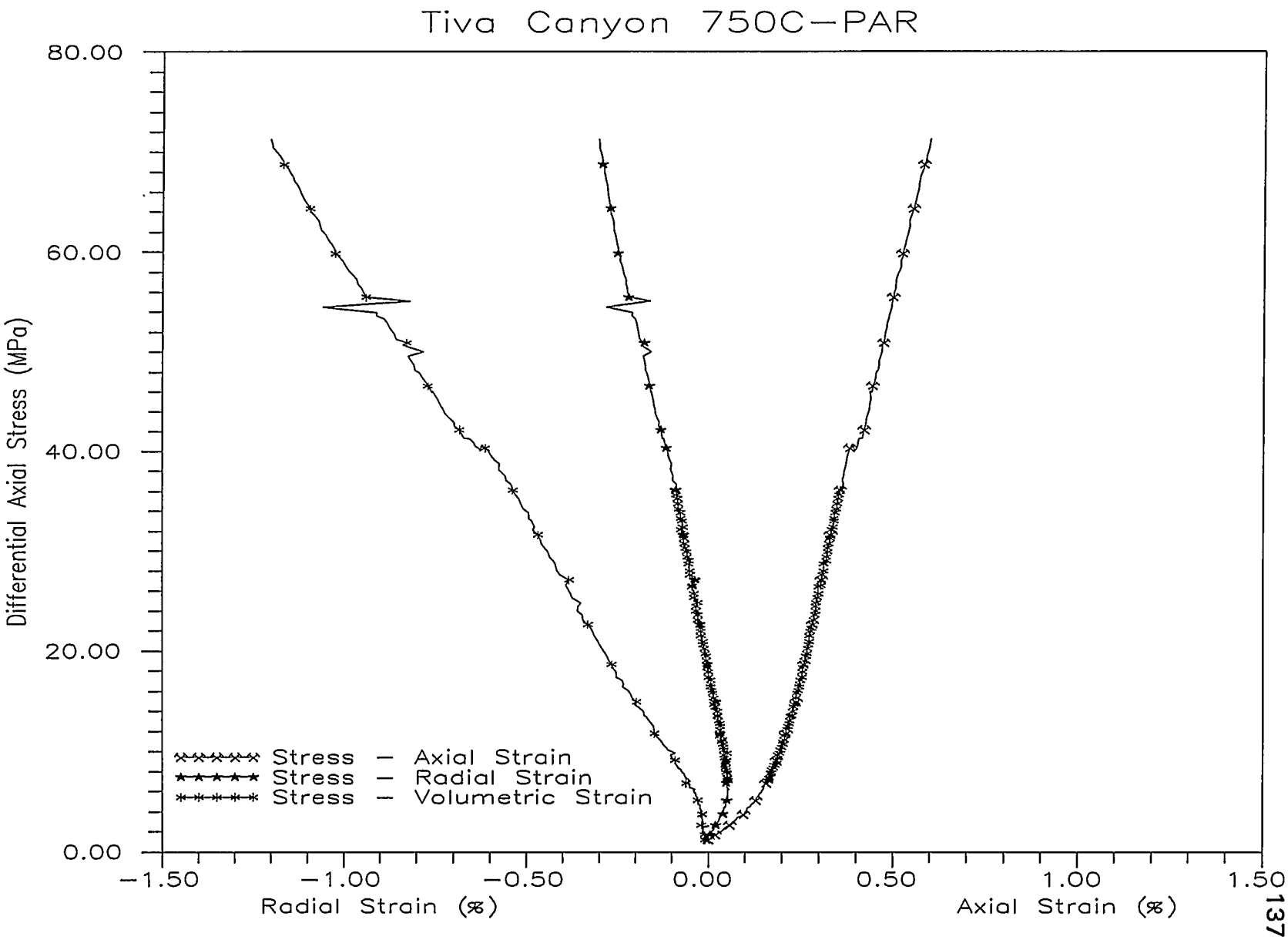
Tiva Canyon 750C—PAR
80.00
60.00
40.00
20.00
0.00
Differential Axial Stress (MPa)
Stress — Axial Strain
Stress — Radial Strain
Stress — Volumetric Strain
−1.50
−1.00
−0.50
0.00
0.50
1.00
1.50
Radial Strain (%)
Axial Strain (%)

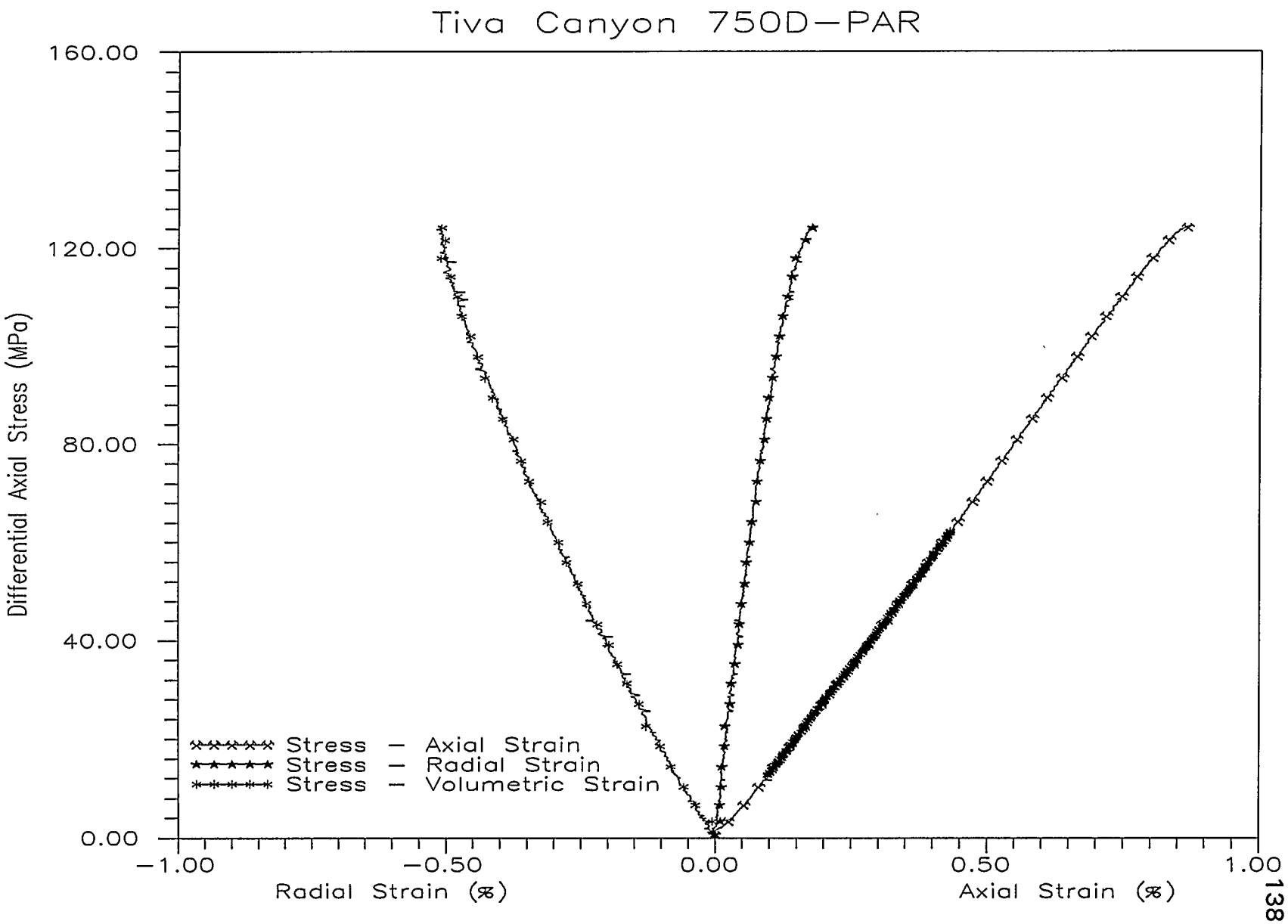
Tiva Canyon 750D—PAR
160.00
120.00
80.00
40.00
0.00
Differential Axial Stress (MPa)
Stress — Axial Strain
Stress — Radial Strain
Stress — Volumetric Strain
−1.00
−0.50
0.00
0.50
1.00
Radial Strain (%)
Axial Strain (%)

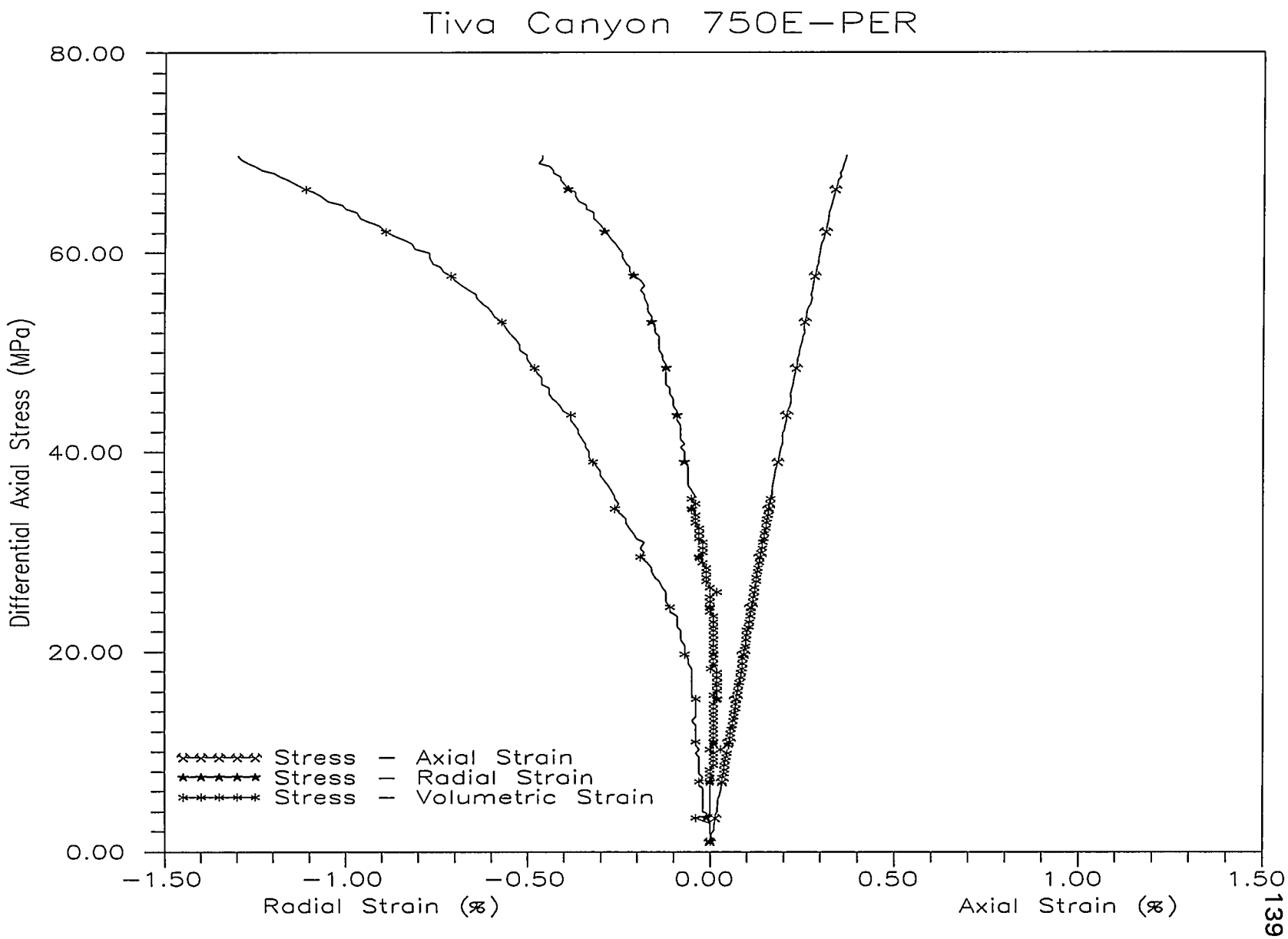
Tiva Canyon 750E—PER
80.00
60.00
40.00
20.00
0.00
Differential Axial Stress (MPa)
Stress — Axial Strain
Stress — Radial Strain
Stress — Volumetric Strain
−1.50
−1.00
−0.50
0.00
0.50
1.00
1.50
Radial Strain (%)
Axial Strain (%)

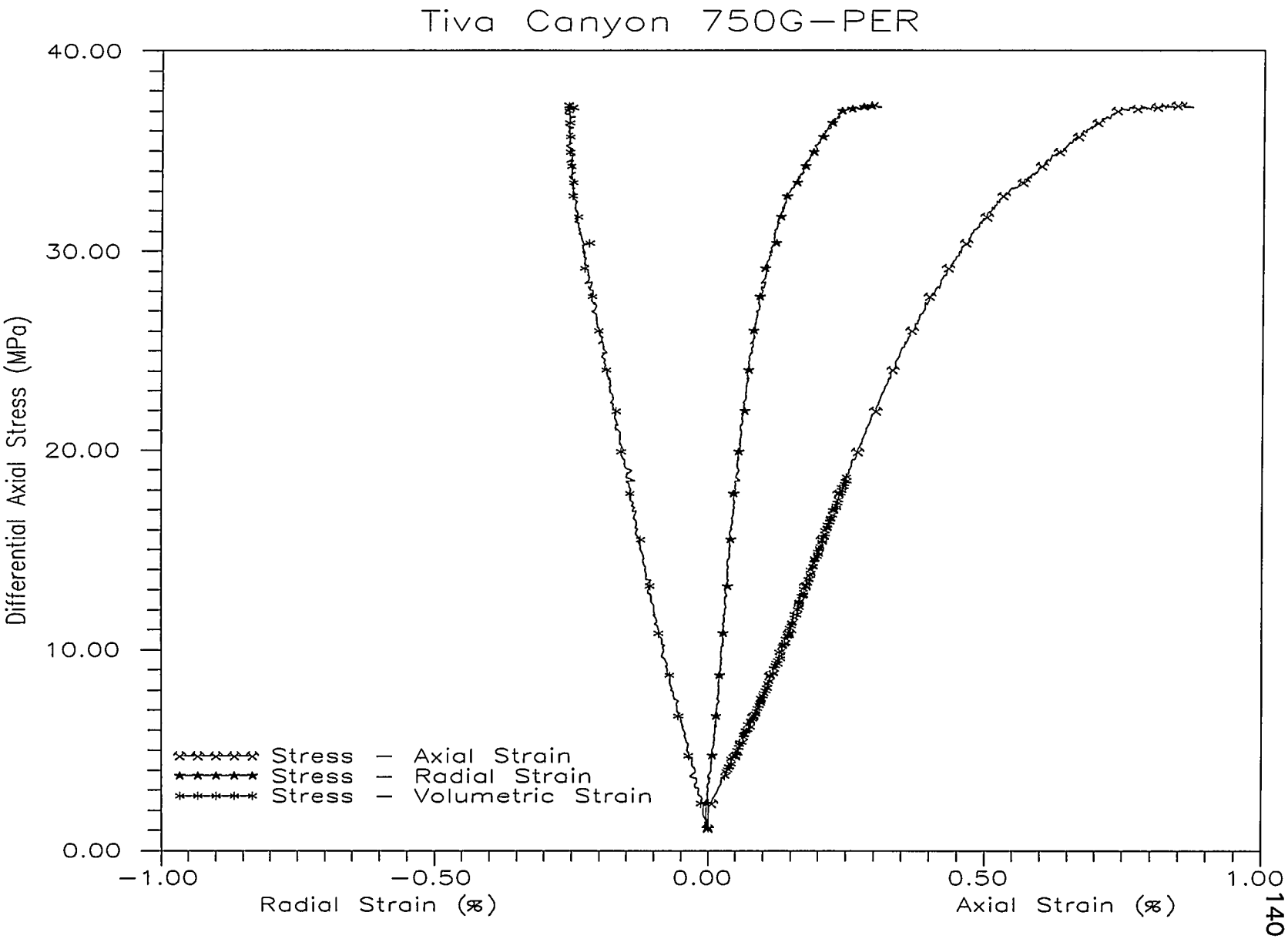
Tiva Canyon 750G—PER
40.00
30.00
20.00
10.00
0.00
Differential Axial Stress (MPa)
Stress — Axial Strain
Stress — Radial Strain
Stress — Volumetric Strain
−1.00
−0.50
0.00
0.50
1.00
Radial Strain (%)
Axial Strain (%)

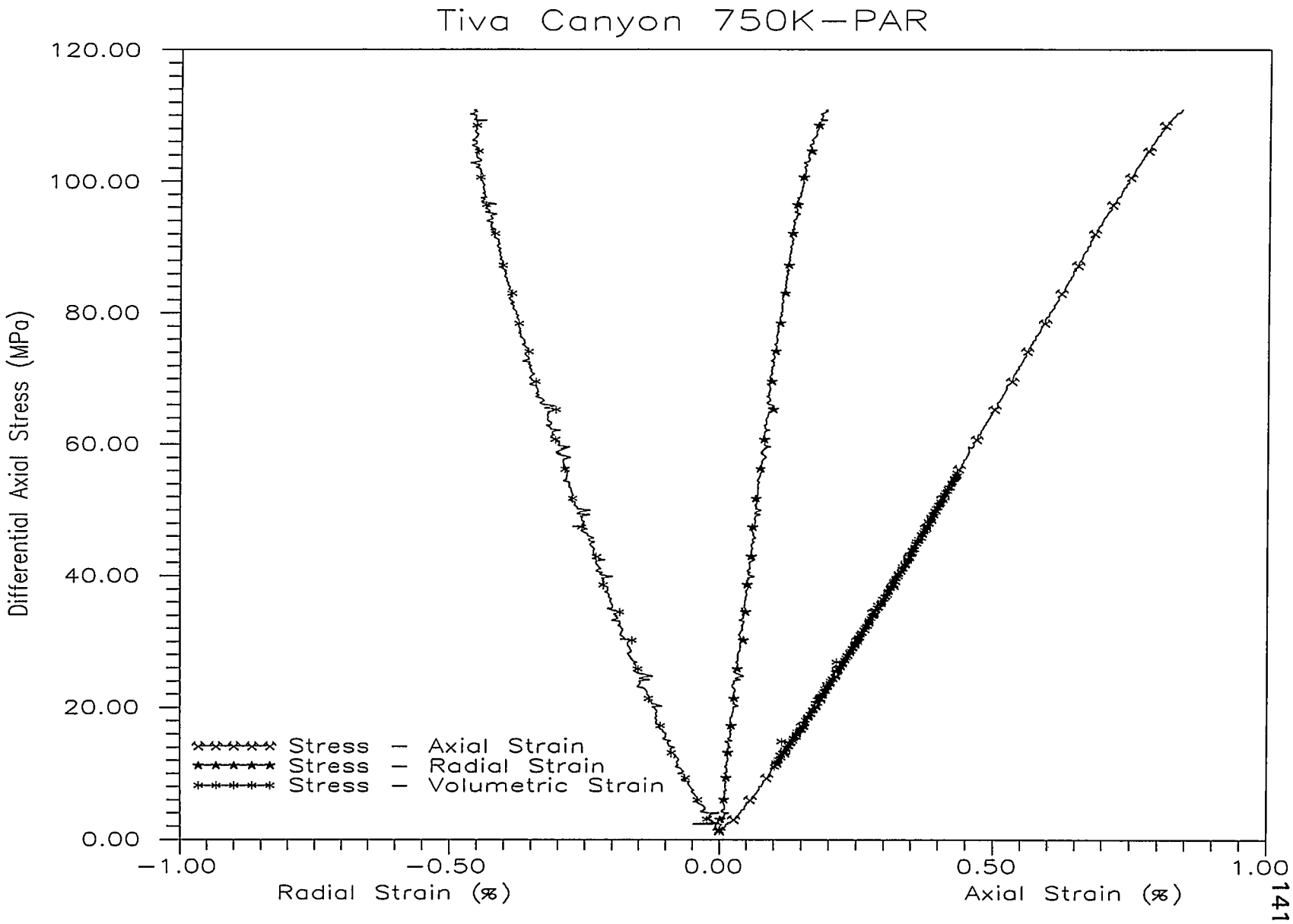
Tiva Canyon 750K—PAR
120.00
100.00
80.00
60.00
40.00
20.00
0.00
Differential Axial Stress (MPa)
Stress — Axial Strain
Stress — Radial Strain
Stress — Volumetric Strain
−1.00
−0.50
0.00
0.50
1.00
Radial Strain (%)
Axial Strain (%)